Structural - Functional Analysis of Plant Cyclic Nucleotide Gated Ion Channels

By

Huda Abdel-Hamid

A thesis submitted in conformity with the requirements for the degree of

Doctor of Philosophy

Graduate Department of Cell and Systems Biology

University of Toronto

Structural - Functional Analysis of Plant Cyclic Nucleotide Gated Ion Channels

Huda Abdel-Hamid

Doctor of Philosophy 2013

Graduate Department of Cell and Systems Biology

University of Toronto

Abstract

The *Arabidopsis thaliana* genome encodes twenty putative cyclic nucleotide-gated channel (CNGC) genes. Studies on *A. thaliana* CNGCs so far have revealed their ability to selectively transport cations that play a role in various stress responses and development, however, the regulation of plant CNGCs is not yet fully understood. Thus, in this study I have attempted to analyze the structure-function relationship of AtCNGCs, mainly by using suppressor mutants of the rare gain-of function mutant, *cpr22*.

The *A. thaliana* mutant *cpr22* resulted from an approximately 3kb deletion that fused the 5' half and the 3' half of two CNGC-encoding genes, *AtCNGC11* and *AtCNGC12,* respectively. The expression of this chimeric CNGC, the *AtCNGC11/12* gene confers easily detectable characteristics such as stunted morphology with curly leaves and hypersensitive response-like spontaneous lesion formation. Through a suppressor screen, twenty nine new alleles were identified in *AtCNGC11/12*. Since the cytosolic C-terminal region contains important regulatory domains, such as a cyclic-

nucleotide binding domain, eleven cytosolic C-terminal mutants, S17, S35, S81, S83, S84, S100, S135, S136, S137, S140 and S144, were analyzed. A detailed analysis of two mutants, S100 (AtCNGC11/12:G459R) and S137 (AtCNGC11/12:R381H), suggested that G459 and R381 are important for basic channel function rather than channel regulation. Site-directed mutagenesis and fast protein liquid chromatography (FPLC) showed that these two amino acids influence both intra- and inter-subunit interactions that are involved in stabilizing the tertiary structure of the channel.

In addition, calmodulin binding domain(s) (CaMBD) and cyclic nucleotide binding domain(s) (CNBD) of some of AtCNGCs were studied using computational modeling and biophysical analyses. The data indicated that AtCNGC12 has two CaMBDs in both N- and C- cytosolic termini, whereas AtCNGC11 has only one CaMBD located in the N-terminal region of the channel. In addition, a thermal shift assay suggested that AtCNGC12 has higher affinity to bind cAMP over cGMP.

Taken together, the current study contributes to identify key residues for channel function and provides new insights into CaMBD and CNBD in plant CNGCs.

List of abbreviations

3D: 3 dimensional

A: alanine

AC: adenylyl cyclase

AKT: *Arabidopsis* K^+ transporter

APG: arginine, phosphoric acid, glucose

ARPK: rice putative protein kinases

Asp: aspartic acid

AtCNGC: *Arabidopsis thaliana* cyclic nucleotide-gated channel

BiFC: bimolecular fluorescence complementation

bp: base pair

C-terminus: carboxyl terminus

C: cysteine

Ca^{2+}:   calcium ion

$CaCl_2$:   calcium chloride

CaM: calmodulin

CaMBD: calmodulin binding domain

CaMK: calmodulin-dependent protein kinases

CaMKK: calmodulin-dependent protein kinase kinase

cAMP: cyclic-3', 5' adenosine monophosphate

Ca$_V$:	voltage-activated calcium channel
cDNA:	complementary deoxyribonucleic acid
cGMP:	cyclic guanosine-3', 5' monophosphate
cm:	centimeter
CML:	calmodulin Like
CN:	calcineurin
CNBD:	cyclic nucleotide binding domain
CNGA :	cyclic nucleotide-gated channel alpha (animal CNGC)
CNGB:	cyclic nucleotide-gated channel beta (animal CNGC)
cNMP:	3', 5'-cyclic nucleotide monophosphate
CPR22:	constitutive expresser of pathogenesis related genes 22
Cs$^+$:	cesium ion
D:	aspartic acid
D$_2$O:	deuterium oxide
Da:	dalton
DAP:	death-associated protein
dATP:	deoxyadenosine triphosphate
dCTP:	deoxycytidine triphosphate
ddH$_2$O:	double distilled water
dGTP:	deoxyguanosine triphosphate

DNA:	deoxyribonucleic acid
DNase:	deoxyribonuclease
DND:	defense no death
dNTP:	deoxyribonucleotide triphosphate
dTTP:	deoxythymidine triphosphate
E:	glutamic acid
E. coli:	*Escherichia coli*
eag:	ether-a-gogo
EDTA:	ethylenediaminetetra-acetic acid
EMS:	ethylmethane sulphonate
EtOH:	ethanol
EV:	empty vector
F:	phenylalanine
FPLC:	fast protein liquid chromatography
FRET:	fluorescence resonance energy transfer
G:	glycine
GAD:	glutamate decarboxylase
GC:	guanylyl cyclase
GFP:	green fluorescence protein
GLR:	glutamate receptor-like

Glu: glutamic acid

H: Histidine

H^+:   proton

HCN: hyperpolarization-activated and cyclic nucleotide-gated pacemaker channels

HEK293:   human embryonic kidney 293

HEPES: 4-(2-hydroxyethyl)-1-piperazineethanesulfonic acid

hERG: eag-related gene family

His: histidine

HLM1:   hypersensitive response-like lesion mimic 1

HR: hypersensitive response

HvCBT1:   *hordeum vulgare* calmodulin binding transporter 1

I: isoleucine

IQ-type: isoleucine glutamine-type

IQGAP: IQ motif containing GTPase activating protein

K: lysine

K^+:   potassium ion

K_2HPO_4:   dipotassium phosphate

KAT: K^+ transporters of *Arabidopsis thaliana*

kb: kilo base

KCl: potassium chloride

KO: knock-out

L: Litre

LB: Luria-Bertani broth

Li^+:   lithium ion

M: methionine

MARCKS: myristoylated alanine-rich C kinase substrate

MCA1:   mechanosensitive channel

Mg: magnesium

mg: milli gram

$MgCl_2$:   magnesium chloride

$MgSO_4$ magnesium sulphate

min: minute

ml: milli litre

MLCK: skeletal and smooth muscle

MlotiK1   *Mesorhizobium loti* K1

mM: milli Molar

MPSS: massively parallel signature sequencing:

MSA: multiple sequence alignment

N-terminus: amino terminus

N: nitrogen ion

N: Asparagine

N. benthamiana: *Nicotiana benthamiana*

Na(V)1.2: voltage-dependent sodium channel.

Na^+: sodium ion

NaCl: sodium chloride

NMR: nuclear magnetic resonance

NOS: endothelial nitric oxide synthase

NtCBP4: *Nicotiana tabacum* calmodulin binding protein 4

º C: degree Celsius

OD600: optical density at 600 nm

P: phosphorus

PAGE: polyacrylamide gel electrophoresis

PCR: polymerase chain reaction

PDB: protein database bank

PDE: phosphodiesterase

pH: potential hydrogen

Phe: phenylalanine

Phyre: protein homology/analogY recognition engine

PIP2: phospholipid phosphatidylinositol 4, 5-bisphosphate

PKG cGMP-dependent protein kinases

PMCA:	plasma membrane ATPase
PR:	pathogenesis-related gene
PyMOL:	python-enhanced molecular graphics tool
Q:	glutamine
R:	arginine
Rb^+:	rubidium ion
RH:	relative humidity
RIa:	type Ia regulatory subunit
RNA:	ribonucleic acid
RNAi:	ribonucleic acid interference
rpm:	round per minute
RT-PCR:	reverse transcription polymerase chain reaction
RT:	room temp
S:	sulphur ion
S:	serine
S1-S6:	transmembrane segment 1 to 6
SA:	salicylic acid
SC:	synthetic complete
SDS:	sodium dodecylsulfate
sec:	second

SpIH:	HCN channel from sea urchin sperm
T:	threonine
TEA:	tetraethylammonium
TPC:	two-pore Channel
Tris:	N, N, N', N'-tetramethylethylethylenediamine
TRK:	tyrosine kinases
V:	volts
v/v:	volume per volume
W:	tryptophan
Ws:	Wassilewskija
Wt:	wilde type
X. laevis:	*Xenopus laevis*
Y:	tyrosine
µg:	micro gram
µl:	micro litre
µM:	micro molar

Table of Contents

Statement of Publications

Abdel-Hamid, H., Chin K., Shahinas D., Moeder, W. Yoshioka K., 2010, Calmodulin binding to arabidopsis cyclic nucleotide gated ion channels. *Plant Signaling & Behavior* 5: 1-3

Abdel-Hamid H., Chin K., Moeder W., Yoshioka K., 2011, High throughput chemical screening supports the involvement of Ca2+ in cyclic nucleotide-gated channel-mediated programmed cell death in Arabidopsis. *Plant Signaling & Behavior* 5: 1147-1149

Abdel-Hamid H., Moeder W., Shahinas D., Chin K., Yoshioka K., A suppressor screen of the chimeric AtCNGC11/12 reveals residues important for inter-subunit interactions of cyclic nucleotide-gated ion channels. Revising for *Plant Physiology*

Abdel-Hamid H*., DeFalco T*., Marshall C., Ikura M., Snedden W., Yoshioka K., *Co-first author, Characterization of calmodulin binding domains in plant cyclic nucleotide gated ion channels (tentative title), in progress.

Contribution was also made to:

Chin K., Moeder W., **Abdel-Hamid H**., Shahinas D, Gupta D, Yoshioka K. J 2010, Importance of the αC-helix in the cyclic nucleotide binding domain for the stable channel regulation and function of cyclic nucleotide gated ion channels in Arabidopsis. *J. Exp Bot*. 9: 2383-93

List of Figures

List of Tables

Appendix

Acknowledgements

First of all, I would like to thank both the Egyptian government and the CSB department for their financial support.

I would like to thank my supervisor Dr. Yoshioka for her kind help and support through my journey in her lab. I also want to thank all the past and present members of the Yoshioka lab, specially Kimberly Chin for all her help since I joined the Yoshioka lab, four years ago, including helping me in revising my thesis and Sol Nievas for all her help and support and for being such a good friend. I also want to thank my committee members, Dr. Campbell and Dr. Desveaux, and their lab members for all their help. I would like to specially thank Dr. Desveaux and Brenden Hurtly for all their help in the FPLC analysis. I also want to thank our collaborators, Dr. Zagotta and Dr. Ikura for their help and advice. Special thanks to Dr. Marshall for all his kind help.

I also want to thank my family for all their emotional and financial support, specially my twin sister Dr. Abdel-Hamid for being there for me at all times. Last but not least, I would like to thank my husband and the love of my life, Dr. El-Maghraby for everything he did and still doing to make it possible for me to be in the lab in weekdays, weekends and holidays, for taking care of our daughter and yet always smiling to make it possible for me to continue, thank you just does not say enough.

Chapter 1

Literature study

1.1. Cyclic Nucleotide-Gated ion Channels (CNGCs)

Plants, like any other living organisms, require nutrients for their survival and development. It has been known that plants require 16 essential ions (Marschner, 1995; Mengel *et al.,* 2001). Those ions can be divided into two groups according to their sources. Carbon, hydrogen, and oxygen are derived from the atmosphere, soil and water. The remaining 13 essential ions, including nitrogen (N), phosphorus (P), potassium (K^+), calcium (Ca^{2+}), magnesium (Mg^{2+}), sulphur (S), iron (Fe), zinc (Zn), manganese (Mn), copper (Cu), boron (B), molybdenum (Mo), and chloride (Cl) are supplied either from soil minerals or soil organic matter (Marschner, 1995; Mengel *et al.,* 2001; White and Brown, 2010). Six of those essential ions, including N, P, K^+, Ca^{2+}, Mg^{2+} and S, are required in large amounts, while the rest are required in less amounts (White and Brown, 2010).

Both Ca^{2+} and K^+, among other essential ions, are well known for their crucial role in pathogen defence responses, where one of the very early responses in pathogen defence is ion fluxes including an influx of H^+ and Ca^{2+} and efflux of H^+ and Cl (Atkinson *et al.*, 1996). Ca^{2+} and K^+ also play an important role in regulating growth and development in plants (Hepler, 2005; Dreyer and Uozumi, 2011). For example, K^+ plays a major role as a stabilizer of plant metabolism and it contributes to cellular growth and responses to environmental changes. A high potassium concentration, in certain cell compartments, is important for enzyme activation, stabilization of protein synthesis, neutralization of negative charges on proteins, formation of membrane potential, and maintenance of cytosolic pH homeostasis (Dreyer and Uozumi, 2011).

Ca^{2+}, on the other hand, is involved in nearly all aspects of plant development and also in the signalling pathways (Hepler, 2005). These pathways connect biotic and abiotic stimuli that have an impact on gene expression and cell physiology (Dodd *et al.*, 2010). In plants, the Ca^{2+} signals are the result of transient increases in cytosolic free Ca^{2+}. This signalling mechanism is only made possible by the electrochemical potential difference for Ca^{2+} across membranes that separate Ca^{2+} sources from the cytosol (Sanders *et al.*, 1999). This electrochemical potential difference for Ca^{2+} is maintained in plants by ATP powered Ca^{2+} pumps or by Ca^{2+}-H^{+} antiporters driven by proton-motive forces (Sanders *et al.*, 2002). This system of pumps and antiporters provide the homeostatic conditions by which Ca^{2+} releasing channels function transiently in order to momentarily elevate cytosolic free Ca^{2+} levels (Sanders *et al.*, 1999).

There are three channel families that are thought to contribute to this transient release of Ca^{2+} in plants (Ward *et al.*, 2009). The smallest is the Two-Pore Channel (TPC) family of which the *A. thaliana* genome contains one member, TPC1. This protein is predicted to form voltage gated homodimers, where each sub-unit has 12 transmembrane domains and 2 pore domains (Peiter *et al.*, 2005). TPC1 is localized to the vacuolar membrane where it is thought to facilitate Ca^{2+} fluxes into the cytosol (Peiter *et al.*, 2005; Pottosin *et al.*, 2009). Next is a much larger channel family, the Glutamate Receptor-like (GLR) channels, which in *A. thaliana* is comprised of 20 members. Unlike TPC1, GLR channels are thought to function as tetramers and each subunit has 3 transmembrane domains and 1 pore loop (Davenport, 2002; Jammes *et al.,* 2011). Plant GLR channels are thought to be plasma membrane localized where they non-selectively channel ions (Jammes *et al.,* 2011) (Figure 1.1).

Figure 1.1
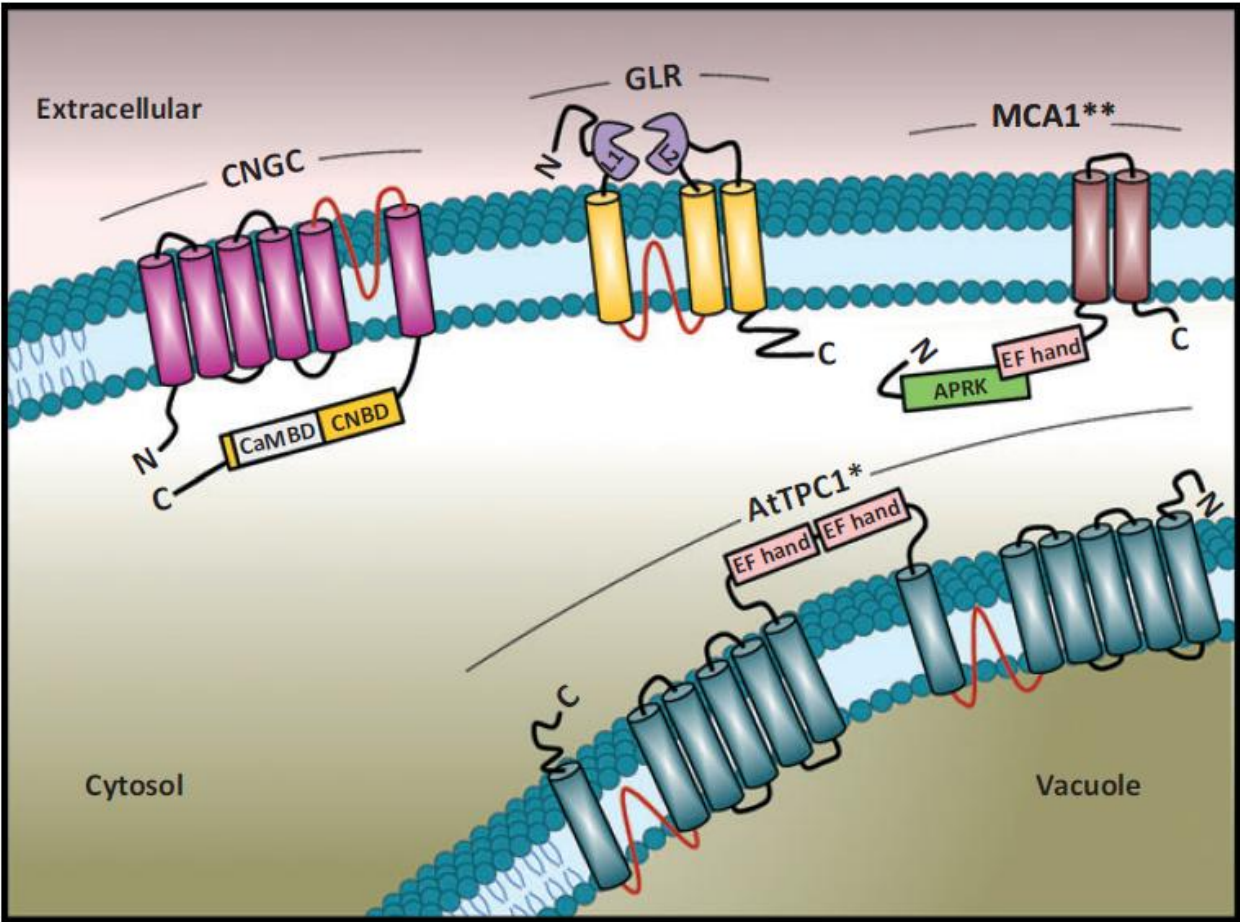
Figure 1.1: Subcellular localization and predicted transmembrane topology of three major families of Ca^{2+}-permeable channels in plants: TPC, GLRs and CNGCs. The *A. thaliana* two-pore channel (AtTPC1) has been predicted to have 12 transmembrane helices and two pores (red lines). A cytosolic loop contains two Ca^{2+} binding EF hands. Glutamate Receptor-like channels (GLRs) are proposed to have three transmembrane domains, a pore-forming domain (red line) and two ligand binding domains L1 and L2 facing the extracellular space. Cyclic nucleotide-gated channels (CNGCs) contain six transmembrane domains with the pore region (red line) located between the fifth and sixth domains. The cyclic nucleotide binding domain (CNBD) overlaps with the calmodulin binding domain (CaMBD). *AtTPC1 has been reported to be localized in the *A. thaliana* tonoplast, whereas other TPCs from different plant species have been reported to be localized to the plasma membrane in heterologous expression systems. Also, the mechanosensitive channel named MCA1 is predicted to have two transmembrane domains. **The prediction of the transmembrane topology of MCA1 is still preliminary (Adapted from Jammes *et al.,* 2011).

The last family is the cyclic nucleotide-gated channel (CNGC) family which is the focus of this thesis work.

Plant and animal CNGCs are members of the super-family of voltage gated ion channels. This super-family also includes the hyperpolarization-activated and cyclic nucleotide-gated pacemaker channels (HCN), the ether-a-gogo (eag) and human eag-related gene family (hERG) of voltage-activated K^+ channels, and several plant K^+ channels that are often referred to as K^+ transporters of *A. thaliana* (KAT) or *A. thaliana* K^+ transporter (AKT) (Kaupp and Seifert, 2002). Members of this super-family share a common structure with 6 membrane-spanning segments designated S1-S6, a pore region between S5 and S6 which is followed by cyclic nucleotide monophosphates (cNMPs) binding domain (CNBD). In some cases a Calmodulin bidning domain (CaMBD) is also present at the amino (N) (animal CNGCs) and/or carboxy (C) (plant and animal CNGCs) terminus (Zagotta and Siegelbaum, 1996; Bradley *et al.*, 2004; Trudeau and Zagotta, 2003) (Figure 1.2).

1.1.1. Discovery of CNGCs

1.1.1.a. Animal CNGCs

CNGCs were first identified in animal retinal photoreceptors plasma membranes (Fesenko *et al.*, 1985). The rod photoreceptor activation occurs in the dark when cyclic guanosine-3', 5' monophosphate (cGMP) molecules bind to the channel and permit its opening, which leads to a Ca^{2+} ion influx. When light hits the retina, a photo transduction cascade occurs and as a result, cGMP is hydrolysed to GMP.

Figure 1.2
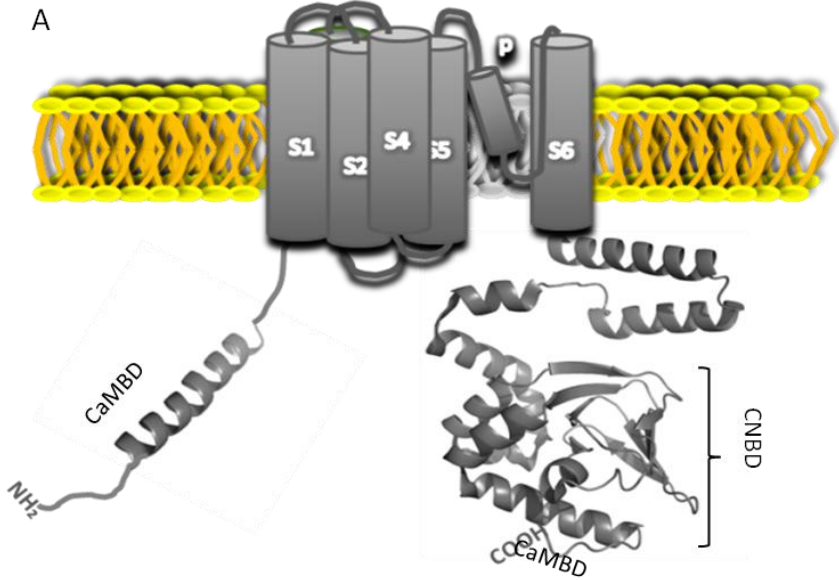
Animal CNGCs (CNGB1b)
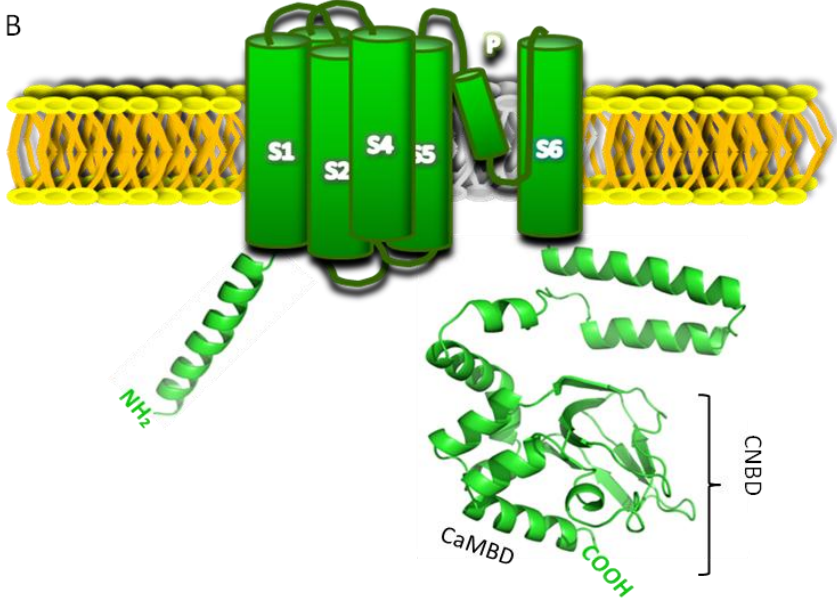
Plant CNGCs

Figure 1.2: The predicted membrane topology and domain structures of a (A) animal and (B) plant CNGC subunits. The N-and C-termini are intracellular and contain domains for channel regulation; a cyclic nucleotide binding domain (CNBD) in the C-terminus and a calmodulin binding domain (CaMBD) in the C- and/or N-terminus of animal CNGCs (CNGB1b is depicted here) and in the C-terminus of plant CNGCs overlapping with the CNBD.

As a response to the decrease of cGMP level in the cell the CNGCs close. The closure of the CNGCs leads to a reduction of the Ca^{2+} level in the cell, which then acts as a negative feedback in the photo transduction cascade (Matulef and Zagotta, 2003).

CNGCs have also been identified in the cone photo receptors and proven to be activated by the same photo transduction cascade that occurs during rod photo receptors activation (Kaupp and Seifert, 2002). CNGCs in both rod and cone photoreceptors are activated by cGMPs, whereas the transduction of odorant signals through olfactory CNGCs is activated by cyclic-3', 5' adenosine monophosphate (cAMP) (Nakamura and Gold, 1987).

CNGCs have also been identified in non-sensory tissues such as liver, kidneys, lungs, olfactory bulbs, testes, spleen and muscles (Zagotta and Siegelbaum, 1996; Kaupp and Seifert, 2002).

A typical mammalian CNGC functions in the form of a heterotetramer, composed of a combination of 2 out of the 6 identified different CNGC subunits; namely CNGA1-CNGA4, CNGB1, and CNGB3. The CNGAs are considered to be the principle subunits (α subunits) as they are able to form functional channels on their own, while the CNGBs are considered to be modulatory subunits (β subunits) as they contribute to the properties of the functional heterotetramer (Dhallan *et al.*, 1990; Weyand *et al.*, 1994; Liman and Buck, 1994; Korschen *et al.*, 1995; Kaupp *et al.*, 1998; Kaupp and Seifert, 2002).

Depending on the tissue, the CNGC heterotetramer is composed of a unique combination of the subunits. For instance, the rod cells CNGCs are composed of

CNGA1 and CNGB1 (Chen *et al.*, 1994; Korschen *et al.*, 1995), while in the cone cells they are composed of CNGA3 and CNGB3 (Bonigk *et al.*, 1999; Gerstner *et al.*, 2000).

Mutations in the rod and cone or olfactory channels cause different kinds of blindness or a loss of odorant signalling, respectively. For example, mutation of the rod channel CNGA1 can cause a degenerative form of blindness in humans (Dryja *et al.*, 1995), whereas mutations in the cone channels CNGA3 and CNGB3 cause complete achromatopsia (total colour blindness) (Kohl *et al.*, 1998, 2000; Sundin *et al.*, 2000; Wissinger *et al.*, 2001). On the other hand, in olfactory neurons, CNGA2 knockout mouse loses the ability to smell (Brunet *et al.*, 1996).

1.1.1.b. Plant CNGCs

The first plant CNGC, *Hordeum vulgare* calmodulin binding transporter 1 (HvCBT1), was identified from barley through a screen for proteins that are able to bind *A. thaliana* calmodulin 2 (AtCaM2) (Schuurink *et al.*, 1998). In this study, an enzyme-linked protein-protein interaction was used to screen a barley aleurone cDNA expression library. This was followed by the identification and cloning of two *A. thaliana* CNGCs, *AtCNGC1* and *2* (Köhler and Neuhaus, 1998). Shortly after, Arazi *et al.* (1999) has identified tobacco CNGC, NtCBP4 (*Nicotiana tabacum* calmodulin binding protein 4), and Köhler *et al.* (1999) identified four more *A. thaliana* CNGCs, *AtCNGC3 – 6*. In 2000, the *A. thaliana* genome sequence became available and the sequence data revealed total of 20 members in *A. thaliana* CNGCs (Mäser *et al.* 2001).

The overall sequence similarity of *A. thaliana* CNGCs ranged from 55% to 83%, and based on their predicted amino acid sequences they were classified into 4 groups:

groups I, II, and III are closely related, while group IV, which can be further subdivided into 2 subgroups. They are distantly related to the other groups as well as to one another (Mäser *et al.*, 2001) (Figure 1.3).

Possible biological functions of group I and group IVB members have been reported (Köhler *et al.*, 2001; Sunkar *et al.,* 2000; Balague *et al.*, 2003; Chan *et al.*, 2003; Li *et al.*, 2005; Ma *et al.*, 2006; Gobert *et al.*, 2006; Yoshioka *et al.*, 2006; Borsics *et al.*, 2007). AtCNGC10 was reported to play an important role in plant development, particularly in root growth, while AtCNGC1 has been shown to participate in heavy metal movement (Sunkar *et al.*, 2000; Ma *et al.*, 2006; Borsics *et al.,* 2007; Christopher *et al.*, 2007). AtCNGC3 has been shown to be involved in the uptake and translocation of K^+ and Na^+ and may be necessary to maintain homeostasis of these ions (Gobert *et al.*, 2006; Balague *et al.*, 2003). Also, *AtCNGC11* and *12* KO mutant plants exhibited decreased resistance to an avirulent isolate of the oomycete pathogen *Hyaloperonospora arabidopsidis* as well as avirulent strains of the bacterial pathogen *Pseudomonas syringae*, indicating a role for these two channels in pathogen defence (Yoshioka *et al.*, 2006; Moeder *et al.*, 2011).

AtCNGC2 and AtCNGC4 of the group IVB share significant similarity in their sequences. Loss of function mutants of *AtCNGC2* and *AtCNGC4,* namely *dnd1* (*defence no death* 1) and *dnd2/hlm1* (*defence no death 2/hypersensitive response-like lesion mimic 1)* respectively, exhibit constitutive disease resistance responses such as expression of *pathogenesis-related* (*PR*) genes, elevated levels of salicylic acid (SA) and hypersensitive response (HR) like spontaneous cell death (Clough *et al.* 2000; Balagué *et al.* 2003; Jurkowski *et al.* 2004). The barley necrotic locus *nec1* mutant,

Figure 1.3
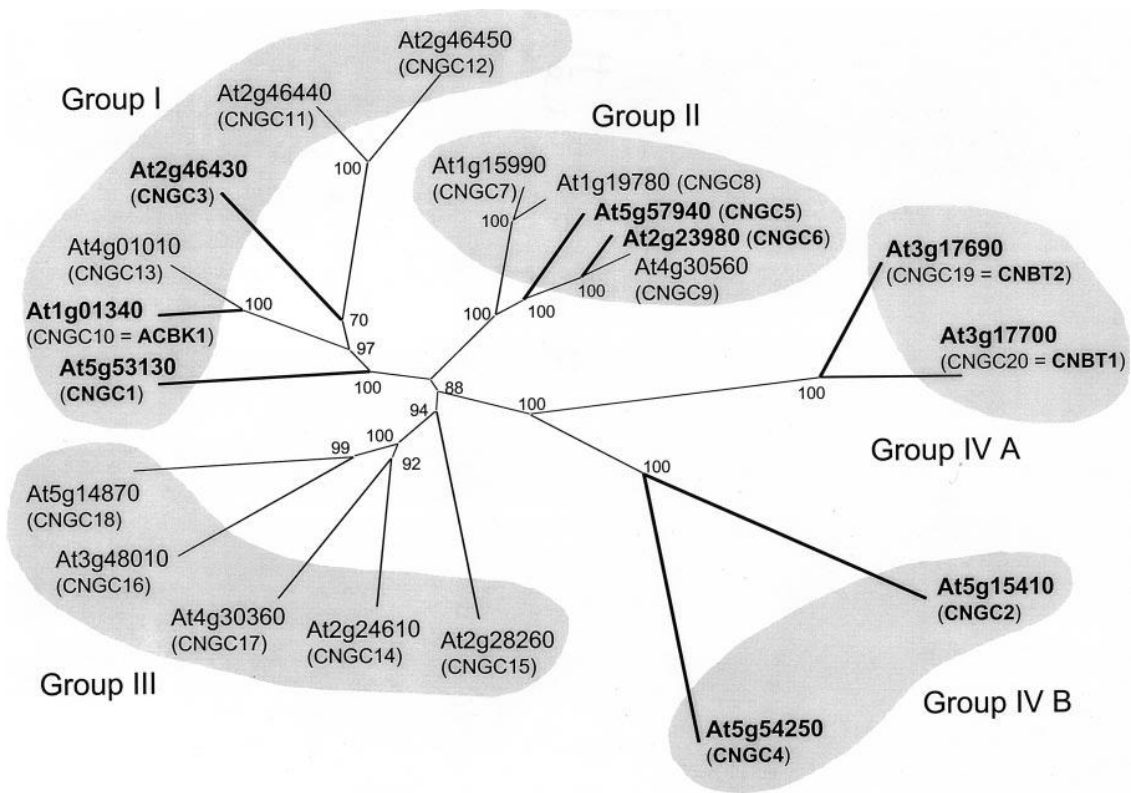
Figure 1.3: Phylogenetic tree using protein sequences of the twenty members of the *A. thaliana* CNGC family. The twenty members are organized into five groups (I-IVB) based on sequence similarity. (Adapted from Mäser *et al.,* 2001).

which shows spontaneous necrotic lesions, has a mutation in the barley homolog of *AtCNGC4* (Rostoks *et al.* 2006).

1.1.1.c. *cpr22* and AtCNGC11/12

Following these findings, Yoshioka *et al.* (2001, 2006) identified the *A. thaliana* mutant *cpr22* (*constitutive expresser of PR genes* 22) that is generated by a 3 kb genomic deletion that fuses the 5' half of *AtCNGC11* and the 3' half of *AtCNGC12* resulting in the chimeric *AtCNGC11/12* gene. *cpr22* exhibits multiple resistance responses without pathogen infection similar to *dnd1* and *dnd2/hlm1* in the hemizygous state and conditional lethality in the homozygous state (Yoshioka *et al.*, 2001). Interestingly, relatively high temperature (28°C) and high humidity (>95%RH) can rescue the lethality of homozygous *cpr22* mutant plants and also related phenotypes in *cpr22* hemizygous mutant plants (Yoshioka *et al.*, 2001; Mosher *et al.*, 2010) (Figure 1.4).

Similarity of phenotypes in *dnd1*, *dnd2/hlm1* and *cpr22* strongly suggested the involvement of AtCNGCs in defence responses. Those phenotypes are induced by the expression of *AtCNGC11/12* in *cpr22* and the absence of *AtCGNC2* and *4* in *dnd1* and *dnd2/hlm1*, respectively. This suggests that a precise cation signal/homeostasis is required to activate defence responses and there may be an intriguing relationship between these four CNGCs.

It has been shown that the phenotype of *cpr22* is caused by the expression of the chimeric *AtCNGC11/12* rather than the absence of either wild type *AtCNGC11* or *12* (Yoshioka *et al.*, 2006). Baxter *et al.* (2008) further reported the requirement of

functionally active AtCNGC11/12 for the *cpr22* phenotype. Although yeast complementation assay showed that AtCNGC11/12 functions Ca^{2+} and K^+ channels (Yoshioka *et al.*, 2006; Baxter *et al.*, 2008; Chin *et al.*, 2010), only the Ca^{2+} channel blockers Gd^{3+} and La^{3+}, but not the K^+ channel blocker tetraethylammonium chloride (TEA), suppress AtCNGC11/12-induced HR-like cell death *in planta* (Urquhart *et al.*, 2007). This suggests that Ca^{2+} influx is involved in AtCNGC11/12-mediated HR-like cell death formation. This result was further supported by a non-biased chemical screen identifying Ca^{2+} channel blockers but not K^+ channel blockers to suppress *cpr22*-related lethality (Abdel-Hamid *et al.,* 2011).

1.1.2. Ion selectivity of CNGCs

Animal CNGCs are strongly selective for cations over anions, and are permeable to monovalent cations as well as Ca^{2+} (Kaupp and Seifert, 2002). The permeability ratios vary between organisms and even tissues within the same organism. For instance, rod CNGCs are most permeable to Li^+, cone ones are most permeable to K^+, while olfactory CNGCs are most permeable to Na^+ (Menini, 1990; Picones and Korenbort, 1992; Frings *et al.*, 1992).

Permeability of CNGCs to Ca^{2+} was found to negatively affect the current of monovalent cations across them because Ca^{2+} must bind to an internal site on the pore region of the channel before it can pass through, which blocks the flow of other cations (Kaupp and Seifert, 2002). The glutamate residue inside of the pore region has been reported to be responsible for Ca^{2+} binding. Replacement of this residue with a neutral residue resulted in suppression of both, Ca^{2+} binding and blocking of the flow of the monovalent cations. Furthermore, when this glutamate was replaced to another

negatively charged residue, aspartic acid, Ca^{2+} binding affinity was enhanced (Eismann *et al.*, 1994; Gavazzo *et al.*, 2000; Root and MacKinnon, 1993; Park and MacKinnon, 1995; Seifert *et al.*, 1999).

Unlike animal CNGCs, the ion selectivity of plant CNGCs has hardly been characterized. So far, two main approaches have been used to study the permeability of AtCNGCs: electrophysiological studies and heterologous expression of the CNGCs in ion uptake deficient mutants in yeast (*Saccharomyces cerevisiae*) and *E. coli* (*Escherichia coli*) (Chin *et al.*, 2009).

AtCNGC2 was found to be permeable for the monovalent cations $K^+ > Li^+ \approx Rb^+ \approx Cs^+ > Na^+$ (Leng *et al.,* 1999, 2002). The higher affinity to K^+ over Na^+ was linked to the presence of specific amino acids (N416, D417) in the pore domain (Hua *et al.*, 2003). In addition, it was found that Ca^{2+} blocks channel function and reduces its permeability for monovalent cations (Leng *et al.*, 2002).

Further functional studies have been reported regarding AtCNGC4, AtCNCG1, and AtCNGC10. *Xenopus laevis* oocytes expressing AtCNGC4 were assessed electrophysiologically, and AtCNGC4 was demonstrated to be equivalently permeable to K^+ and Na^+ (Balagué *et al.*, 2003). A similar result was demonstrated for AtCNGC1 by electrophysiological studies in human embryonic embryonic kidney (HEK293) cells (Hua *et al.*, 2003). AtCNGC10 could conduct an inward current of K^+ when expressed in HEK293 cells (Christopher *et al.*, 2007). To date, characterization of plant CNGCs by electrophysiological methods has only been performed for the above mentioned subunits. One of the reasons is the instability of the expression of plant CNGCs in such heterologous systems (Leng *et al.*, 1999; Balagué *et al.*, 2003).

Figure 1.4

A

Ws-wt   cpr22

Morphology

HR

Bar = 50µM

B

Ws-wt   cpr22

PR-1

rRNA

C

Ws-wt   cpr22

Resistance
phenotype
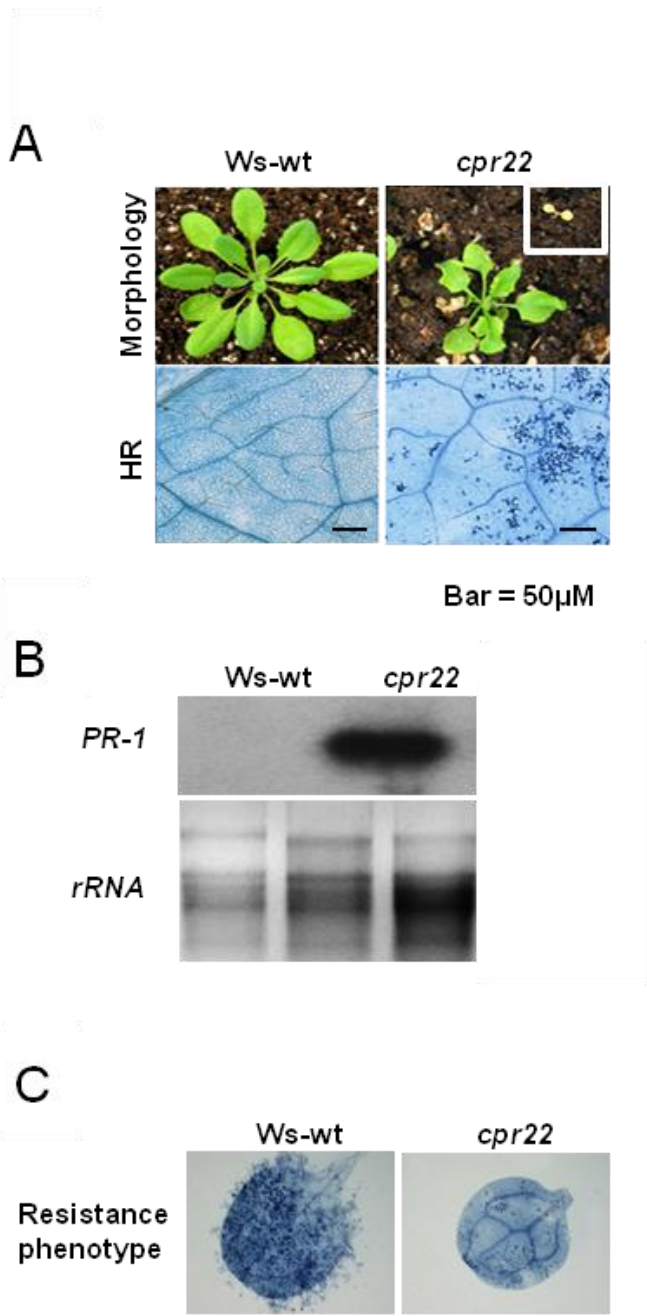
Figure 1.4: Characterization of *cpr22*. (A) Morphological phenotypes and spontaneous HR cell death formation of wild type (Ws-wt) and *cpr22*. A *cpr22* homozygous plant is shown in the white square. (B) Northern blot analysis for *PR-1* gene expression in Ws-wt and *cpr22*. Ethidium bromide staining of ribosomal RNA (rRNA; lower panel) served as a loading control. (C) Growth of *Hyaloperonospora arabidopsidis*, isolate Emwa1 in Ws-wt and *cpr22*. The Trypan blue analysis was done to visualize pathogen growth. (Adapted from Chin *et al.,* 2010).

Table 1.1: Ion selectivities and physiological roles identified in plant CNGCs.*

Gene	Gene ID	Ion selectivity	Suggested physiological role	Reference
Arabidopsis thaliana				
AtCNGC1	AT5G53130	K^+, Na^+, Ca^{2+}, Pb^{2+}	Cation uptake from soil	Hua _et al._ 2003a; Mercier _et al._ 2004
			Heavy metal uptake	Sunkar _et al._ 2000; Ali _et al._ 2005
AtCNGC2	AT5G15410	K^+, Ca^{2+}, Li^{2+}, Cs^+, Rb^+	Developmental cell death and senescence	Leng _et al._ 1999, 2002; ercier _et al._ 2004
			Growth and development	Ko¨hler _et al._ 2001; Chan _et al._ 2003
			Thermal sensing and acquired thermotolerance	Finka _et al._ 2012
			Pathogen resistance	Ali _et al._ 2007; Clough _et al._ 2000
AtCNGC3	AT2G46430	K^+, Na^+	Distribute and translocate ions from xylem	Gobert _et al._ 2006
AtCNGC4	AT5G54250	K^+, Na^+	Pathogen resistance	Mercier et al. 2004; Balague´ _et al._2003; Jurkowski _et al._ 2004
AtCNGC10	AT1G01340	K^+, Ca^{2+}, Mg^{2+}	Light modulated development	Li _et al._ 2005; Borsics _et al._ 2007;Christopher _et al._ 2007; Guo _et al._ 2010
AtCNGC11	AT2G46440	K^+, Ca^{2+}	Pathogen resistance	Yoshioka _et al._ 2006; Urquhart _et al._ 2007
			Gravitropic bending and dark-induced senescence	Urquhart _et al._ 2011
AtCNGC12	AT2G46450	K^+, Ca^{2+}	Pathogen resistance	Yoshioka _et al._ 2006; Urquhart _et al._ 2007
			Gravitropic bending and dark-induced senescence	Urquhart _et al._ 2011
AtCNGC18	AT5G14870	Ca^{2+}	Polarized pollen tube growth	Frietsch _et al._ 2007
Nicotiana tabacum				
NtCPB4	AF079872	Pb^{2+}	Heavy metal uptake	Arazi _et al._ 1999
Hordeum vulgare				
HvCBT1	AJ002610	Unknown	Ion transport in aleurone	Schuurink _et al._ 1998
NEC1	AY972627	Unknown	Pathogen resistance	Rostoks _et al._ 2006

Modified from Chin _et al.,_ 2009

An alternative assay for assessing channel permeability is the complementation of ion uptake deficient yeast or *E. coli* mutants through the heterologous expression of *CNGCs.* A number of AtCNGCs have been characterized by this way. Köhler *et al.* (1999) reported that both AtCNGC1 and 2 were able to partially rescue the growth of the K^+ uptake deficient yeast mutant, CY162, which lacks two major K^+ transporters, *TRK1* and *TRK2*. This mutant cannot survive in low-K^+ media (Ko and Gaber, 1991). Similar approcach has been taken using Ca2+ yeast mutant (R). Heterologous expression studies of plant CNGCs in such mutants are summarized in Table 1.1 (modified from Chin *et al.*, 2009).

There is some debate on how well these heterologous expression systems reflect the *in vivo* function of these channels. Therefore, careful interpretation and further assessment is required (Kaplan *et al.*, 2007).

1.2. Structure of CNGCs

1.2.1. Structure-function analysis of Animal CNGCs

The structure of the cytoplasmic C-terminal region of animal CNGCs, including the CNBD and the C-linker domains of hyperpolarization-activated cyclic-nucleotide gated channel 2 (HCN2) and sea urchin SpIH1 channel, has been solved by X-ray crystallography (Zagotta *et al.* 2003; Flynn *et al.*, 2007). The HCN channels belong to a super-family of voltage-gated channels that play an essential role in conducting electrical signals involved in cardiac and neuronal pacemaker activities in animals (Zagotta *et al.*, 2003). In addition, these channels are similar to those of the CNGC, eag- (ether a go-go), and KAT1-related Shaker-type K^+ channels (Zagotta and

Siegelbaum, 1996; Bruggemann *et al.,* 1993; Hoshi *et al,* 1995; Zagotta *et al.* 2003). The C-terminal region of both SpIH1 and HCN2 has a tetrameric configuration.

The C-linker is composed of six α-helices and the CNBD is composed of four α-helices and a β-roll in which cyclic nucleotides bind and interact with the C-linker (Figure 1.5). The CNBD has a similar fold to that of the *E. coli* catabolite gene activator protein (CAP) and the regulatory domain of the cAMP dependent protein kinase A, indicating the conservation of this structure (Zagotta *et al.* 2003; Flynn *et al.*, 2007). HCN is fully regulated by cAMP although cGMP interactions can occur as well. It was postulated that cAMP binding results in a conformational change in the CNBD, which is then coupled with a conformational change in the C-linker leading to the opening of the channel (Zagotta *et al.* 2003; Flynn *et al.*, 2007) (Figure 1.5). It has been shown that CNGCs are likely to function as heterotetramers in animals (Craven and Zagotta 2006; Flynn *et al.*, 2007), but whether this also is true in plants remains to be elucidated.

1.2.1.a. CNBD of animal CNGCs

Many cellular processes have been reported to be regulated by cNMPs. These processes include retinal phototransduction, smooth muscle tone, heart rate and sperm chemotaxis. This regulation by cNMPs is carried out by direct binding to a variety of effector proteins. Examples of these effector proteins are kinase A, ion channels, transcription factors, and the Rap guanine nucleotide-exchange proteins (Baruscotti and Difrancesco, 2004; Biel *et al.*, 2002; Pape, 1996; Robinson and Siegelbaum, 2003; Flynn *et al.,* 2007).

In general, the CNBD is composed of two subdomains: a roll sub domain and a C-helix subdomain. The roll subdomain consists of two α-helices: "A-helix" and "B-helix" and between the two helices there are eight β-sheets (β1-β8). Between the sixth and the seventh β-sheets there is a short "P-loop". The C-helix subdomain is a single α-helix located in the end of the CNBD (Figure 1.5).

The reported crystal structure and electrophysiological analysis for both HCN2 and SpIH1 suggested that cNMPs (cAMP or cGMP) bind inside of the β-roll before they interact with the C-helix, where cGMP binds to the syn conformation, in contrast to the anti-configuration seen with cAMP (Zagotta *et al.* 2003; Flynn *et al.*, 2007). Mammalian CNGCs were found to be activated by cGMP, whereas HCN channels are activated fully by cAMP (full agonist) and partially by cGMP (partial agonist) (Altenhofen *et al.*, 1991, Kumar and Weber, 1992, Scott *et al.*, 1996; Weber *et al.*, 1989, Zagotta *et al.*, 2003, Flynn *et al.,* 2007; Zhou and Siegelbaum*,* 2007). In general, the specificity of binding cGMP over cAMP is coming from a threonine/serine residue in the β-roll and an aspartate residue in the C-helix that stabilize the docking of cGMP in the syn configuration in the CNBD (Figure 1.6).

Figure 1.5
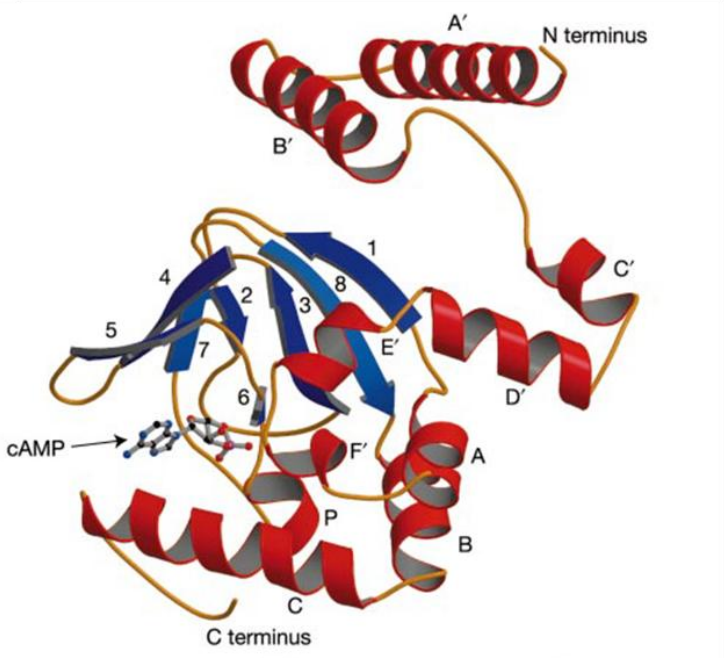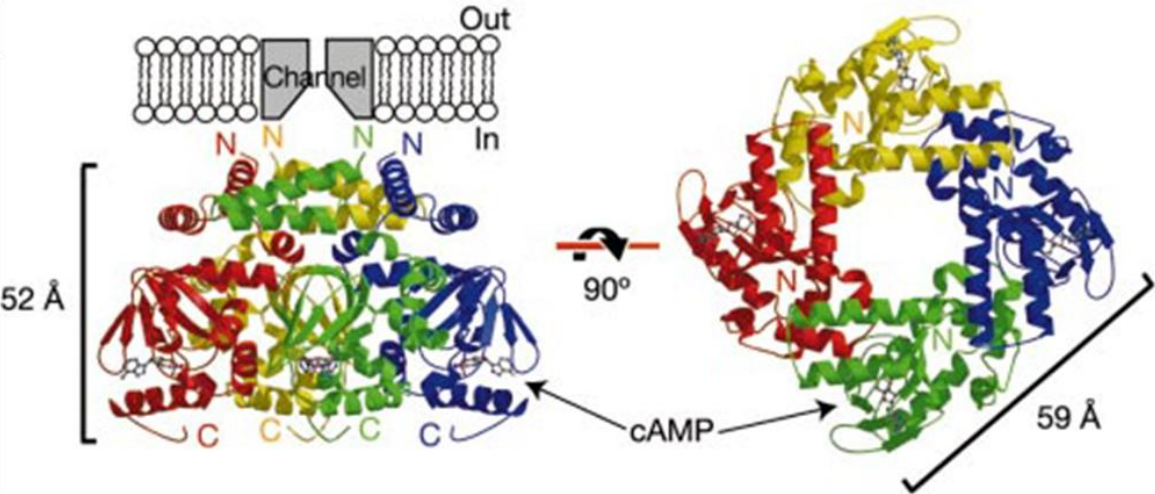
Figure 1.5: Structure of the mouse HCN2 C-linker (six α-helices; A'-F') and CNBD (four α-helices; A, P, B, C with eight β-sheets between A- and B-helices) with cAMP (PDB DI 1Q5O). (A) Ribbon representation of a single protomer of HCN2 with cAMP. (B) HCN2 tetramer viewed perpendicular (left) and parallel (right) to the four-fold axis. Each subunit is shown in a different colour. (Adapted from Zagotta *et al.,* 2003).

Figure 1.6
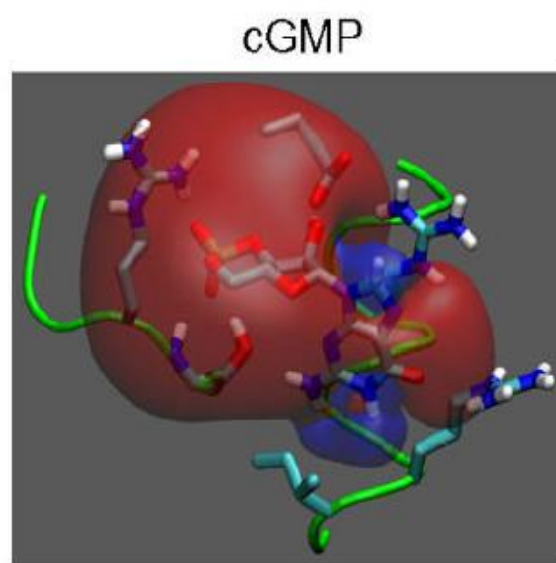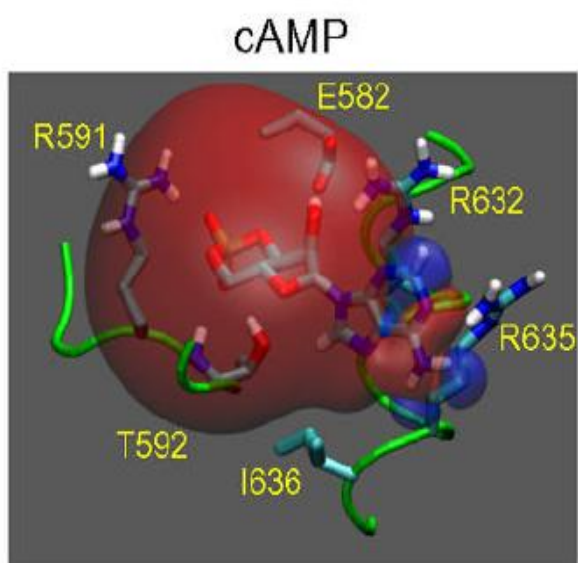
Figure 1.6: Molecular dynamics simulation of the cNMP-bound HCN2 CNBD: The relative positions of cAMP (left) or cGMP (right) and key interacting residues are shown. The colored isosurface shows the cNMP electrostatic potential (red, negative; blue, positive). (Adapted from Zhou and Siegelbaum*, 2007).

1.2.1.b. CaMBD of animal CNGCs

A typical animal CNGC has a minimum of one CaMBD on either the N-terminus (as in CNGA1 and 3), the C-terminus (as in CNGA1 and 4), or on both (as in CNGB1a, 1b, and CNGB3) (Ungerer *et al.,* 2011). Plant CNGCs are suggested to have a slightly different structure, where both CaMBD and CNBD are found in an overlapping region on the C-terminus that extends in the cytosol (Köhler and Neuhaus, 2000; Hua *et al.*, 2003, Figure 1.2).

Animal CNGCs are negatively regulated upon binding to CaM (Zufall *et al.*, 2001; Menini, 1999; Fain *et al,* 2001; Trudeau and Zagotta, 2003). Specific subunit interactions mediate CaM-dependent inhibition in CNGC tetramers. For instance, in olfactory CNGA2 channels, CaM disrupts an interaction between the N- and C-terminal regions upon binding to the N-terminus (Varnum and Zagotta, 1997). A similar disruption occurs between the N- and C- termini of rod CNGB1 and CNGA1 upon CaM binding to the N-terminal region of CNGB1 subunits (Trudeau and Zagotta, 2002, 2003). The precise N- and C-terminal regions that form these interactions in olfactory channels are different from those in rod channels (Trudeau and Zagotta, 2003).

1.2.1.c. Pore domain of animal CNGCs

CNGCs form as tetramers with each subunit containing six putative transmembrane segments (S1-S6), a pore region and cytoplasmic amino and carboxyl termini. The pore domain connects the S5 and S6 segments of the transmembrane domain, forming a loop that extends toward the central axis of the channel (Figure 1.2, Sun *et al.*, 1996; Becchetti *et al.*, 1999; Wang *et al.*, 2007). Although residues in the S4–

S5 loop and in the S5 and S6 transmembrane segments affect ion conduction, the pore region is the major determinant of ion selectivity in CNGCs (Giorgetti *et al.*, 2005; Becchetti *et al.*, 1999). Moreover, these regions (S5 and S6) determine the pore diameter of animal CNGCs (Sun *et al.*, 1996). The center of the iris forms a short, narrow region of the pore that serves as the selectivity filter. Since the channel must contain a gate to prevent ion permeation in the closed state, the pore region itself, in addition to forming the ion selectivity filter, must function as the channel gate, the structure of which changes when the channel opens (Wang *et al.*, 2007; Biel *et al*, 2009).

1.2.2. Plant CNGCs

1.2.2.a. Structure of plant CNGCs

The overall structure of plant CNGCs is similar to that of animal CNGCs. The only predicted difference is the location of CaMBD. It has been suggested that the CaMBD is located at the αC-helix of the CNBD in tobacco CNGC, NtCBP4 as well as *A. thaliana* AtCNGC1 and AtCNGC2 (Köhler *et al.*, 1999; Arazi *et al.*, 2000; Köhler and Neuhaus, 2000). A conditional suppressor of AtCNGC11/12 (*cpr22*), S58, was found to contain a mutation in the putative CaMBD (Chin *et al.*, 2010; Abdel-Hamid *et al*, 2010) (Figure 1.7). This indicates the importance of CaM in the regulation of plant CNGCs. So far, little is known about the molecular mechanism of the regulation of CNGCs by CaM in plants (Hua *et al.*, 2003; Bridges *et al.*, 2005; Kaplan *et al.*, 2007; Chin *et al.*, 2010).

No complete crystal structure of a plant CNGC has been reported so far. The CNBD of AtCNGC2, however, has been modeled (Hua *et al.*, 2003*b*). Using the

previously solved structure of the cAMP dependent protein kinase A, RIa, it was shown that cAMP resides in the β barrel in the syn-conformation in AtCNGC2 which is remarkably different from the anti-conformation seen in animals (Hua *et al.* 2003*b*; Zagotta *et al.* 2003; Flynn *et al.*, 2007).

Different plant CNGC subunits were shown to exhibit different cNMP selectivity. For example, electrophysiological studies shown that AtCNGC4 is activated by cGMP more strongly than by cAMP (Balagué *et al.*, 2003), while AtCNGC2 is activated to a similar extent by both cAMP and cGMP (Leng *et al.*, 1999, Leng *et al.*, 2002). AtCNGC11/12 and AtCNGC12 complement K^+-deficient yeast mutant more effectively in the presence of cAMP than cGMP, indicating that they are activated by cAMP more efficiently than by cGMP (Yoshioka *et al.*, 2006).

Baxter *et al.* (2008) and Chin *et al.* (2010) identified functionally important amino acids of AtCNGC12 and/or AtCNGC11/12 by a genetic screen for suppressor mutants of *cpr22* (*AtCNGC11/12*). Computational modelling and *in vitro* cAMP-binding assays indicated that E519 in the CNBD of AtCNGC11/12(12) is a key residue for the structural stability and functionality of AtCNGCs through the interaction of the C-linker and the CNBD (Baxter *et al.* 2008). E519, which is conserved among AtCNGCs, aligns well to Y573 in human CNGA3, where a mutation in this residue causes achromatopsia in human (Wissinger *et al.* 2001), suggesting that this amino acid position plays a functionally important role for CNGCs in general. On the other hand, Chin *et al.* (2010) reported that R557, located in the αC-helix of the CNBD, is important in the regulation of the channel, where the αC-helix is predicted to contain the CaMBD as well (Figure 1.7).

Figure 1.7
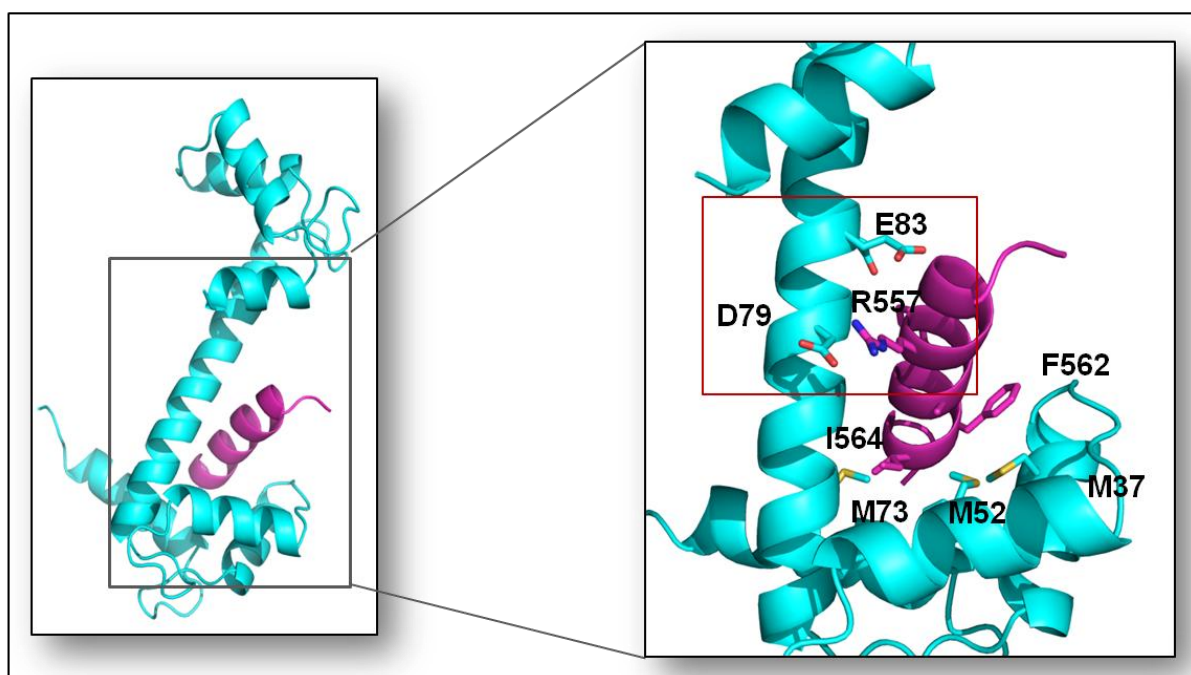
Figure 1.7: Computational modeling of CaM binding with CNBD αC-helix of AtCNGC12. Modeling of the tertiary structure of AtCaM1, and the αC-helix of AtCNGC12 was conducted using the crystal structures of the potato CaM, PCM 6 (PDB# 1RFJ) and the cytoplasmic C-terminus of the invertebrate CNGC, SpIH (Flynn *et al.* 2007, PDB# 2PTM), respectively, as templates. The protein fold recognition server (Phyre) was used to model these proteins. The binding modeling was performed using an algorithm for molecular docking (PatchDock). The images were generated using PyMOL. CaM is colored in cyan and the αC-helix is shown in magenta. Left panel: overall binding model between AtCaM1 and AtCNGC12, Right panel: close up of the boxed area of the left panel in AtCNGC12, M73, M52 and M37 of AtCaM1 create a hydrophobic pocket together with F562 and I564 of AtCNGC12, which is a typical binding configuration between CaM and target proteins. R557 (Chin *et al.,* 2010) creates salt bridges with both D79 and E83. (Adapted from Abdel-Hamid *et al.*, 2010).

1.3. Research objectives

The main objective of my doctoral thesis is to better understand the structure-function relationship of plant CNGCs with an emphasis on the characterization of subunit interactions, CaM binding and cNMP selectivity. I hypothesized that the constitutive active AtCNGC11/12 can be used as a tool to achieve this main objective. There are a number of attributes that make AtCNGC11/12 an excellent model for structure-function analysis. It is thought to be a constitutively active channel that induces a number of measurable phenotypes in the well characterized *Arabidopsis* mutant *cpr22*. These morphological phenotypes make it possible to perform suppressor screens to identify intragenic mutations that affect channel function and regulation. Indeed, this approach has been used in the past in our laboratory, but without extensive biochemical and biophysical analysis to validate these mutants.

In this study, I extended these past studies with an in depth experimental validation. I analyzed a total of eleven intragenic suppressor mutants of *cpr22* by computational modeling and generated various hypotheses regarding the structure-function relationship of specific mutants. These hypotheses were then verified by molecular and biochemical analyses. I also utilized *in silico* analyses to identify putative CaMBDs and the predictions were experimentally confirmed by biophysical analyses. Finally, the preference of cNMP binding of specific AtCNGCs was predicted by computational modeling and was also validated experimentally.

Thus, this thesis work was conducted using a combination of genetics, various biochemical and biophysical analyses, and computational modeling to expand our current knowledge of plant CNGCs.

Chapter 2

Materials and Methods

2.1. Plant Growth condition

Arabidopsis thaliana plants were grown on Pro-Mix soil (Premier Horticulture Inc., Red Hill, PA, USA) in a growth chamber under ambient humidity as described by Silva *et al*. (1999). *Nicotiana benthamiana* plants were grown on the same soil in a growth chamber under a 9:15 h light: 14:45h dark regime at 22°C (day) and 20°C (night) with 65% humidity.

2.2. Suppressor screening and identification of the S35, S83, S100, S135, S137 and S144 mutants

Approximately 10,000 *cpr22* homozygous M0 seeds were mutagenized with 0.3% (v/v) EMS solution (Sigma-Aldrich®, http:// www.sigmaaldrich.com/) for 8h at room temperature, followed by rinsing more than 15 times in water. The M0 seeds were grown under high humidity (RH >90%) to obtain M1 plants. The M2 seeds were collected and then screened for suppressor mutants under normal humidity.

2.3. *Agrobacterium*-mediated transient expression

Agrobacterium-mediated transient expression in *Nicotinana benthamiana* was performed as described by Urquhart *et al*. (2007). The expression of these genes was confirmed by semi-quantitative RT-PCR (see 2.13.5) and confocal microscopy (see 2.7).

2.4. Ion leakage analysis and trypan blue staining for cell death detection

For ion leakage analysis, 4 leaf discs (0.5 cm) were floated in 5 ml of distilled water. After 15 min the conductivity was determined using an Oakton Con5 Acorn series conductivity meter (Oakton Instruments, Vermont Hills, USA). Trypan blue staining was performed as described previously (Yoshioka *et al.*, 2001).

2.5. Plasmid construction and site direct mutagenesis

For constructions of pYES-AtCNGC11/12:R372W, pYES-AtCNGC11/12:D408N, pYES-AtCNGC11/12:E359K, pYES-AtCNGC11/12:D364N pYES2-AtCNGC12:G459R and pYES2-AtCNGC12:R381H, total RNA was extracted from suppressors S135, S144, S35, S83, S100 and S137, respectively, and cDNA was generated. Cloning of the genes of interest from cDNAs into pYES2 was performed as described previously for S58 in Chin *et al.* (2010). For site-directed mutagenesis, D433S and E412L, were created in the AtCNGC11/12 cDNA in pBluescript (Stratagene, La Jolla, CA, USA) as described previously (Baxter *et al.*, 2008) using the QuikChange site-directed mutagenesis kit (Stratagene, La Jolla, CA, USA) according to the manufacturer's instructions. Primer sequences used for cloning and site-direct mutagenesis are listed in Appendix, Table 1. All constructed plasmids were sequenced for fidelity.

For protein expression, the portions from the beginning of the C-linker to the end of the CNBD (T1048-G1708) of the cDNA of AtCNGC11/12, AtCNGC11/12:R381H, AtCNGC11/12:G459D, AtCNGC11/12:D433S and AtCNGC11/12:E412L were subcloned into the BamHI–NheI sites of the *E. coli* expression vector, modified-pET28, which contains a his-tag in the C-terminus. This vector was provided by the Christendat

laboratory, Department of Cell and System Biology, University of Toronto (Novagen, http:// www.emdbiosciences.com/html/NVG/home.html) All constructed plasmids were sequenced for fidelity and transformed into *the E. coli* strain BL21 (DE3 codon plus).

2.6. Functional complementation in yeast

The K$^+$ uptake-deficient yeast strain RGY516 (*trk1, 2*) was transformed with the yeast expression vector, pYES2 (empty vector) and pYES2 containing AtCNGC11/12, AtCNGC11/12:R381H, AtCNGC11/12:R372W, AtCNGC11/12:D408N, AtCNGC11/12:E359K, AtCNGC11/12:D364N and AtCNGC11/12:G459R. Overnight cultures were grown in an ampicillin selective synthetic complete (SC) medium supplemented with 100mM KCl. Cultures were then washed 5 times with sterile water prior to inoculation. Growth assays were performed by inoculating transformed RGY516 yeast in 3 ml of arginine, phosphoric acid, glucose (APG) medium (10mM arginine, 8mM phosphoric acid, 2% glucose, 2mM MgSO$_4$, 1mM KCl, 0.2mM CaCl$_2$, trace minerals/elements, vitamins; pH 3.2) in sterile 12-well-plates supplemented with 15 mM K$^+$. Yeast growth at 30°C was monitored by measuring OD600 at 24, 48 and 72 hours (Ali *et al.*, 2006).

2.7. Green fluorescence protein (GFP) visualization by confocal microscopy

Agrobacterium-mediated transient expression *in N. benthamiana* was performed as described in Urquhart *et al.* (2007) at 22°C, and protein expression was confirmed by monitoring the expression of green fluorescence protein (GFP) which was fused at the C-terminal of each protein at 30h post infiltration of *Agrobacterium*. Sections of the

infiltrated area were excised and used for confocal microscopy. Confocal fluorescence images were acquired using a Leica TCS SP5 confocal system with AOBS® (HCS PL APO CS 403 immersion oil objective; NA, 1.25) with the AOTF for the argon laser (488 nm) set at 35% and the detection window at 500–600 nm (Leica Microsystems Inc., Wetzlar, Germany).

2.8. Computational modeling and sequence alignment

The tertiary structure modeling of AtCNGC11/12 was conducted as described previously (Baxter *et al.*, 2008). In this study, the crystallized structure of the cytoplasmic C-terminus of both SpIH (Flynn *et al.*, 2007, PDB ID 2PTM) and HCN2 (Zagotta *et al*, 2003 PDB DI 1Q5O) were used. The protein fold recognition server (Phyre; Kelley and Sternberg, 2009) as well as SWISSMODEL (Schwede *et al.*, 2003) were used to model the protein coordinates with an estimated precision of 100%. The homotetramer structures modeling of the C-terminus of AtCNGC11/12, AtCNGC2, AtCNGC4 and CNGA3 were conducted using SymmDock (Prediction of Complexes with Cn Symmetry by Geometry Based Docking, http://bioinfo3d.cs.tau.ac.il/SymmDock/, Schneidman-Duhovny *et. al*, 2005), where the top 20 solution structures were compared to the symmetric unit of the structure of SpIH (Flynn *et al.*, 2007). The symmetry that resembled the SpIH homotetramer was usually in the first 5 top solution structures. The heterotetramer structure modeling of the C-terminus of CNGA3+CNGB3 was conducted the same way using SymmDock, where the homotetramer structure of each subunit was conducted first and compared to the symmetric unit of the structure of SpIH. The heterotetramer was generated manually

using the modeled homotetramers. The superimpositions were generated using DaliLite (Holm and Park, 2000). All the images were generated using PyMOL (DeLano, 2002). No water molecules were assigned in these models, where there were no conserved water molecules detected in the known crystal structures of channels that belong to this family (Flynn *et al*., 2007; Zagotta *et al*, 2003).

The sequence alignments of the amino acid sequences of the 20 *A. thaliana* CNGCs and other ion channels, starting from the beginning of the C-linker to the end of the CNBD, were performed with CLUSTALW (Thompson *et al*., 1994).

2.9. Recombinant protein expression and Fast Protein Liquid Chromatography (FPLC) analysis

Protein expression in BL21 cells was induced by auto-induction as described in Studier (2005). An overnight culture was sub-cultured in the auto-induced medium (Studier 2005) and grown at 37°C for 3hrs and then at 16°C overnight. Proteins were extracted in lysis buffer (150mM NaCl, 50mM TRIS-HCl pH 7.5, 5mM Imidazole, 5% Glycerol and 1% Triton X-100) by sonication with maximum intensity for at least 5 min/1L culture. Subsequently, His-tagged proteins were purified using nickel-nitrilotriacetic acid (Ni-NTA) affinity chromatography.

Fractions were pooled together and concentrated using Amicon Ultra spin columns with a molecular weight cut off of 10,000 Da (Millipore, Bedford, MA, USA) at 2,800 ×g and 4°C. Each 3L bacterial culture gives ~0.2-0.3mg pure protein. The concentrated proteins (~0.3mg/injection) were separated on a HiLoad 16/60 Superdex 200 prep grade column (GE Healthcare) in 150mM NaCl, 50mM TRIS-HCl pH 7.5 at a

flow rate of 1ml/min. The FPLC fractions of the two peaks were pooled separately and concentrated as described above. Proteins were separated on a 12% SDS PAGE gel and immunoblotted using an α-His antibody (Bioshop, Burlington, Canada) at 150V for 30 min as previously described (Baxter *et al.*, 2008).

2.10. Nuclear Magnetic Resonance (NMR) spectroscopy

Four peptides corresponding to predicted CaMBDs were designed. The sequences of these peptides are listed in Appendix, Table 3.

All peptides used in this experiment were synthesized (purification grade <90%) and FPLC and MS analysed by Peptide 2.0 Inc USA. NMR data were collected at 20°C on a 800-MHz Bruker AVANCE II spectrometer, equipped with a 5-mm TCI CryoProbe, and on a four channel Varian Inova 600-MHz spectrometer equipped with z axis pulsed field gradient units and room temperature shielded triple resonance probes using 100μl NMR tubes. Chemical shift assignments were obtained using a 0.2mM ^{15}N -labelled black rat CaM (PDB ID 3CLN, Mal and IKura, 2006). All NMR samples were prepared in a buffer containing 10mM TRIS-HCl (pH 7), 150mM NaCl, 10mM $CaCl_2$, 10% D_2O. Except for the AtCNGC12 C-terminus peptide samples were prepared in 50mM HEPES (pH 5.9), 100mM NaCl, 10mM $CaCl_2$, 10% D_2O. All samples were prepared as a 40μl reaction with a peptide concentration of 0.2mM.

2.11. Tryptophan fluorescence spectroscopy

Fluorescence spectra were recorded on a Shimadzu RF-5301 spectrofluorophotometer at room temperature (Abu-Abed *et al.,* 2004). Tryptophan fluorescence was determined

by titrating AtCaM2 (DeFalco *at al.,* 2010) into samples containing 1.6µM peptide, 10mM TRIS-HCl (pH 7.5), 2mM Ca^{2+}, without or with 2mM EDTA using an excitation wavelength of 295 nm and monitoring emission between 300 and 450 nm. The range of titration used was peptide:CaM=1:(0.1-2.5)

2.12. Protein structural modeling for ligand docking prediction

All models used in the ligands docking were conducted using a stochastic global energy optimization procedure in Internal Coordinate Mechanics (ICM) (Abagyan *et al.,* 1994) with the ICMPro package version 3.7 (MolSoft LLC, San Diego, CA). This procedure consists of three iterative steps: (*a*) random conformational change of a dihedral angle according to the biased probability Monte Carlo method (Abagyan *et al.,* 1994), (*b*) local minimization of all free dihedral angles, and (*c*) acceptance or rejection of the new conformation based on the Metropolis criterion at the simulation temperature (usually 600 K) (Metropolis *et al.,* 1953). The initial model of the cytoplasmic C-terminus of AtCNGC12 was generated using the crystallized structure of the cytoplasmic C-terminus of HCN2 (Zagotta *et al*, 2003 PDB DI 1Q5O) as template.

2.13. Protein structural modeling for prediction of the Ligand-Binding Pocket

The ICMPocketFinder function was used to identify the retinal binding pocket in the cytoplasmic C-terminus of AtCNGC12. The algorithm builds a grid map of a binding potential, and the position and size of the ligand-binding pocket were determined based on the construction of equipotential surfaces along those maps

2.14. Computational modeling for ligand docking

The flexible ligand/grid receptor docking methodology was applied as implemented in ICM using an extension of the Empirical Conformational Energy Program for Peptides 3 (ECEPP/3) (Halgren, 1995) force field parameters and Merck Molecular Force Field (MMFF) partial charges (Nemethy *et al.,* 1992). Five potential maps (electrostatic, hydrogen bond, hydrophobic, and two for vander Waals) were calculated, followed by a global optimization of the flexible ligand in the receptor field, (Totrov and Abagyan, 2001) so that both the intramolecular ligand energy and the ligand–receptor interaction energy were optimized during the calculation.

For each ligand (either cAMP or cGMP), the best solution is scored by an empirical scoring function based on its fit into the binding pocket of the receptor (Totrov *et al.,* 2001; Totrov *et al.,* 1999). This score takes into account continuum and discrete electrostatics, and hydrophobic and entropy loss (Totrov *et al.,* 2001).

2.15. Thermal shift cNMP binding assay

Thermal denaturation of the C-terminus of AtCNGC12 and HCN2 (courtesy of Dr. Zagotta, University of Washington) was conducted with varying concentrations of either cAMP or cGMP to determine their binding affinity. SYPRO® orange dye (Sigma-Aldrich®) was used as a fluorescent indicator to follow the denaturation of the protein. The protocol was optimized from Vedadi *et al.*, 2006. 15μg of protein was used. The reaction buffer consisted of 10mM TRIS-HCl pH 7.5, 150mM NaCl and 5X SYPRO® orange dyes, where the original concentration of the sypro orange dye is 5000X. The

concentration of either cAMP or cGMP was varied between 0-500mM. A Chromo4 real-time PCR system (Bio-Rad USA) was used to analyse the denaturation of the C-terminus of AtCNGC12. A temperature range from 20-80°C with an incremental increase of 0.2°C every 7 seconds was chosen as the optimal denaturation condition.

2.16. General molecular biology

2.16.1. DNA extraction

All plasmid extractions from *E.coli* strains were performed using an alkaline extraction protocol as described in Sambrook and Russel (2001), or using the NucleoSpin® plasmid kit (MACHEREY-NAGEL GmbH & Co. KG, Düren · Germany). The kit was used according to the manufacturer's protocol.

From yeast, all plasmids were extracted by pelleting a 1ml yeast culture grown for 2 days at 30°C and vortexing the pellet with 100μl of lysis solution (2% Triton X-100, 1% SDS, 100mM NaCl, 10mM TRIS-HCl, pH 8, and 1mM EDTA). Following this, 100μl of phenol/chloroform and 0.1g of acid-washed glass beads were added. The samples were then vortexed at high speed for 2 min and centrifuged for 2 min at 13,000 rpm. The supernatants were transferred to clean tubes and precipitated with 250μl of 100% Ethanol for 5 min at room temperature. This was followed by another centrifugation at 13,000 rpm for 5 min. The supernatant was removed and the pellet was washed with 50μl of 70% EtOH and then re-centrifuged at 13,000 rpm for 2 min. The supernatant was discarded and the pellet was air-dried and resuspended in 10μl of TE.

2.16.2. DNA Ligations

All ligations were carried out in 10µl reactions using 1µl (5 Units) of T4 DNA ligase and the companion ligation buffer both obtained from Fermentas (Fermentas, Burlington, ON, CA). Reactions were incubated overnight in a 16°C water bath.

2.16.3. Bacterial Transformations

Both chemically competent and electro-competent *E. coli* cells were made and used for transformations. For chemically competent cells ~100ng (or 4µl from a 10µl ligation) of plasmid was added to the cells and then left on ice for 20 min followed by a 30 sec incubation in a 37°C water-bath and then another 5 min incubation on ice. For the electro-competent cells 50-100ng (or 1-2µl from a ligation) of plasmid was added to the cells and chilled on ice for 5 min and then transferred to a chilled 0.2cm electroporation-cuvette and was electroporated in a BioRad MicroPulsar™ at 2.5 kV. Both chemical and electro-competent cells had 1 ml of LB added to the cells and then placed in a 37 °C shaker at 250 rpm for 1 hr and plated onto LB agar plates containing the appropriate antibiotic selection and incubated overnight at 37 °C.

The introduction of plasmids into *Agrobacterium* was performed by the same protocol that was used for *E. coli* electro-competent transformations. *N. benthamiana* transformations were performed using the *Agrobacterium* strain, GV2260. Transformation for GV2260 required a slightly different heat-shock method. After the plasmid DNA was added, the cells were put into liquid nitrogen for 5 min and then kept for 25 min at 37°C. After adding 1ml of LB to either strain and incubating at 37°C for 1 hr, the cells were plated on LB agar containing rifampicin plus the appropriate selection

antibiotic and grown for 2-4 days at 28°C. Positive colonies were screened by PCR detection and confirmed by restriction digest.

2.16.4. Polymerase Chain Reaction (PCR)

Each PCR reaction contained 50-100ng of template DNA, 0.125mM working concentration dNTPs (from 1.25mM stock mixture of dATP, dCTP, dGTP, and dTTP) (Fermentas, Burlington, ON, CA), 20µmol of each primer (IDT), and 1x PCR buffer (from 5x PCR buffer) (BIO RAD, USA) and one unit of iProof high-fidelity DNA polymerase (BIO RAD, USA) in a final volume of 40µl.

2.16.5. RNA extraction and RT-PCR

Small-scale RNA extraction was carried out using the TRIzol reagent (Invitrogen, Carlsbad, MO, CA), according to the manufacturer's instructions. Reverse transcriptase (RT)-PCR was performed using cDNA generated by SuperScript II Reverse Transcriptase (Invitrogen, Carlsbad, MO, CA) according to the manufacturer's instructions. For the detection of β-tubulin gene expression in *A. thaliana*, the same sets of primers described by Baxter *et al*. (2008) were used (Appendix, Table 1).

.

Chapter 3

Identification of the key functional residues of plant CNGCs using *cpr22* (*AtCNGC11/12*)

3.1. Summary of research

Functionally important residues in *A. thaliana* CNGCs were identified through suppressor screening of *cpr22* (*AtCNGC11/12*). Characterization of suppressor mutants from this screen identified amino acid residues that are essential for either general function of CNGCs or the constitutive character of the chimeric *AtCNGC11/12*.

Twenty nine intragenic mutant alleles had been identified in the suppressor mutant screen. In order to understand the possible effect of the mutations on the channel function, *cpr22*-related phenotypes such as morphology and HR development were analyzed in eleven of the mutants. Furthermore, the mutation positions were identified and computational modeling and functional analysis, using yeast complementation assay, were conducted. The current work not only identified the functionally important residues for plant CNGCs, but also demonstrated the validity of usage of *AtCNGC11/12* as a model for structure-function analysis of plant CNGCs.

3.2. Introduction

CNGCs were first identified in animals in the retinal photoreceptors plasma membranes (Fesenko *et al*., 1995). To understand how the primary structure of the CNGCs affects light and chemical perception, a number of mutagenesis and domain swapping analyses have been conducted. One approach was to use chimeric constructs consisting of bovine rod and rat olfactory subunits to study the domains involved in channel activity (Gordon and Zagotta, 1995). It was observed that channel activity is determined by several regions, namely the N-terminus, the S5 transmembrane domain, and a region extending from S2 to S6. A further study ruled out

the cytosolic loop between S3 and S4 from contributing to channel activity (Mottig *et al.,* 2001). Other studies focused on the residues in the C-linker region that links the CNBD to the S6 transmembrane domain. These studies showed that the C-linker plays a key role in determining cNMP sensitivities among different CNGCs (Gordon and Zagotta, 1995; Zong *et al.*, 1998; Paoletti *et al.,* 1999).

A different approach has been used to identify important residues within the CNGCs: humans and rats were screened for olfactory and light perception abnormalities. Such studies have identified over forty functionally important residues in retinal CNGC subunit (Kohl *et al.*, 1998; Wissinger *et al.*, 2001). Many of which are located within the C-linker or the CNBD.

The structure-function analysis of plant CNGCs, on the other hand, has been relatively limited. The residues important for ion selectivity have been studied by site-directed mutagenesis of AtCNGC2 (Hua *et al.*, 2003). The CaMBD of AtCNGC1 has been shown to regulate ion flow in another study by Ali *et al.* (2007). Two more studies demonstrated the functional importance of particular residues in AtCNGC11/12 and AtCNGC12. These residues are glutamate 519 (E519), which facilitates the interaction between the C-linker and the CNBD (Baxter *et al.,* 2008), and arginine 557 (R557) located in the putative CaMBD within the CNBD, which contributes to channel regulation rather than function (Chin *et al.*, 2010).

Further studies are needed to elucidate the structural and functional properties of plant CNGCs. AtCNGC11/12 is thought to form a constitutively active channel that causes the conditionally-lethal lesion mimic phenotype of the well-characterized *A. thaliana* mutant *cpr22* (Yoshioka *et al.*, 2001, 2006). This phenotype makes it easy to

perform a suppressor screen (Baxter *et al.*, 2008; Chin *et al.*, 2010). This chapter will focus on the structure-function analysis of plant CNGCs using the chimeric *AtCNGC11/12* gene that was identified in *cpr22* (Yoshioka *et al.*, 2001).

3.3. Results

3.3.1. Identification of intragenic suppressor mutants of *cpr22* (*AtCNGC11/12)*

Previously, homozygous *cpr22* seeds were mutagenized by ethane methylsulfonate (EMS) (Baxter *et al.*, 2008). The plants were grown in high relative humidity (RH) >95% to ensure that recessive suppressor mutants are survived in this generation. The M_2 self-pollinated plants were then grown in ambient RH at approximately 65% to select suppressor mutants.

A total of twenty nine intragenic mutant alleles in *AtCNGC11/12* have been identified. The summary of the positions of these new alleles will be discussed in Chapter 4.

3.3.2. Basic characterization of the selected intragenic mutants

Eleven cyctosolic C-terminal mutants, S17, S35, S81, S83, S84, S100, S135, S136, S137, S140 and S144 were selected for detail analyses since the C-terminal region contains the important regulatory domains of the channel. Additionally, the solved crystal structures of the C-termini of HCN2 and SpIH (Zagotta *et al.*, 2003 and Flynn *et al.*, 2007, respectively) make it possible to model the mutants to generate hypotheses.

Figure 3.1 shows the morphology and HR-like cell death development of these mutants. All eleven mutants showed similar morphological phenotype to wild type and

did not develop HR-like cell death under normal conditions (22°C, 65% RH), indicating that these mutations suppress *cpr22*-related phenotypes as expected.

To further characterize these mutants, a temperature shift assay (22°C to 16°C) was conducted. It has been known that *cpr22* phenotypes are enhanced in colder temperature (Mosher et al., 2010) and the suppressor mutant S58 showed HR-like cell death when it was shifted to 16°C indicating that S58 is a conditional suppressor (Chin *et al.*, 2010). As shown in Figure 3.2, S35, S83 and S144 started to exhibit HR-like cell death when they were shifted to 16°C. The level of cell death was quantified by ion leakage (Figure 3.3). The results confirmed that S35, S83 and S144 had significantly higher ion-leakage than in wild type after temperature shift, suggesting that E359K, D364N and D408N mutations in the C-linker in S35, S83 and S144, respectively, conditionally suppress the *cpr22* phenotype, similar to S58.

3.3.3. Structural modeling of the mutants

3.3.3.a. Primary structural analysis

Multiple sequence alignment (MSA) of the amino acid sequence of the cytosolic C-termini of the twenty AtCNGCs revealed that two residues, G395 and R372, mutated in S81 and S135, respectively, are conserved in all twenty AtCNGCs. Three residues, D364, R381 and G459, mutated in S83, S137 and S100, respectively, are conserved in nineteen out of the twenty members. C441 and D408 mutated in S17 and S144, respectively, were conserved in eighteen out of the twenty AtCNGCs.

Figure 3.1
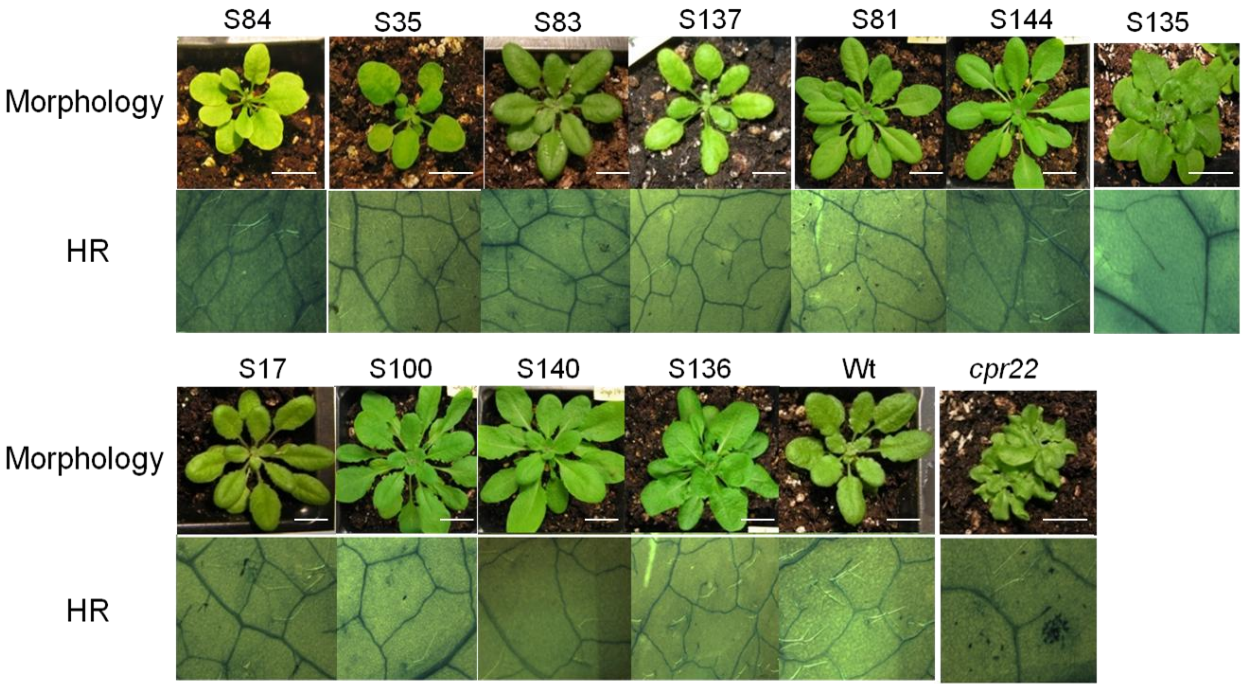
Figure 3.1: Characterization of the suppressor mutants S17, S35, S81, S83, S84, S100, S136, S137, S140, and S144. Morphological phenotypes and spontaneous cell death formation of wild type (Wt), *cpr22*, and suppressor S17, S35, S81, S83, S84, S100, S136, S137, S140, S144. Cell death was detected by trypan blue staining. Approximately 4-week-old plants were used.

Figure 3.2
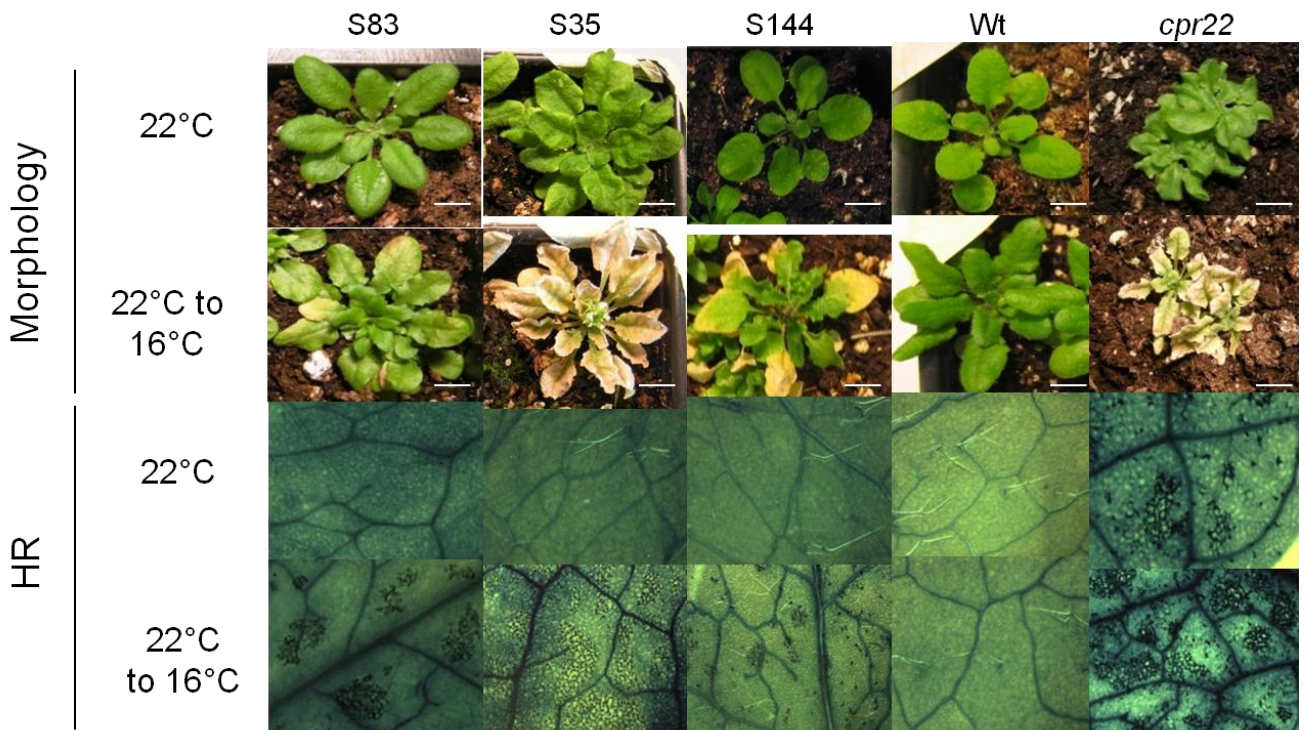
Figure 3.2: Temperature sensitivity of *cpr22*-related phenotypes in *cpr22*, S83, S35, S144 and wild type (Wt) plants after a shift from 22 °C to 16 °C. S83, S35 and S144 displayed *cpr22*-morphology after temperature shift. *cpr22* showed enhancement of cell death and S83, S35 and S144 induced cell death and *cpr22*-related phenotypes after the temperature shift. No cell death induction was observed in wild type (Wt) under both conditions. Photographs were taken 7 days after the shift.

Figure 3.3
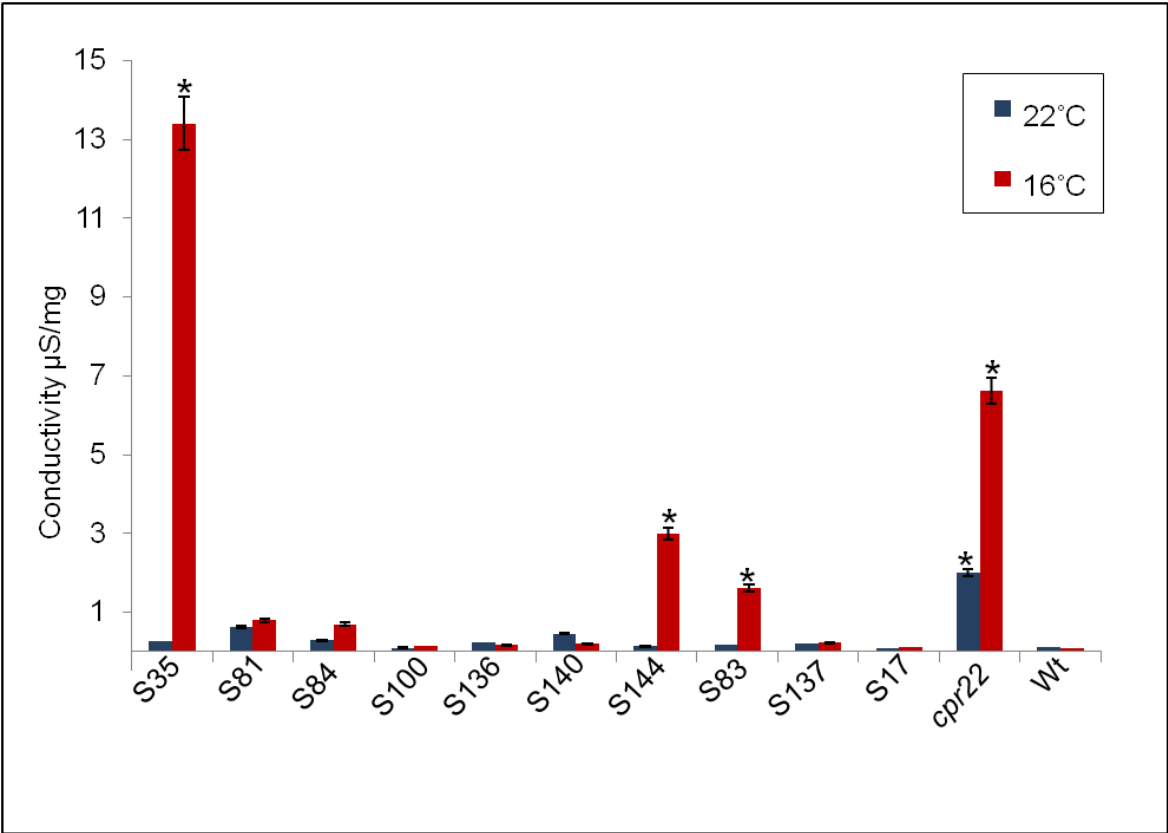
Figure 3.3: Quantitative analysis of cell death by electrolyte leakage in *cpr22*, S35, S81, S84, S100, S135, S136, S137, S17, S140, S144 , S83 and wild type (Wt) plants after a shift from 22 °C to 16 °C. *cpr22* showed enhancement of cell death and S83, S35 and S144 induced cell death after the temperature shift. No cell death induction was observed in wild type (Wt), S81, S84, S100, S135, S136, S137, S17 and S140 under both conditions. Asterisks represent statistically significant differences ($P > 0.05$) when compared to Wt. Samples were taken 7 days after the shift (from the plants presented in Figure 3.2). Data are the average of three biological repeats ±SE.

Two residues, S350 and T513, mutated in S84 and S140, respectively, were conserved in seventeen out of the twenty members. Lastly, E359 and Q543, mutated in S35 and S136, respectively, were not conserved well (Figure 3.4). Considering that CNGCs in both plants and animals maintain similar structure, conserved mutation positions could be important for channel structure universally. Furthermore, R372, R381 and G459, mutated in S135, S137 and S100, respectively aligned well to the previously reported mutation positions of the human cone photoreceptor CNGA3 named R427, R436 and G513 (Wissinger *et al.*, 2001) (Figure 3.5). Mutations in these residues cause complete colour blindness, photophobia and nystagmus, suggesting the importance of these three residues for channel function (Wissinger *et al.*, 2001; Goto-Omoto *et al.*, 2006; Koeppen *et al.*, 2008).

To further assess this alignment, I conducted a structural comparison of *AtCNGC11/12* and CNGA3, with Swiss-Model© (http://swissmodel.expasy.org//SWISS-MODEL.html) using the solved crystal structure of SpIH1 as a template (Flynn *et al.,* 2007) . This will be discussed in 3.3.3.b.

3.3.3.b. Secondary and tertiary structural analysis

CNGCs and HCNs are two channel families that belong to the cyclic nucleotide-regulated channels (Craven and Zagotta, 2006). The similarities between these two channel families are apparent when examining their structural and functional characteristics. Both CNGs and HCNs are gated by direct binding of cNMPs to the cytosolic C-terminal region. Furthermore, both are composed of four subunits with each subunit consisting of six transmembrane domains and cytosolic N- and C-termini (Craven and Zagotta, 2006).

Figure 3.4
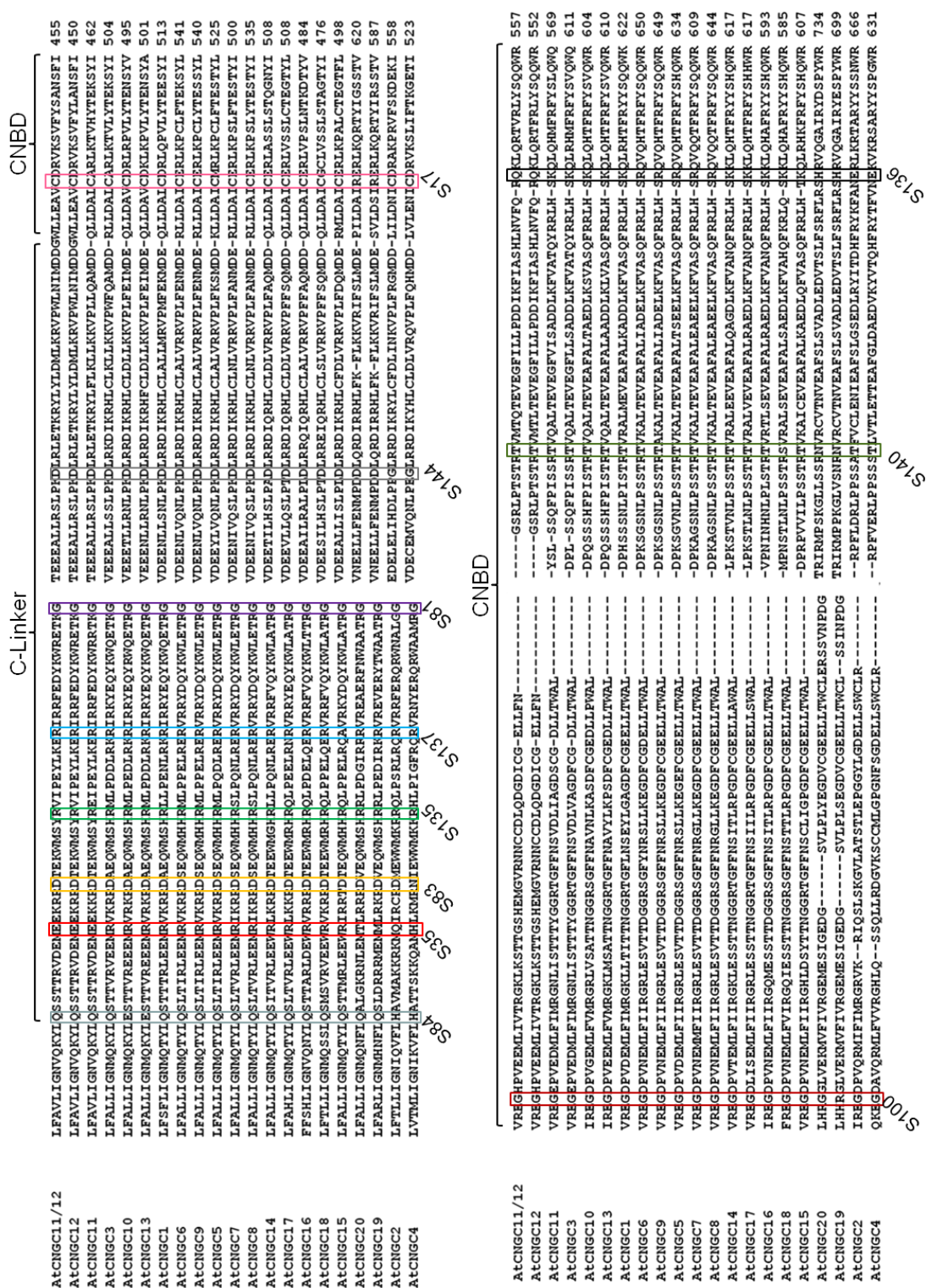
Figure 3.4: Alignment of the area of the C-linker and CNBD in 20 AtCNGCs, NCBI accession # of AtCNGCs are listed in Appendix, Table 2. The boxes, blue, dark red, yellow, light green, light blue, purple, gray, pink, dark red, dark green and black indicate the positions of S84, S35, S83, S135, S137, S81, S144, S17, S100, S140 and S136, respectively.

Figure 3.5


```
                                       S135        S137
HCN2          ALIQSLDSSRRQYQEKYKQVEQYMSFHKLPADFRQRIHDYYEHRYQ-GKM 62
CNGA3         SMISNMNASRAEFQAKIDSIKQYMQFRKVTKDLETRVIRWFDYLWANKKT 450
AtCNGC11/12   KYLQSSTTRVDEMEEKRRDTEKWMSYRVIPEYLKLRIREFEDYKWRETKG 64


HCN2          FDEDSILGELNGPLREEIVNFNCRKLVASMPLFANADPNF-VTAMLTKLK 111
CNGA3         VDEKEVLKSLPDKLKAEIAINVHLDTLKKVRIFQDCEAGL-LVELVLKLR 499
AtCNGC11/12   TEEEALLRSLPKDLRLETKRYLYLDMLKRVPWLNIMDDGWLLEAVCDRVK 114
                                   S100
HCN2          FEVFQPGDYIIREGTIGKKMYFIQHGVVSVLTKGNKEM--KLSDGSYFGE 159
CNGA3         PTVFSPGDYICKKGDIGKEMYIINEGKLAVVADDGVTQFVVLSDGSYFGE 549
AtCNGC11/12   SVFYSANSFIVREGHPVEEMLIVTRGKLKS-TTGSHEMGCDLQDGDICGE 163
```

Figure 3.5: Alignment of the areas of R372, R381 and G459 mutated in S135, S137 and S100, respectively, in HCN2 (NP _001185), CNGA3 (NP_001289) and AtCNGC11/12 (12) (EU541495).

The crystal structures of the C-terminus regions of HCN2 (Zagotta *et al.,* 2003) and SpIH1 (Flynn *et al.,* 2007) have been solved. These C-terminal fragments assemble as a 4-fold symmetric tetramer directly below the transmembrane portion of the channel.

Structural modeling of the C-terminal domain of AtCNGC11/12 (same as AtCNGC12) was performed using both SpIH1 and HCN2 as templates, where they showed the highest structural similarity to AtCNGC11/12 among the currently available crystal structures of cytosolic C-termini. Overall, higher structural similarity was seen with SpIH1 than with HCN2 (Figure 3.6). Therefore, SpIH1 was used as a template for all computational modeling conducted in this study.

In my models, positions R372, R381 and G459, mutated in S135, S137 and S100, respectively, superimposed perfectly with the three residues of human CNGA3 mentioned previously (Figure 3.7). This indicates that the positions of those three residues are structurally important for CNGC function in both plants and animals.

To predict how the eleven identified intragenic mutations affects the structure of the channel to suppress *cpr22*-conferred phenotypes, a bioinformatics approach was taken to investigate the secondary and tertiary structures of the eleven suppressors. Previously, E519K in S73 was discovered in the eighth β-strand in the CNBD and was postulated to impede predicted stabilizing interactions between the C-linker and the CNBD (Baxter *et al.*, 2008). The structure prediction tools, Swiss-Model© (http://swissmodel.expasy.org//SWISS-MODEL.html) and SymmDock (http://bioinfo3d.cs.tau.ac.il/SymmDock/) were used for the analysis to test the above mentioned postulation. Using the same approach, two possible types of mechanisms for *cpr22* phenotype suppression were revealed in seven suppressors out of eleven. The

first suggested mechanism includes intra-subunit interaction (between residues in the same subunit), in S81, S144, and S17, (Figure 3.8). The second suggested mechanism is inter-subunit interaction (between residues in different subunits), in S83, S135, S137 and S100 (Figure 3.9). The possible mechanism of interaction for both S100 and S137 will be discussed in detail in Chapter 4. S35 and S140 were predicted to have different kinds of interactions that will be discussed below, whereas S84 (S350L) could not be modeled because it was too close to the membrane domain of the channel. S136 was previously characterized (Chin *et al.,* 2010).

For S81 (G395R), located in the lobe connecting the αB-helix with the αC-helix of the C-linker, the model showed that the change from glutamin (G) to the positively charged arginine (R) appears to create a novel interaction between R395 and G398 in the form of a salt bridge (Figure 3.8.A). This predicted interaction could affect the flexibility of this region of the C-linker resulting in the suppression of the *cpr22*-conferred phenotypes associated with this mutant.

The predicted model for S144 (D408N), located in the αD-helix of the C-linker, revealed a possible disruption of a salt bridge between D408 and K407 when the negatively charged aspartic acid (D) was mutated to the neutral asparagine (N) (Figure 3.8.B). This salt bridge disruption could attribute to the conditional suppression of the *cpr22*-conferred phenotype associated with this mutant.

The possible mechanism of suppression predicted for S17 (C441Y), located in the last α-helix of the C-linker, could be due to the change from a small polar residue (C) to a more bulky one (Y). This change may affect the orientation of the side chains of the surrounding residues, where both L437 and M421 side chains were pushed further

away compared to their original positions in the wild type structure (Figure 3.8.C). This change in the configuration of those two residues, might be the reason of the suppression of *cpr22*-related phenotypes in S17 mutant.

The computational modeling of S83 (D364N) predicted novel inter-subunit interactions instead of an intra-subunit interaction (Figure 3.8.D). The model revealed a possible inter-subunit interaction between D364, located in the first α-helix of the C-linker and both R354 and K394, located in the lobe connecting αB-helix and αC-helix of the C-linker and located in first α-helix of the C-linker, respectively, on the neighbouring subunit. These interactions can be salt bridges because D364 is negatively charged and R354 and K394 are positively charged. In S83, D364N mutation likely disrupt these two salt bridges. (Figure 3.9.A, B and C). This can be the reason of the suppression of the *cpr22*-related phenotypes in S83 mutant. .

The 3D model of S135 (R372W), like S83, did not predict any possible interaction within the same subunit (Figure 3.8.E). It predicts, however, a possible inter-subunit interaction in the form of a salt bridge between the positively charged R372, located in the end of the αA-helix of the C-linker and negatively charged D420 located in the αD-helix of the C-linker of the neighbouring subunit. This salt bridge was disrupted when the positively charged arginine (R) was replaced with a neutral tryptophan (W) in this mutant (Figure 3.9.A, D and E). Therefore, it is likely that the disruption of the salt bridge in S135 causes the wild type-like phenotypes associated with this mutant.

Neither intra- nor inter- subunit interactions were predicted for S35 through computational modeling. The mutation, E359K, was predicted to locate in the αA-helix of the C-linker in close proximity to the cell membrane (Figure 3.8.D). This residue,

however, aligned well with R478 in SpIH1 (data not shown). R478 in SpIH1 was reported to have a possible interaction with phospholipid phosphatidylinositol 4, 5-bisphosphate (PIP2) in the membrane during the stabilization of the closed state of the channel (Flynn and Zagotta, 2011). This suggested a similar role for E359 in the regulation of AtCNGC11/12. Therefore, this substitution of glutamate to lysine could interrupt similar interaction with PIP2, thereby causing the suppression of *cpr22*-related phenotype associated with this mutant.

The computational modeling of S140 (T513I), located between the P-helix and the 6th-β sheet of the CNBD, revealed a configuration change in the entire CNBD (Figure 3.8.G). This configuration change of the CNBD might have caused the suppression of *cpr22*-related phenotype associated with this mutant.

The combination of the basic characterization of suppressor mutants' phenotype and computational modeling revealed six interesting positions. E359K (S35), D364N (S83) and D408N (S144) characterized as conditional suppressor mutants, and G459R (S100), R372W (135), and R381H (S137) as nonconditional (perfect) suppressor mutants that structurally aligned well with previously reported human CNGA3 mutants (Wissinger *et al.*, 2001). This indicates that these positions are universally important positions for CNGC in general. These six mutants were further investigated.

Figure 3.6

A

Channel properties	HCN2 PDB no. 1Q5O	SpiH PDB no. 2PTM
Channel type	HCN	HCN
Full agonist	cAMP	cAMP
Organism	Mouse	Sea Urchins sperm
Z-score to AtCNGC11/12(12)	24.1	30.5
Residue aligned with AtCNGC11/12	180 (80%)	192 (85.7%)

B
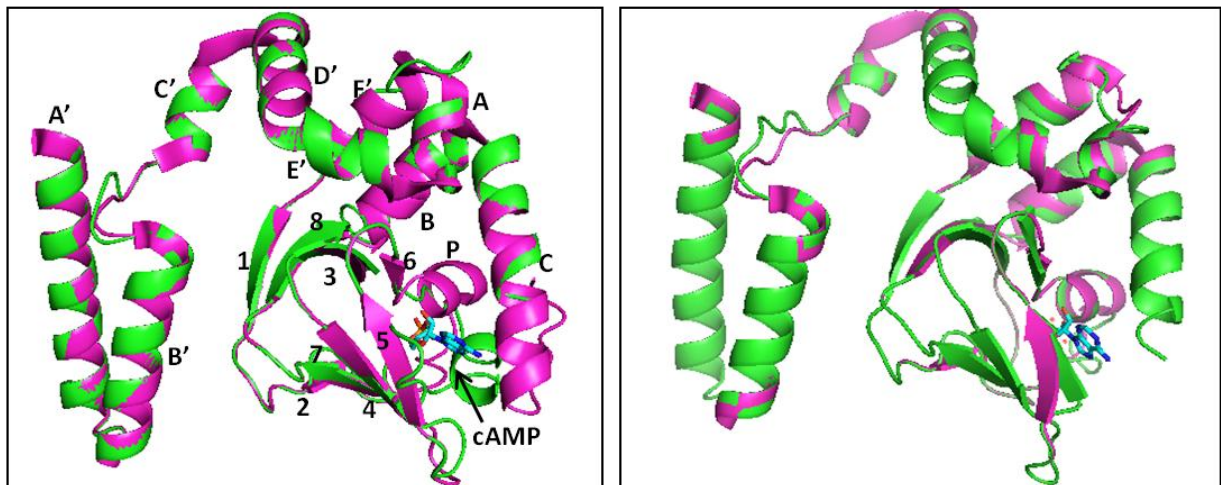
Figure 3.6: Overall structural similarity between SpIH1 and HCN2 to AtCNGC11/12(12). (A) Table showing channel properties of both SpIH1 and HCN2 C-termini to AtCNGC12 C-terminus. (B) Computational modeling and superimposition of the cytoplasmic C-terminal region of AtCNGC11/12(12) (green) containing the C-linker (six α-helices; A'-F') and the CNBD (four a-helices; A, P, B, C with 1-8 β-sheets between A- and B-helices) and both HCN, left, and SpIH1, right (magenta).

Figure 3.7
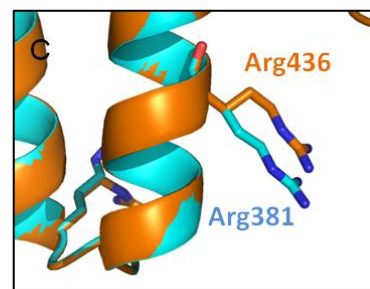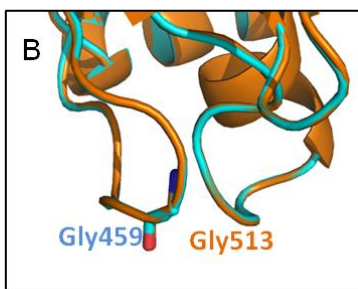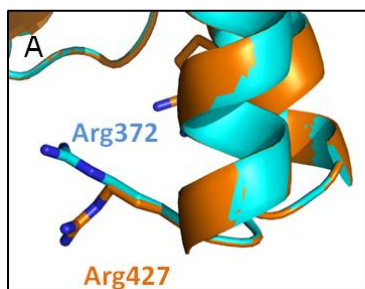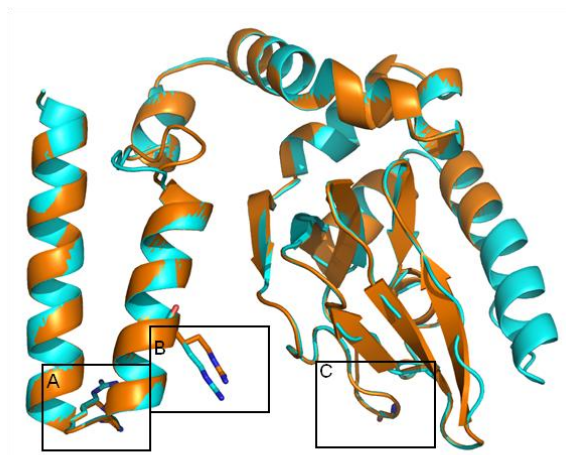
Figure 3.7: Computational structural modeling and superimposition of the cytoplasmic C-terminal region of AtCNGC11/12 (blue) and human CNGA3 (brown). Mutation positions of S135 (A), S100 (B) and S137 (C). The protein sequence from the residues after the sixth transmembrane domain (S350 to A641 in AtCNGC11/12; EU541497 and N398 to E586 in CNGA3; NP_001289) was modeled to the crystallized SpHI structure (Flynn *et al.*, 2007, PDB ID 2PTM).

Figure 3.8
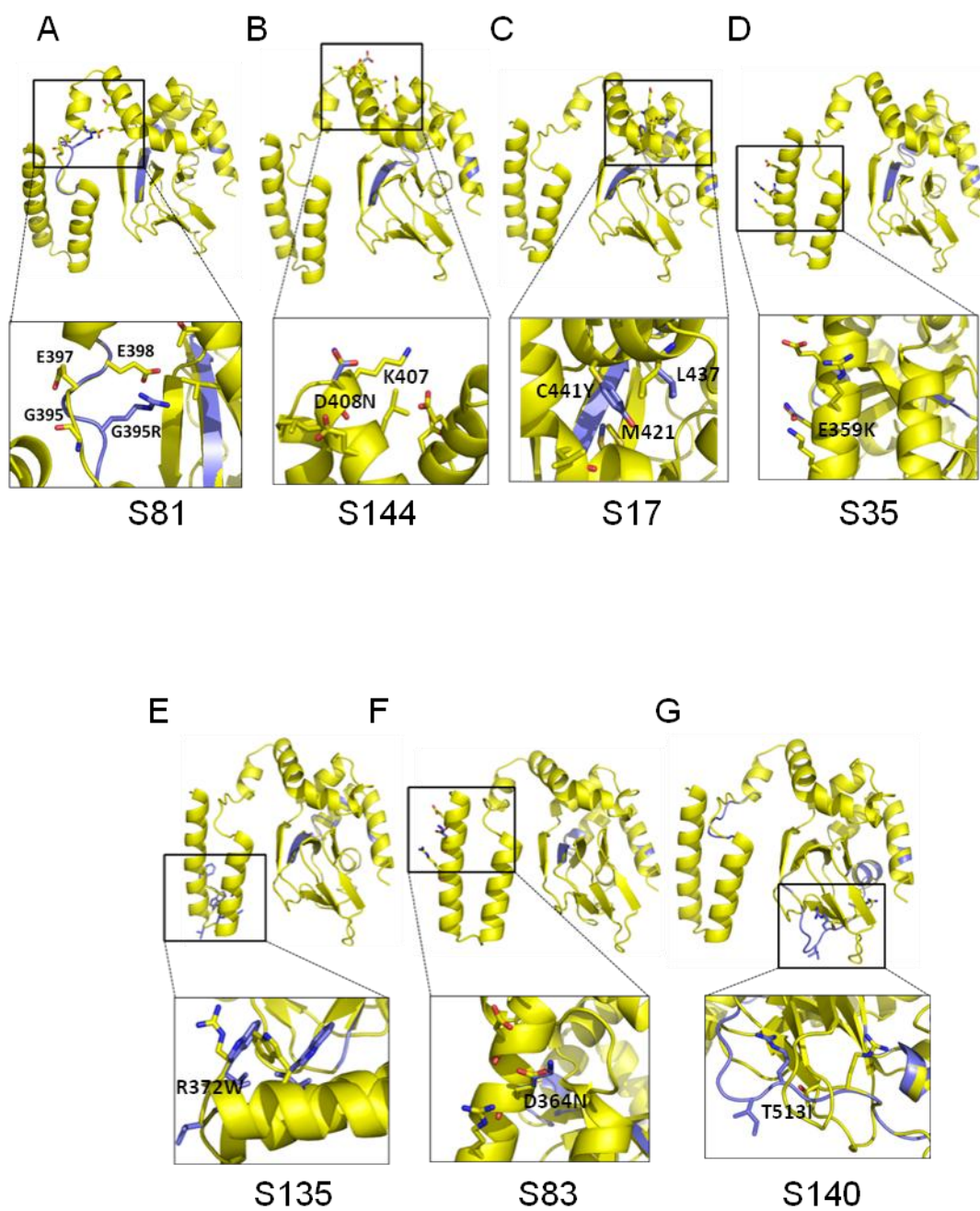
Figure 3.8: Computational structural modeling of the cytoplasmic C-terminal region of AtCNGNC11/12 and seven suppressor mutants. Yellow color indicates AtCNGC11/12 (12), blue color indicates the mutants. (Overlaid models of AtCNGNC11/12 and the equivalent area of (A) S81, (B) S144, (C) S17, (D) S35, (E) S135, (F) S83, (G) S140. The protein sequence from the residues after the sixth transmembrane domain (S350 to A641 in AtCNGC11/12; EU541497) with and without mutations was modeled to the SpHI structure (Flynn *et al.*, 2007, PDB ID 2PTM).

Figure 3.9
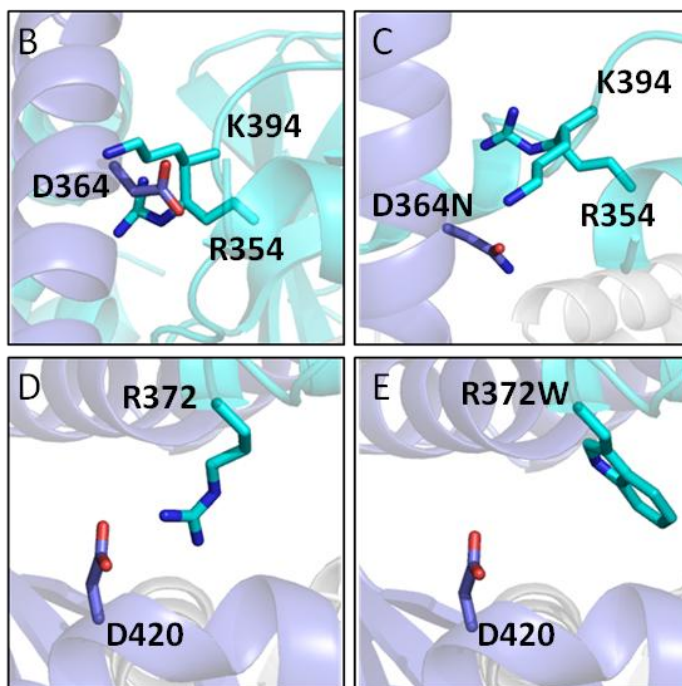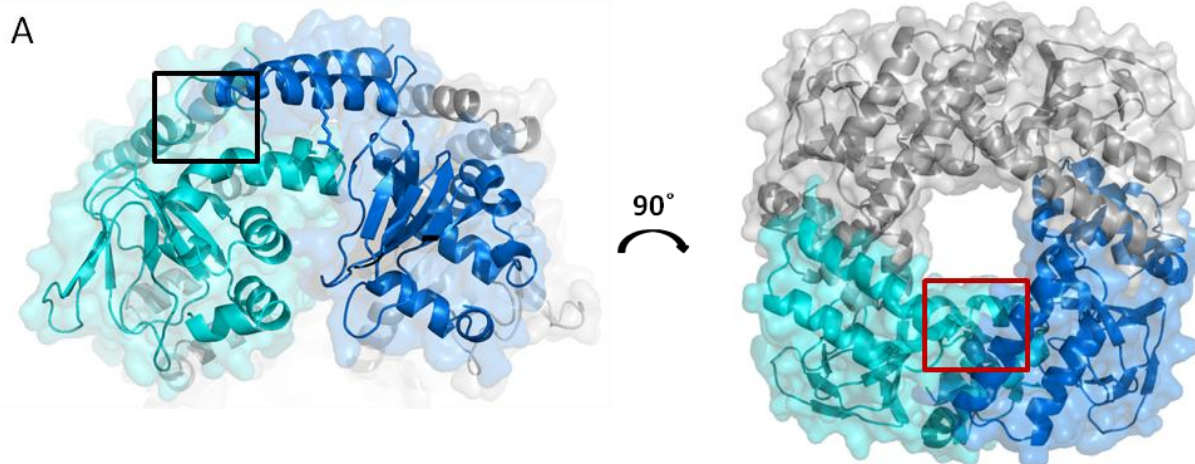
Figure 3.9: Computational structural modeling of tetramer structure of the cytoplasmic C-terminal region of AtCNGNC11/12 (12), S83 and S135. (A) AtCNGC11/12 (EU541497) tetramer viewed perpendicular (left) and parallel (right). All subunits are shown by different colors to depict their interaction. (B) Close-up of the red box in (A) and (C) the equivalent area of S83. (D) Close-up of the black box in (A) and (E) the equivalent area of S135.

3.3.4. Functional analysis of S135 (R372W), S137 (R381H), S100 (G459R), S35 (E359K), S83 (D364N), and S144 (D408N) by yeast complementation assay

Channel function in several plant CNGCs have been assessed with a complementation assay using ion-uptake deficient yeast mutants (Chin *et al.*, 2009). AtCNGC11/12 has been shown to function as K^+ and Ca^{2+} channels by this way (Yoshioka *et al.*, 2006; Urquhart *et al.*, 2007; Baxter *et al.*, 2008). It has been reported that AtCNGC11/12:E519K (S73) was unable to complement K^+ uptake-deficient yeast mutant growth. Furthermore, AtCNGC12 harbouring the S73 mutation (E519K) also failed to complement K^+ uptake-deficient yeast mutants, indicating that E519 is essential not only for AtCNGC11/12 function but also for basic channel function of wild type AtCNGC12 (Baxter *et al.*, 2008). On the other hand, the AtCNGC11/12:R557C (S58) was able to complement the yeast mutants strain RGY516 with similar efficiency as AtCNGC11/12. This suggested that the R557C mutation alters the constitutively active nature of the chimeric channel rather than disrupting basic channel function (Chin *et al.*, 2010). The same assay using K^+ uptake-deficient yeast mutant was conducted to investigate the functionality of the six selected mutants in this study.

Full length cDNA of *AtCNGC11/12:*E359K (S35), *AtCNGC11/12:*D364N (S83), *AtCNGC11/12:*D408N (S144), *AtCNGC11/12:*G459R (S100), *AtCNGC11/12:*R372W (135), and *AtCNGC11/12:*R381H (S137) were cloned into the yeast expression vector pYES2, and transformed into a K^+-uptake deficient yeast strain RGY516 (Ali *et al.,* 2005). As shown in Figure 3.10, RGY516 carrying *AtCNGC11/12:*E359K (S35), *AtCNGC11/12:*D364N (S83) or *AtCNGC11/12:*D408N (S144) were able to grow in low potassium media with similar efficiency as AtCNGC11/12, whereas RGY516 carrying

*AtCNGC11/12:*G459R (S100), *AtCNGC11/12:*R372W (135), or *AtCNGC11/12:*R381H (S137) could not. Expression of the genes in yeast was confirmed by RT-PCR and no significant difference between AtCNGC11/12 and mutants was found (data not shown). Similar result was obtained using three different colonies of transformed yeast.

Taken together, the data suggests that E359K, D364N and D408N mutations in S35, S83 and S144 respectively, do not affect basic channel function, whereas R372W, R381H and G459R mutations in S135, S137 and S100 respectively, are essential for channel function.

3.4. Discussion

In order to understand the structural basis of plant *CNGCs*, Baxter *et al.* (2008) conducted a genetic screen for *cpr22* suppressor mutants. Through this screening, 29 new alleles were identified. Among those, S73 was analyzed in the same study. This mutant possessed an E519K substitution in the CNBD in *AtCNGC11/12*. This substitution was found to abolish channel function and suppressed *AtCNGC11/12*-mediated phenotypes (Baxter *et al.*, 2008).

Through this study, eleven additional mutants, located in the cytosolic C-terminus of AtCNGC11/12, were investigated. Basic characterization regarding morphology and HR-like cell death development was conducted. All eleven mutants displayed wild type-like morphology and complete suppression of HR-like cell death development under normal conditions (22°C and 65% RH). Three of the eleven characterized mutants, S35, S83 and S144, were revealed to be conditional suppressors where they developed HR-like cell death at 16°C.

Another conditional suppressor, S58 (R557C), was also identified in the same screen. Chin *et al.* (2010) reported that R557 in the αC-helix of the CNBD plays an important role in stable channel regulation. R557C mutation was shown to suppress cell death formation and other *cpr22*-related phenotypes under normal conditions (22°C and 65% RH). The *cpr22*-related phenotypes were induced in lower temperatures (16°C), suggesting an alteration in channel regulation rather than loss of channel function. This finding suggests that the conditional suppression associated with S35, S83 and S144 could also be attributable to an alteration in the regulation of the channel, rather than basic channel function. Indeed, yeast complementation analysis supported this notion.

To investigate possible mechanisms of suppression associated with these mutants, 3D computational modeling was conducted. Through this analysis, I found two possible mechanisms of interaction to suppress *cpr22*-phenotypes in seven out of the eleven mutants; intra- and inter-subunit interactions. The intra-subunit interaction between residues in the same subunit was previously reported in *AtCNGC11/12*, where Baxter *et al.* (2008) suggested a possible salt bridge between E517 located in the CNBD and R384 located in the C-linker. It has suggested that the substitution of E519 to K519 led to the disruption of this interaction by breaking the R384–E519 salt bridge, resulting in a complete loss of *cpr22*-associated phenotypes and channel function.

Figure 3.10
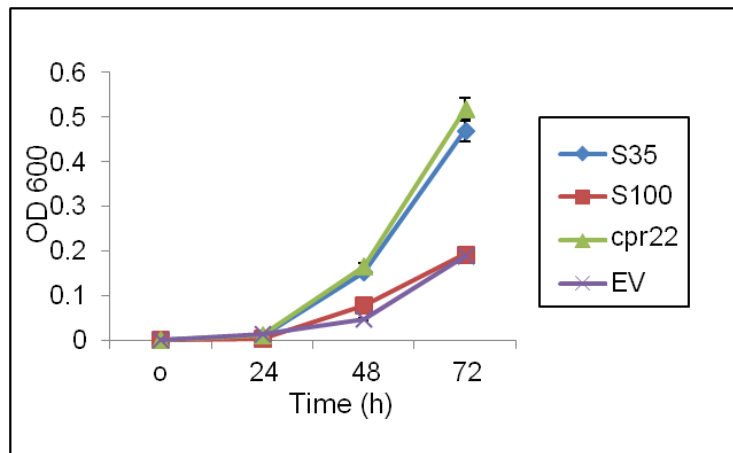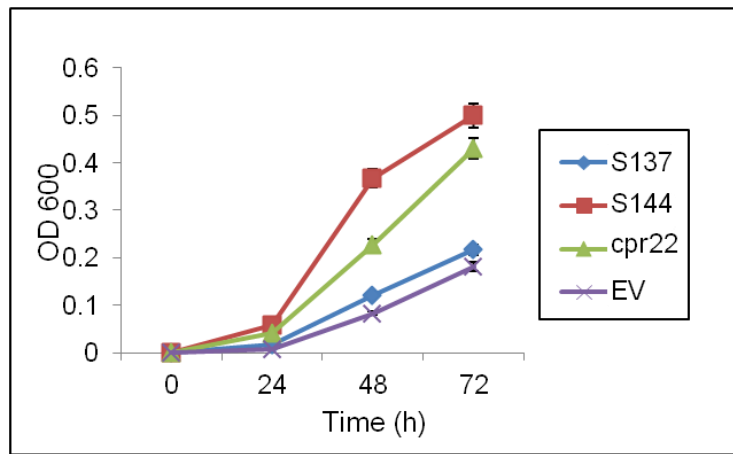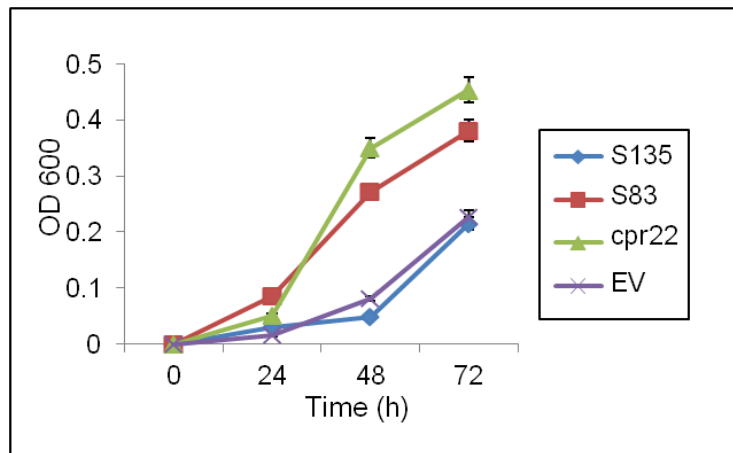
Figure 3.10: Yeast complementation analysis using the K^+-uptake-deficient mutant RGY516. Expression of *AtCNGC11/12*, *AtCNGC11/12:*E359K (S35), *AtCNGC11/12:*D364N (S83) or *AtCNGC11/12:*D408N (S144) but not *AtCNGC11/12:*G459R (S100), *AtCNGC11/12:*R372W (135), *AtCNGC11/12:*R381H (S137) or empty vector (EV) complemented the K^+-uptake deficiency of RGY516 in low potassium media. Data are the average of three biological repeats ±SE.

I hypothesized that the suppression of *cpr22*-related phenotypes associated with S81, S144 and S17 is due to the alteration of the possible intra-subunit interaction, similar to S73 mutation. My computational modeling indicated 1) a creation of a novel salt bridge in S81, 2) a disruption of an existing salt bridge in S144 and 3) an overall change in the orientation of the surrounding residues in S17.

The computational modeling also indicated possible inter-subunit interactions between residues in neighbouring subunits in S83, S135, S137 and S100. The models predicted a possible interaction, in the form of salt bridges, between D364 (in the C-linker of one subunit) and both R354 and K394 (in the C-linker of the neighbouring subunit) that can be disrupted by the substitution of D364 to N364 (S83). Another salt bridge was predicted between R372 and D420 (located in the C-linker of different subunits). Substituting of R372W (S135) may have caused the disruption of this predicted salt bridge.

The inter-subunit interaction between residues on neighbouring subunits was reported previously in the animal HCN2 channel, another family of ion channels highly similar to animal CNGCs (Craven and Zagotta, 2004; Craven *et al.,* 2008). It was revealed by crystallography that an important intra- and inter-subunit interaction occurred between three residues, K468 in the C-linker (which align with S137 mutation R381H), D542 in the CNBD of the same subunit and E502 in the C-linker of the neighbouring subunit (Zagotta *et al.,* 2003). It was further investigated in CNGA1 by site direct mutagenesis and patch clamping and suggested that this interaction is essential for normal gating of both HCN2 and CNGA1 channels (Craven and Zagotta, 2004; Craven *et al.,* 2008). Similarly, I hypothesized that the loss of inter-subunit interaction in

S83 and S135, caused the loss of *cpr22*-like phenotypes in these mutants. The mechanism of interaction of S100 and S137 will be discussed in details in Chapter 4.

The computational modeling did not reveal any possible interaction for both E359 and T513 mutated in S35 and S140, respectively. E359 aligned well with a positively charged residue in SpIH1 that was believed to have a possible role in the regulation of this channel through the cell membrane signalling pathway (Flynn and Zagotta, 2011). This suggests a similar role for E359 in the regulation of *AtCNGC11/12*, one that has yet to be investigated. The 3D model of S140 revealed a configuration change in the entire CNBD compared to wild type. In animal systems, it has been reported that cNMPs bind within the pocket formed by the αC-helix and the β-barrel composed of the eight β sheets in the CNBD (Weber and Steitz, 1987; Rehmann *et al.*, 2007). This suggests that the configuration change in the CNBD predicted in S140 would likely affect the proper binding of cNMP within the CNBD, which resulted in the phenotypes associated with this mutant.

Future work could include further functional analyses using the aforementioned yeast complementation assay for the other seven mutants. Additionally, *Agrobacterium*-mediated transient expression in *Nicotiana benthamiana* could be conducted. This method was previously used to detect the HR-like programmed cell death by the expression of *AtCNGC11/12* (Yoshioka *et al.,* 2006; Urquhart *et al.,* 2007). The same method was used more recently to confirm that the loss of HR-like cell death observed in S73 and S58 were attributable to their respective mutations (Baxter *et al.,* 2008; Chin *et al.,* 2010). The *Agrobacterium*-mediated transient expression in *Nicotiana*

benthamiana was conducted for two mutants (S100 and S137) that will be discussed in Chapter 4.

Future studies could also include site-directed mutagenesis to test the proposed interactions in the investigated suppressors. So far, the current work shown here has identified residues that are important for either channel regulation or channel function, and has further demonstrated the utility of *AtCNGC11/12* as a tool for CNGC structure-function research.

Chapter 4

A suppressor screen of the chimeric *AtCNGC11/12* reveals residues important for inter-subunit interactions of cyclic nucleotide-gated ion channels

Huda Abdel-Hamid, Wolfgang Moeder, Dea Shahinas, Kimberley Chin, Deepali Gupta and Keiko Yoshioka

H.A. provided the data for Figures 4.1, 4.2, 4.3, 4.4 (a and c), 4.5, 4.6, 4.7, 4.8, 4.9, 4.10 (except b, lower panel), 4.11, and 4.12 and Table 4.2

4.1. Summary of research

To investigate the structure-function relationship of plant cyclic nucleotide-gated ion channels (CNGCs), we identified a total of 29 mutant alleles of the chimeric *AtCNGC11/12* gene that induces multiple defense responses in the *Arabidopsis thaliana* mutant, constitutive expresser of *PR* genes 22 (*cpr22*). Based on computational modeling, two new alleles, S100 (AtCNGC11/12:G459R) and S137 (AtCNGC11/12:R381H), were identified as counterparts of human CNGA3 (a human CNGC) mutants. Transient expression in *Nicotiana benthamiana* as well as functional complementation in yeast showed that both AtCNGC11/12:G459R and AtCNGC11/12:R381H have alterations in channel function. Site-directed mutagenesis coupled with fast protein liquid chromatography using recombinantly expressed C-terminal peptides indicated that both mutations significantly influence subunit stoichiometry to form multimeric channels. Further computational models suggested similar molecular mechanisms for the equivalent human mutants. Taken together, we have identified two residues that are likely important for subunit interaction for both plant and animal CNGCs.

4.2. Introduction

Cyclic nucleotide-gated ion channels (CNGCs) were first discovered in retinal photoreceptors and olfactory sensory neurons (Zagotta and Siegelbaum, 1996; Kaupp and Seifert, 2002). CNGCs play crucial roles for the signal transduction in these neurons that are excited by photons and odorants, respectively. In mammalian genomes, six CNGC genes have been found and named *CNGA1–4*, *CNGB1*, and

CNGB3 (Kaupp and Seifert, 2002). It has been reported that in mammalian cells, CNGCs function as heterotetramers that are composed of A and B subunits with cell-specific stoichiometry (Kaupp and Seifert, 2002; Cukkemane *et al.*, 2011). For example, CNGCs in rod photoreceptors are composed of three A1 subunits and one B1a subunit, whereas in cone photoreceptors they are believed to be composed of two A3 and two B3 subunits (Zhong *et al.*, 2002; Peng *et al.*, 2004). The structure of each subunit is similar to that of the voltage gated K^+-selective ion channel (Shaker) proteins, including a cytoplasmic N-terminus, six membrane-spanning regions (S1–S6), a pore domain located between S5 and S6, and a cytoplasmic C-terminus (Zagotta and Siegelbaum, 1996). CNGCs are only weakly voltage-dependent and are opened by the direct binding of cyclic nucleotides (CN, cAMP and cGMP), which are universally important secondary messengers that control diverse cellular responses (Fesenko *et al.*, 1985). The cytoplasmic C-terminus contains a cyclic nucleotide-binding domain (CNBD) and a C-linker region that connects the CNBD to the S6 domain. CNG channel activity is also regulated by feedback inhibitory mechanisms involving the Ca^{2+} sensor protein, calmodulin (CaM). CaM binding sites in animal CNGCs have been found in various regions of both the C- and N-terminal domains (Ungerer *et al.*, 2011). It has been reported that the subunit composition has significant influence on the mode of CaM-mediated regulation (Kramer *et al.*, 1992; Bradley *et al.*, 2004; Song *et al.*, 2008).

On the other hand, plant CNGCs have only been investigated much more recently. The first plant CNGC, HvCBT1 (*Hordeum vulgare* calmodulin (CaM)-binding transporter), was identified as a CaM-binding protein in barley (Schuurink *et al.*, 1998). Subsequently, several CNGCs were identified from *A. thaliana* and *Nicotiana tabacum*

(Arazi *et al.*, 1999; Köhler and Neuhaus, 1998; Köhler *et al.*, 1999). The *A. thaliana* genome sequencing project identified a large family comprising of twenty members (*AtCNGC1-20*), indicating a significant expansion of *A. thaliana* CNGCs that suggests a higher level of diversity and functional importance in plants (Mäser *et al.*, 2001). To date, possible biological functions of *A. thaliana* CNGCs in development, ion homeostasis as well as pathogen resistance have been reported. (Kaplan *et al.*, 2007; Chin *et al.*, 2009; Dietrich, 2010; Moeder *et al.*, 2011). With respect to structure, plant CNGCs are believed to have a similar architecture to their animal counterparts (Chin *et al.*, 2009). On the other hand, only a handful of studies on the structure–function analysis of plant CNGCs has been published so far and this field is still very much in its infancy (Hua *et al.*, 2003; Bridges *et al.*, 2005; Kaplan *et al.*, 2007; Baxter *et al.*, 2008; Chin *et al.*, 2010).

Previously, we have reported two functionally important residues in plant CNGCs (Baxter *et al.*, 2008; Chin *et al.*, 2010). These residues were discovered using a suppressor screen of the rare gain-of-function *A. thaliana* mutant *constitutive expresser of PR gene* 22 (*cpr22*) (Yoshioka *et al.*, 2006). The *cpr22* mutant, which has a deletion between *AtCNGC11* and *AtCNGC12* resulting in a novel, but functional chimeric CNGC (*AtCNGC11/12*), exhibits multiple resistance responses without pathogen infections in the hemizygous state and conditional lethality in the homozygous state (Yoshioka *et al.*, 2001; Yoshioka *et al.*, 2006; Moeder *et al.*, 2011). It has been reported that the *cpr22* phenotype is attributable to the expression of *AtCNGC11/12* and its channel activity (Yoshioka *et al.*, 2006; Baxter *et al.*, 2008), thereby making the suppressor screen an

invaluable tool for identifying intragenic mutants to further elucidate the structure-function relationship of plant CNGCs (Baxter *et al.*, 2008; Chin *et al.*, 2010).

In this study, we describe a total of 29 mutant alleles of *AtCNGC11/12* including the three previously published alleles (Baxter *et al.*, 2008; Chin at al., 2010) and compare their predicted 3D structural positions to equivalent mutations of a human CNGC, CNGA3. Two *AtCNGC11/12* mutations emerged as counterparts of human mutations. Both the AtCNGC11/12 as well as the human mutations were computationally predicted to affect inter-subunit interactions. This prediction was followed up with size exclusion chromatography (FPLC) in combination with site-direct mutagenesis using recombinant C-terminal peptides.

4.3. Results

4.3.1. Chimeric AtCNGC11/12 (*cpr22*) suppressor screening identified 29 mutant alleles of AtCNGC11/12

The suppressor screen of *cpr22* was reported previously (Baxter *et al.*, 2008). Through this screen, a total of 29 mutant alleles in *AtCNGC11/12* have been discovered. Figure 4.1 shows a summary of the positions of these new alleles. This includes 6 premature stop codon mutations in various domains (Figure 4.1 and Table 4.1) which further supports the previously reported notion that *cpr22* (*AtCNGC11/12*)-mediated phenotypes are attributable to the expression of *AtCNGC11/12* (Yoshioka *et al.*, 2006; Baxter *et al.*, 2008). The remaining 23 mutations involve single amino acid substitutions caused by point mutations. In agreement with the mutagenizing effect of the alkylating agent, ethyl methanesulfonate (EMS), 22 out of 23 mutations are G/C to

Figure 4.1
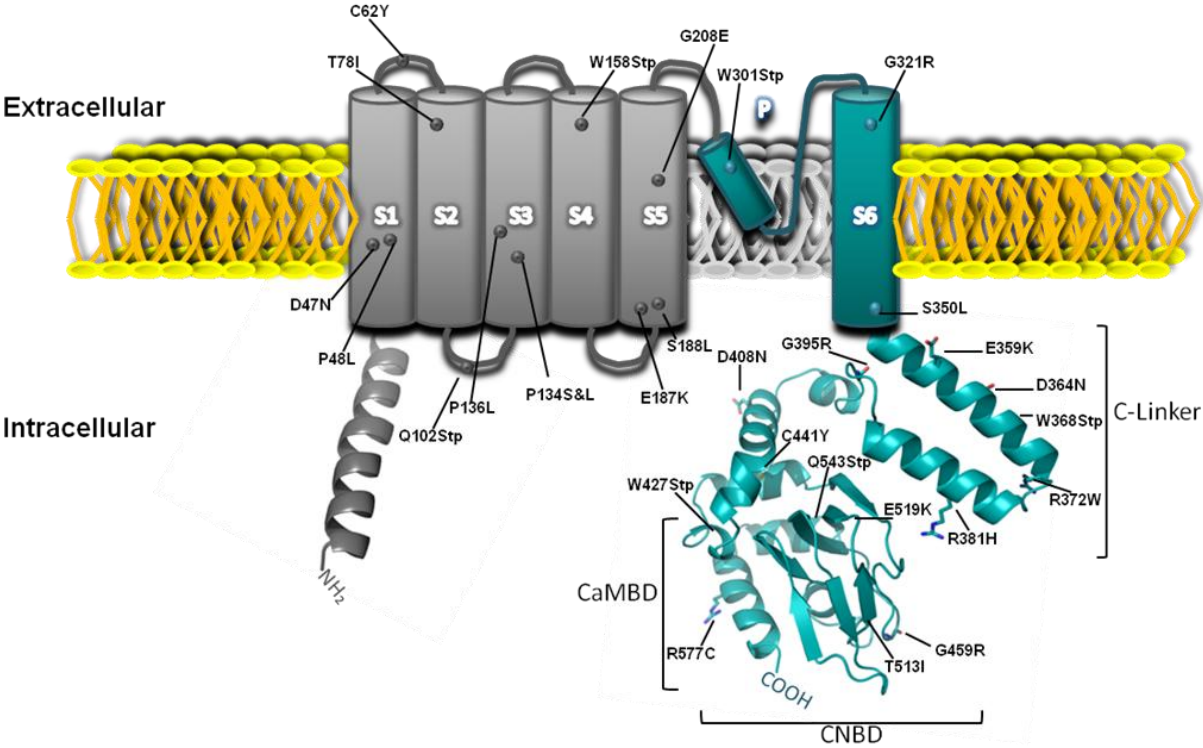
Figure 4.1: Location of the 29 mutations with respect to the proposed topological model of AtCNGC11/12 (12) including the six transmembrane domains (S1–S6), the ion pore (P), the C-linker and the cyclic nucleotide-binding domain (CNBD). See Table 4.1 for details.

Table 4.1: Summary of intragenic mutations in *AtCNGC11/12*

ID No.	Residue No.	Original seq.	Mutated Seq.	Residue change[a]	Location
S1	158	TGG	TGA	W:STP	S_3-S_4 loop
S5	301	TGG	TGA	W:STP	Pore
S13	187	GAA	AAA	E:K	S_4-S_5 loop
S17	441	TGC	TAC	C:Y	CNBD
S23	427	TGG	TGA	W:STP	C-linker
S35	359	GAG	AAG	E:K	C-linker
S56	188	TCA	TTA	S:L	S_4-S_5 loop
S58[b]	557	CGC	TGC	R:C	CNBD
S73[c]	519	GAA	AAA	E:K	CNBD
S80	62	TGC	TAC	C:Y	S_2 Domain
S81	395	GGA	AGG	G:R	C-linker
S82	47	GAT	AAT	D:N	S_2 Domain
S83	364	GAC	AAC	D:N	C-linker
S84	350	TCA	TTA	S:L	C-linker
S85	368	TGG	TGA	W:STP	C-linker
S88	102	CAA	TAA	Q:STP	S_2-S_3 loop
S89	134	CCC	TCC	P:S	S_3 Domain
S92	136	CCT	CTT	P:L	S_3 Domain
S94	78	ACT	ATT	T:I	S_2 Domain
S100	459	GGG	AGG	G:R	CNBD
S101	208	GGG	GAG	G:E	S_5 Domain
S104	48	CCT	CTT	P:L	S_1 Domain
S134	134	CCC	CTC	P:L	S_3 Domain
S135	372	CGG	TGG	R:W	C-linker
S136[b]	543	CAA	TAA	Q:STP	CNBD
S137	381	CGC	CAC	R:H	C-linker
S138	321	GGG	AGG	G:R	S_6 Domain
S140	513	ACC	ATC	T:I	CNBD
S144	408	GAC	AAC	D:N	C-linker

[a]; STP: stop codon; [b]; previously described in Chin *et al.*, 2010; [c]; previously described in Baxter *et al.*, 2008.

A/T conversions (Table 4.1). One exception, suppressor 81 (S81), has two single nucleotide mutations within one triplet which include a rare conversion of A to G. The mutations are located across all domains except the cytosolic N-terminus. All mutants exhibited no readily discernible phenotypes compared to wild type plants, similar to the previously published mutants, S58, S73 and S136 (data not shown; Baxter *et al.*, 2008, Chin *et al.*, 2010).

4.3.2. S100 and S137 are counterparts of achromatopsic human CNGA3 mutants and show complete suppression of AtCNGC11/12-induced phenotypes in planta and lost channel function in yeast

CNGA3 is a human *CNGC* gene that encodes one subunit of the cGMP-gated cone photoreceptor CNGC (Kaupp and Seifert, 2002). Wissinger *et al.* (2001) reported the first comprehensive screen for *CNGA3* mutations in families with hereditary cone photoreceptor disorders. They described 46 mutations in *CNGA3* that cause autosomal recessive complete achromatopsia linked to chromosome 2q11. Previously, we reported that the *AtCNGC11/12* suppressor 73 (S73) that has a mutation in the CNBD, is a counterpart of one of these human mutants (Figure 4.1; Table 4.1; Baxter *et al.*, 2008). This suggested an inherent level of conservation between plant and animal CNGCs, and further indicated that the suppressor screen for *cpr22* is a useful tool to discover residues that are functionally important for CNGCs in general. In this study, we further investigate other mutations in *AtCNGC11/12* that are in structurally equivalent positions to those in human mutants.

First, three dimensional computational analysis was conducted for 12 suppressor mutations (S17, S23, S35, S81, S83, S84, S85, S100, S135, S137, S140, S144) that are located in the cytoplasmic C-terminal region (Figure 4.1 and Table 4.1), since this region contains important regulatory domains. As a template, the crystal structure of the cytoplasmic C-terminal region of a hyperpolarization-activated cyclic nucleotide modulated (HCN) channel, SpIH (crystallized with cAMP; Flynn *et al*., 2007; PDB ID: 2PTM) that possesses the highest structural similarity to AtCNGC11/12 among the currently available crystal structures of cytosolic C-termini, was used. Simultaneously, human CNGA3 mutations from Wissinger *et al*. (2001) that are located in similar areas to the selected 12 suppressor mutations were also modeled using the SpIH crystal structure. Two mutants, S100 and S137, were identified to be equivalent to two CNGA3 mutants. S100 has a single amino acid substitution Glycine (G) 459 to Arginine (G459R) that is located at the loop between the first and the second β sheet (β1 and β2) in the β-barrel structure in the CNBD (Figure 4.2). S137 also has a single amino acid substitution Arginine (R) 381 to Histidine (R381H) that is located in the B' helix of the C-linker domain (Figure 4.2). From a structural point of view, AtCNGC11/12:G459R (S100) and AtCNGC11/12:R381H (S137) are located in equivalent positions as the human mutations, CNGA3:G513E and CNGA3:R436W, respectively (Figure 4.3, Wissinger *et al*. 2001). These two residues are well conserved in both plants and animals. Both G459 and R381 are conserved in nineteen out of twenty *A. thaliana* CNGCs. The conservation of R381 and G459 was investigated using various CNGCs from different organisms. As shown in Table 4.2, both residues were remarkably well conserved among a diverse range of organisms except the bovine olfactory epithelium

CNGC channel, which has a lysine (K) instead of an arginine (R), where lysine and arginine share similar biochemical properties. Thus, the high degree of conservation of these two residues among CNGCs of various organisms strongly suggests the importance of these two locations for CNGC channel function.

As shown in Figure 4.4a (upper panels), the *A. thaliana* suppressor mutants, S100 and S137, show no detectable morphological differences compared to wild type plants, indicating an alteration of AtCNGC11/12 channel function. The original mutant, *cpr22,* induces multiple pathogen resistance responses, including hypersensitive response-like programmed cell death without pathogen infection (Yoshioka *et al.*, 2001). Thus, spontaneous cell death was analyzed by microscopic analysis using trypan blue staining. As shown in Figure 4.4a (lower panels), spontaneous cell death is also suppressed in both S100 and S137, which correlated with the suppression of morphological phenotypes (*i.e.* lethality). The loss of spontaneous cell death formation was also confirmed quantitatively by ion leakage analysis (Figure 4.4b). The expression of *AtCNGC11/12* (*AtCNGC11/12:G459R* in S100 and *AtCNGC:R381H* in S137) were confirmed by semi-quantitative reverse transcription-PCR (RT-PCR). No significant difference in the expression levels of *AtCNGC11/12* was detected in S100 and S137 compared to *cpr22* (Figure 4.4c), indicating that the suppression of the *cpr22*-related phenotypes in S100 and S137 is attributable to alterations in channel function rather than a loss of expression of *AtCNGC11/12*.

Figure 4.2
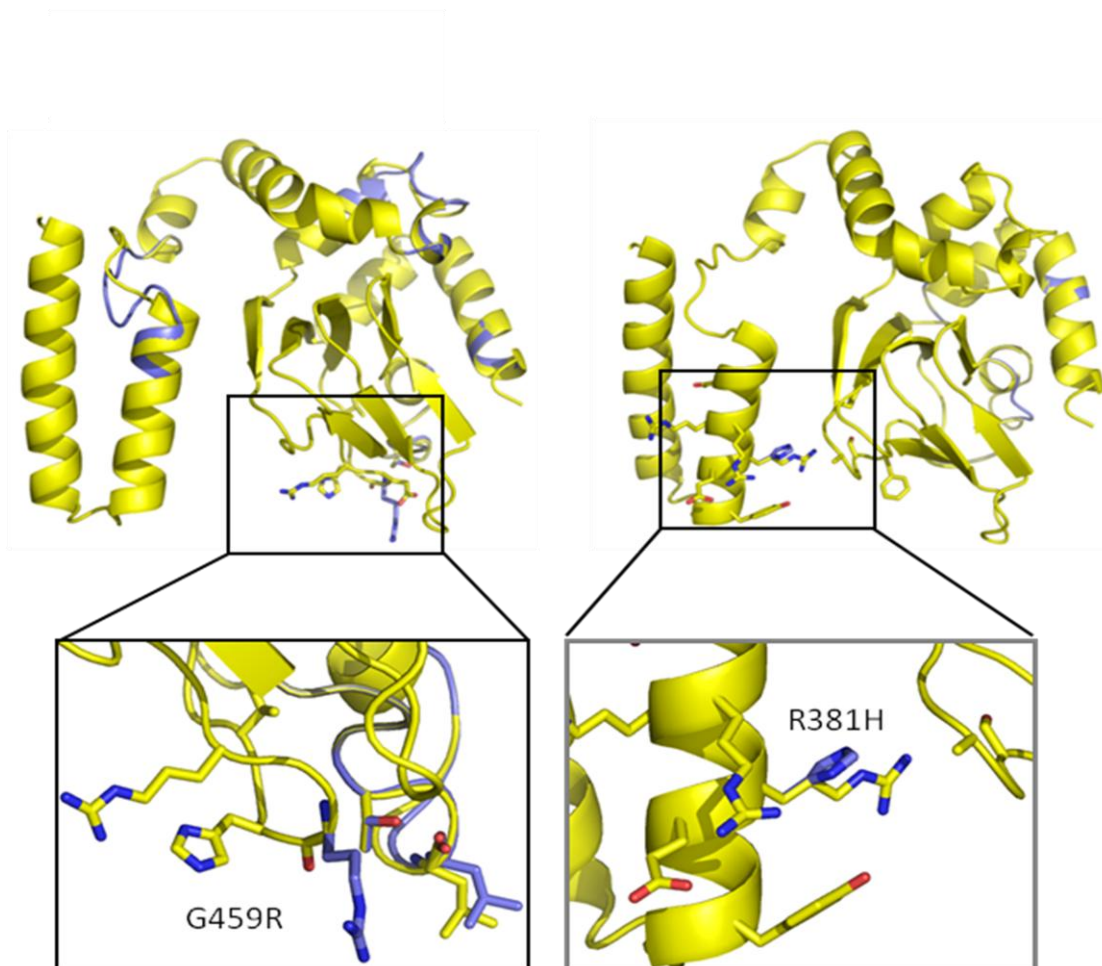
Figure 4.2: Computational structural modeling of the cytoplasmic C-terminal region of AtCNGNC11/12, AtCNGC11/12:G459R and AtCNGC11/12:R381H. Yellow color indicates AtCNGC11/12, blue color indicates the mutants. Left panel: overlaid models of AtCNGNC11/12 and AtCNGC11/12:G459R. Right panel: overlaid models of AtCNGNC11/12 and AtCNGC11/12:R381H. The protein sequence from the residues after the sixth transmembrane domain (S350 to R569 in AtCNGC11/12; EU541497) with and without mutations was modeled to the crystallized SpIH structure (Flynn *et al*., 2007, PDB no. 2PTM).

Figure 4.3
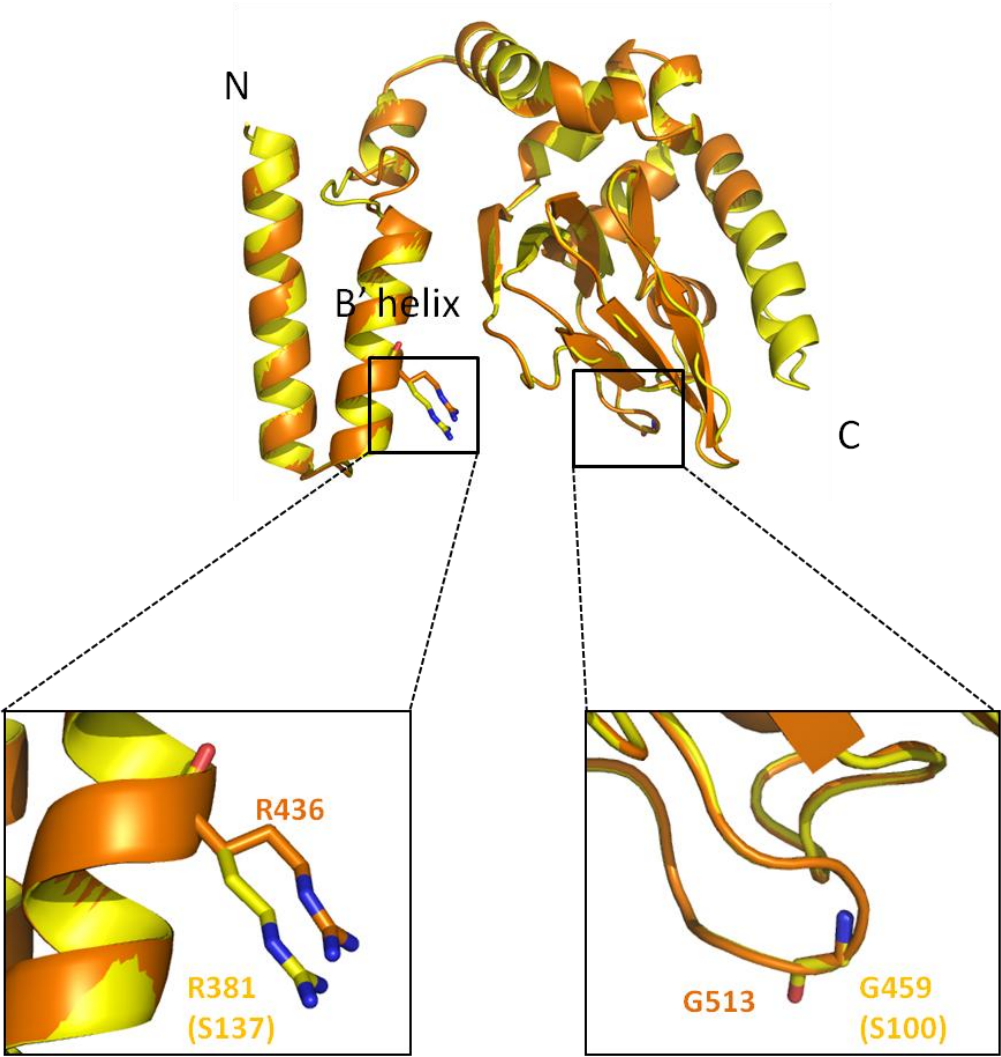
Figure 4.3: Superimposition of structural models of AtCNGC12 and CNGA3. Yellow: AtCNGC 12, Orange: CNGA3. Mutant ID numbers are indicated in parenthesis

Table 4.2: Conservation of R381 and G459 among various organisms

	Organism[a]						
Residue No.[b]	HC	MC	CC	HR	BO	DM	CE
R381	R	R	R	R	K	R	R
G459	G	G	G	G	G	G	G

[a] HC; human cone photoreceptors CNGA3 (NP_001289), MC; mice cone photoreceptor a-subunits CNG(A)3 (CAB89685), CC; chicken cone photoreceptor a-subunit CNG channel (CAA61757), HR; human rod photoreceptor alpha subunit CNGA1(NP_000078), BO; bovine olfactory epithelium CNG channel (CAA38754), DM; *Drosophila melanogaster* CNG channel (CAA61760), CE; *Caenorhabditis elegans* tax4 CNG channel (CAP16270)

[b] Residue No. in AtCNGC11/12

Figure 4.4

(a)

Bar = 50 μM

(b)

(c)
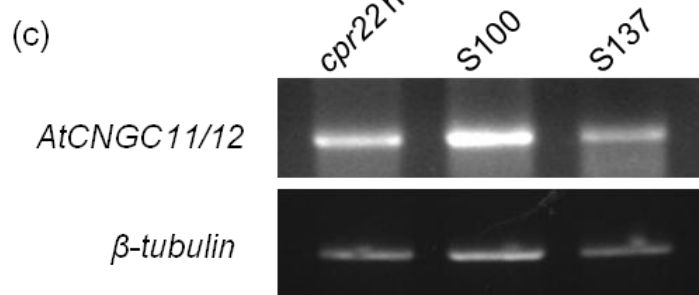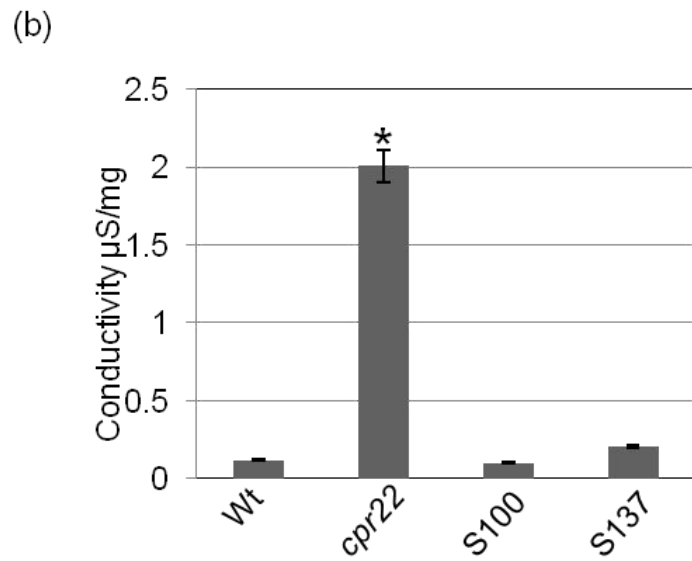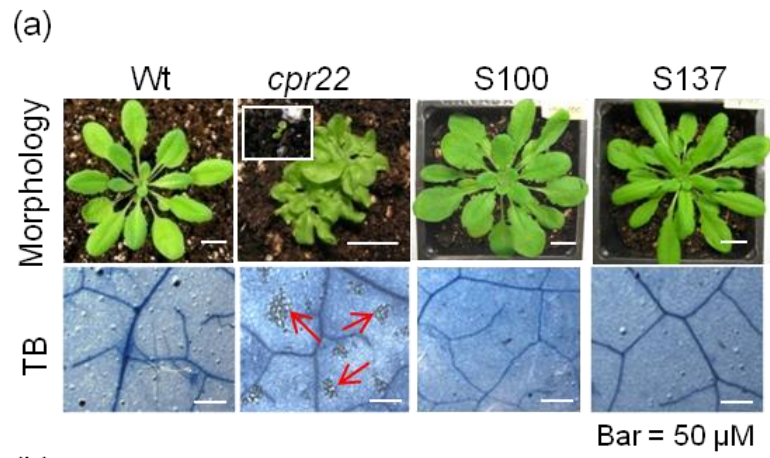
Figure 4.4: Characterization of the suppressor mutants S100 and S137 (a) Morphological phenotypes and spontaneous cell death formation of wild type (Wt), *cpr22*, and suppressor S100 and S137. A *cpr22* homozygous plant is shown in the white square. *cpr22* homozygotes are lethal after the cotyledon stage under ambient temperature and humidity (22°C, 65% RH). Cell death was detected by trypan blue (TB) staining (red arrows indicate dead cells). Approximately 4-week-old plants were used. (b) Quantitative analysis of cell death by electrolyte leakage in *cpr22*, S100, S137, and Wt. Asterisks represent statistically significant differences ($P>0.05$) when compared to Wt (c) RT-PCR analysis of *cpr22*, S100 and S137 for *AtCNGC11/12* expression. *β-tubulin* served as a loading control. 25 cycles for each analysis were applied.

To confirm the suppression of *AtCNGC11/12*-induced phenotypes, *Agrobacterium*-mediated transient expression of *AtCNGC11/12:G459R* and *AtCNGC11/12:R381H* was conducted in *Nicotiana benthamiana.* This system was previously established to analyze HR cell death development and was recently used to show that AtCNGC11/12 induces cell death in a synchronized manner (Urquhart *et al*., 2007). As shown in Figure 4.5a, cell death was induced by the transient expression of *AtCNGC11/12* but not *AtCNGC11/12:G459R*, *AtCNGC11/12:R381H,* or empty vector control. Transcription and translation of *AtCNGC11/12, AtCNGC11/12:G459R* and *AtCNGC11/12:R381H* were monitored by semi-quantitative RT-PCR and fluorescence of green fluorescence protein (GFP) that was fused to the C-terminal end of each gene. As shown in Figure 4.5b and 4.5c, there is no significant difference between the expression of the original *AtCNGC11/12* and the two mutated genes. Therefore, the suppression of cell death is not due to the expression levels of the mutated genes. Taken together, the two mutations, *G459R and R381H,* in *AtCNGC11/12* suppress the induction of *AtCNGC11/12*-mediated phenotypes *in planta.*

So far, precise characterizations of S73 and S58 have been reported and it has been suggested that the two mutations affect AtCNGC11/12 function in fundamentally different ways; S73 (AtCNGC11/12:E519K) abolished basic channel function of AtCNGC11/12, whereas S58 (AtCNGC11/12:R557C) retains its channel function, but displayed alterations in its regulation (Baxter *et al*., 2008, Chin *et al*., 2010; Abdel-Hamid *et al*., 2010). To investigate whether *AtCNGC11/12:G459R* and *AtCNGC11/12:R381H* have lost basic channel function, functional complementation analysis was conducted in the *trk1, trk2* K$^+$ uptake-deficient yeast mutant, RGY516 (Ali

et al., 2006). Enhanced growth of mutant yeast has been previously demonstrated upon expression of various plant CNGCs (Köhler *et al.*, 1999; Leng *et al.*, 1999; Ali *et al.*, 2006; Urquhart *et al.*, 2007; Baxter *et al.*, 2008; Chin *et al.*, 2010). RGY516, transformed with AtCNGC11/12, *AtCNGC11/12:G459R* or *AtCNGC11/12:A381H* was tested in APG medium. As shown in Figure 4.6a, AtCNGC11/12 was able to complement the *trk1*, *trk2* growth defect phenotype as expected, whereas *AtCNGC11/12:G459R* and *AtCNGC11/12:R381H* could not. Expression of the genes in yeast was confirmed by semi-quantitative RT-PCR and no significant difference between AtCNGC11/12 and mutants was detected (Figure 4.6b).

Collectively, these data indicated that both G459R and R381H mutations in *AtCNGC11/12* suppress *AtCNGC11/12*-induced phenotypes by abolishing *AtCNGC11/12* channel function.

4.3.3. Computational analysis suggests an effect of G459R and R318H on inter-subunit, but not intra-subunit interactions of CNGCs

To investigate the molecular mechanisms that cause the suppression of channel function by the G459R or R381H mutations, further computational analyses were conducted. A previously published mutation, *AtCNGC11/12:E519K* (S73), caused alterations in intra-subunit interactions (Baxter *et al.*, 2008). Our computational modeling did not find any obvious disruption of intra-subunit interactions by G459R or R381H (Figure 4.2). This was also the case with equivalent mutants in human CNGA3, 513E and R436W (Figure 4.7), suggesting that these residues/mutations do not play

Figure 4.5

(a)

(b)

(c)

Bar = 10 μM
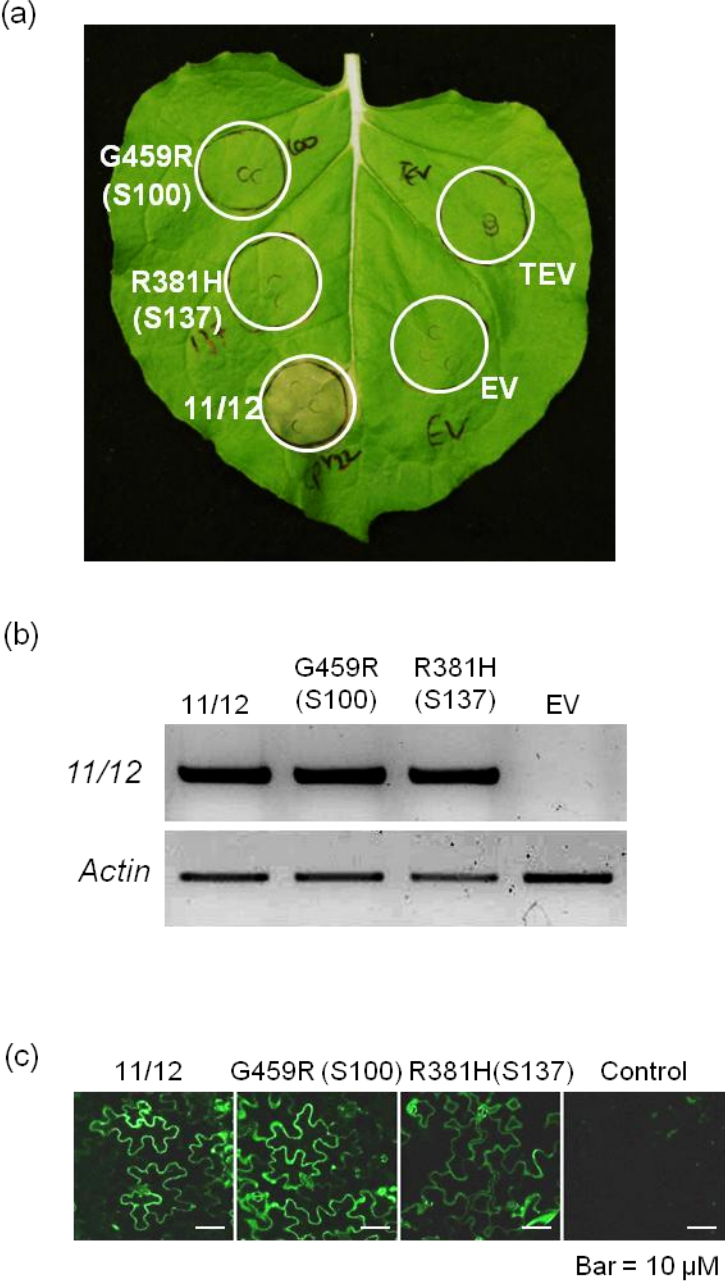
Figure 4.5: Cell death induced by *AtCNGC11/12* in *Nicotiana benthamiana* was suppressed by S100 (G459R) and S137 (R381H). (a) Induction of cell death in *N. benthamiana* after infiltration of *Agrobacterium* carrying *AtCNGC11/12:GFP, AtCNGC11/12:G459R:GFP, AtCNGC11/12:R381H:GFP*, empty vector (EV). (b) RT-PCR analysis of leaf discs from *N. benthamiana* leaves expressing *AtCNGNC11/12:GFP*, *AtCNGC11/12:G459R:GFP* or *AtCNGC11/12:R381H:GFP* 24h after infiltration. *Actin* served as a loading control (25 cycles). (c) Expression of *AtCNGNC11/12:GFP*, *AtCNGC11/12:G459R:GFP* or *AtCNGC11/12:R381H:GFP* in *N. benthamiana* leaves at 32 h post-infiltration was monitored by confocal microscopy.

Figure 4.6
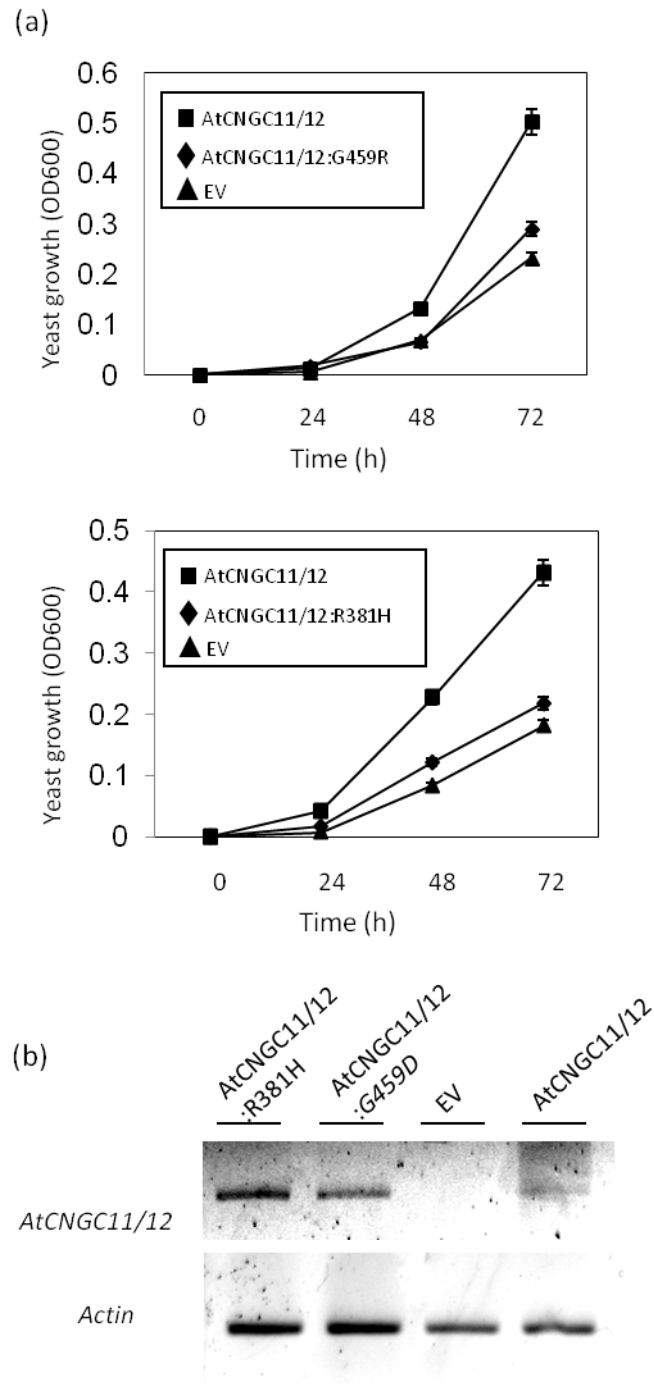
Figure 4.6: Yeast complementation analysis using the K$^+$-uptake-deficient mutant RGY516. (a) *AtCNGC11/12*, but not *AtCNGC11/12:G459R*, *AtCNGC11/12:R381H* or empty vector (EV) complemented the K$^+$-uptake deficiency of RGY516. (b) RT-PCR analysis of yeast carrying *AtCNGNC11/12*, *AtCNGC11/12:G459R*, *AtCNGC11/12:R381H* or empty vector (EV). Data are the average of three biological repeats ±SE. *Actin* served as a loading control (25 cycles).

significant roles in mediating intra-subunit interactions. We then analyzed the possible alterations of these mutations on inter-subunit interactions. It has been reported that native photoreceptor CNGCs are heterotetrameric complexes composed of two structurally related subunit types, A and B subunits (Kaupp and Seifert 2002). On the other hand, so far there is no experimental evidence that indicates the multimerization of plant CNGC subunits. In analogy to animal CNGCs, it has been speculated that plant CNGCs also form tetramers. Thus, the tetramer of the cytosolic C-terminal region of AtCNGC11/12 (same as wild type AtCNGC12) was modeled (Figure 4.8a). This model was created as a homotetramer since there is no information about the composition of plant CNGCs, except that both AtCNGC11 and 12 subunits can function as homomeric channels when expressed in yeast (Yoshioka *et al*., 2006; Urquhart *et al*., 2007; Baxter *et al*., 2008). As shown in Figure 4.8b, G459 does not have any interactions with a neighboring subunit in this tetramer model (Figure 4.8b upper left panel), whereas G459R creates a new salt bridge with D433 in a neighboring subunit (Figure 4.8b upper right panel). This was also the case when we modeled the equivalent mutant of CNGA3, CNGA3:G513E (Figure 4.8b lower panels). It has been suggested that in CNG channels of native rod cells, two distinct subunits, CNGA3 and CNGB3, form heterotetramers comprising of three CNGA3 and one CNGB3 subunits (Kaupp and Seifert, 2002). Thus, such a heterotetramer was modeled to examine the role of G513, which is equivalent to G459 in AtCNGC11/12 (Figure 4.8b). Figure 4.8b lower panels show the area of G513 in CNGA3-CNGA3 interaction in this heterotetramer. G513 in CNGA3 does not interact with another subunit, similar to G459 in AtCNGC11/12 (Figure 4.8b lower left panel), whereas G513E created a repulsion with E457 in a neighboring subunit (Figure 4.8b

lower right panel). A similar model was made for G513 in a CNGA3-CNGB3 interaction (Figure 4.9b). Collectively, these data suggest that both G459R in AtCNGC11/12 and G513E in CNGA3 created a new interaction and a repultion with a residue in a neighboring subunit respectively, which may cause the disruption of channel function.

On the other hand, the inter-subunit interaction model of AtCNGC11/12 indicates that R381 forms a salt bridge with E412 in a neighboring subunit (Figure 4.8c upper left panel). This salt bridge was disrupted by the R381H mutation (Figure 4.8c upper right panel). As expected, the counterpart mutation of AtCNGC11/12:R381H in CNGA3, R436W, also disrupts a salt bridge between R436 and E467 of the neighboring subunit in the CNGA3-CNGA3 interaction (Figure 4.8c lower panels). Additionally, R436W also disrupts an additional salt bridge formed between R436 and D507 in the same subunit (intra-subunit interaction). Again, a similar prediction was made for the CNGA3-CNGB3 interaction (Figure 4.9c).

Taken together, these computational models strongly suggest that G459 and R381 in AtCNGC11/2 likely influence the interaction between subunits similar to their counterparts in human CNGA3. Furthermore, these models demonstrate that the structural roles of these residues in both plant and animal CNGCs are conserved.

Figure 4.7
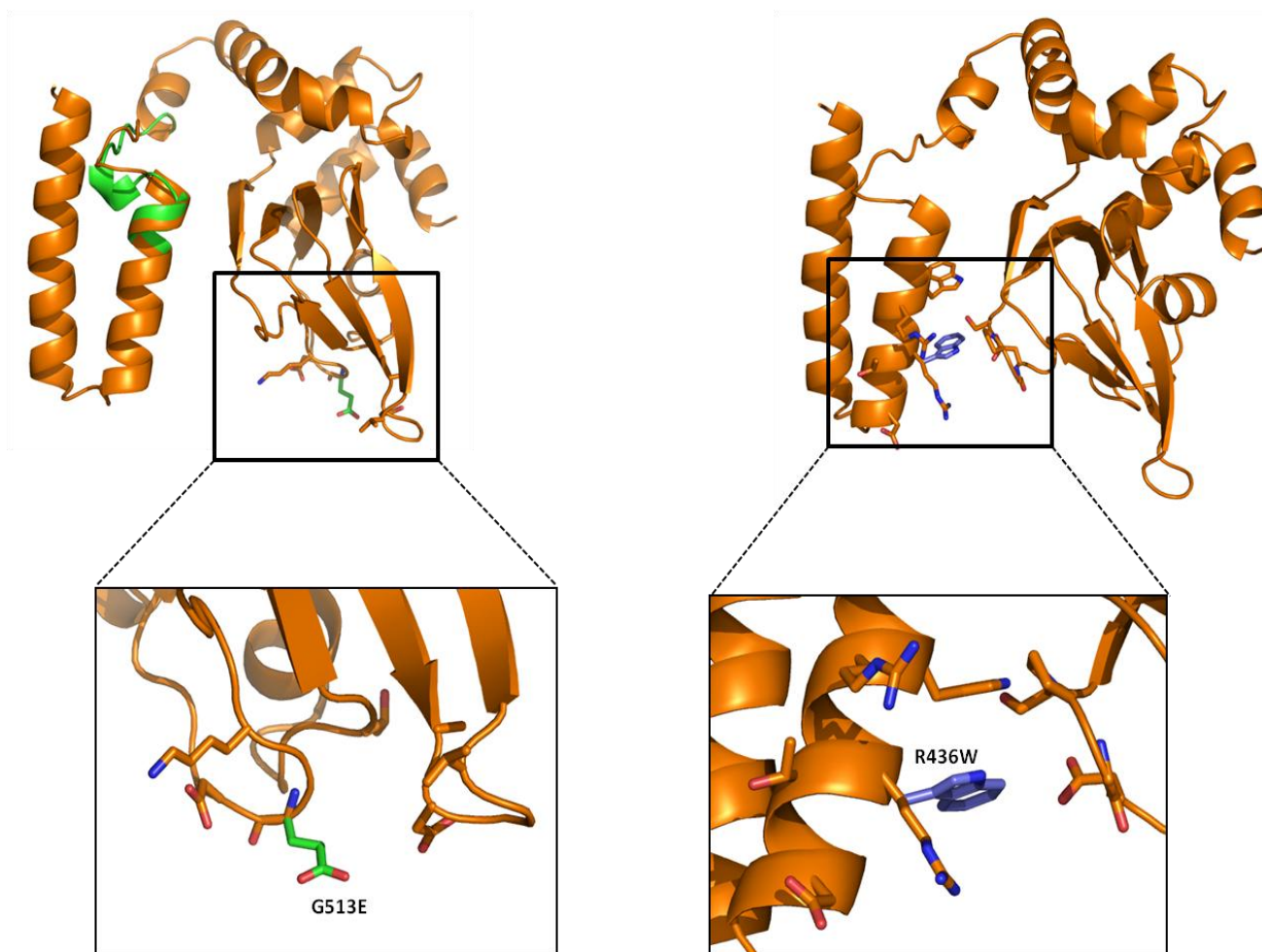
Figure 4.7: Computational structural modeling of the cytoplasmic C-terminal region of CNGA3:G513E and CNGA3:R436W. Yellow color indicates CNGA3, blue color indicates the mutants. Left panel: overlaid models of CNGA3 and CNGA3: G513E. Right panel: overlaid models of CNGA3and CNGA3: R436W. The protein sequence from the residues after the sixth transmembrane domain (N407 to E600 in CNGA3; NP_001289) with and without mutations was modeled to the crystallized SpIH structure (Flynn *et al.*, 2007, PDB no. 2PTM).

Figure 4.8
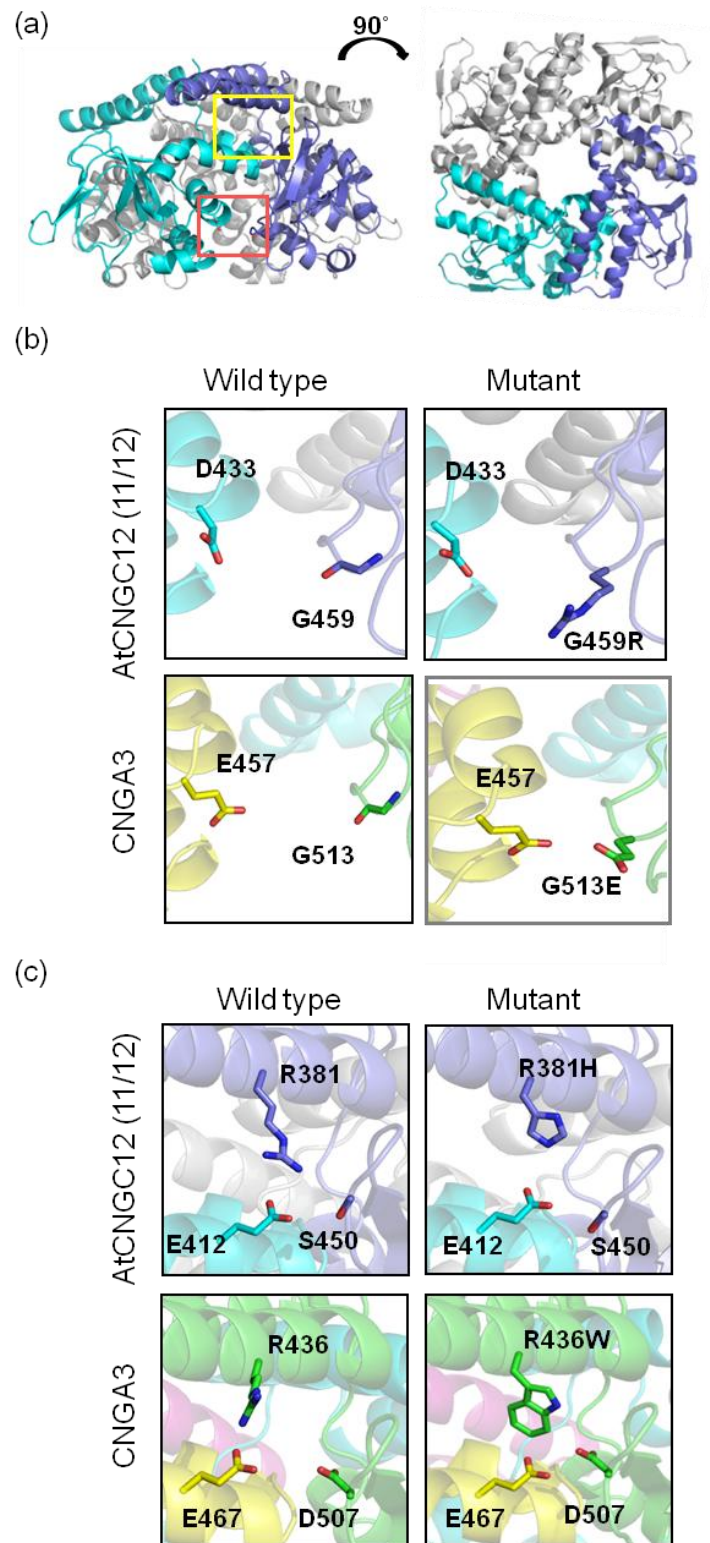
Figure 4.8: Computational structural modeling of tetramer structure of the cytoplasmic C-terminal region of AtCNGNC11/12 (12), AtCNGC11/12:G459R, AtCNGC11/12:R381H, CNGA3, CNGA3:G513E, and CNGA3:R436W. (a) AtCNGC11/12 (EU541497) tetramer viewed perpendicular (left) and parallel (right). Two subunits are shown by different colors to depict their interaction. (b) Close-up of the red box in (a) and the equivalent area of CNGA3 (NP_001289). (c) Close-up of the yellow box in (a) and the equivalent area of CNGA3.

Figure 4.9

(a)

(b)

Wild type   Mutant

(c)

Wild type   Mutant
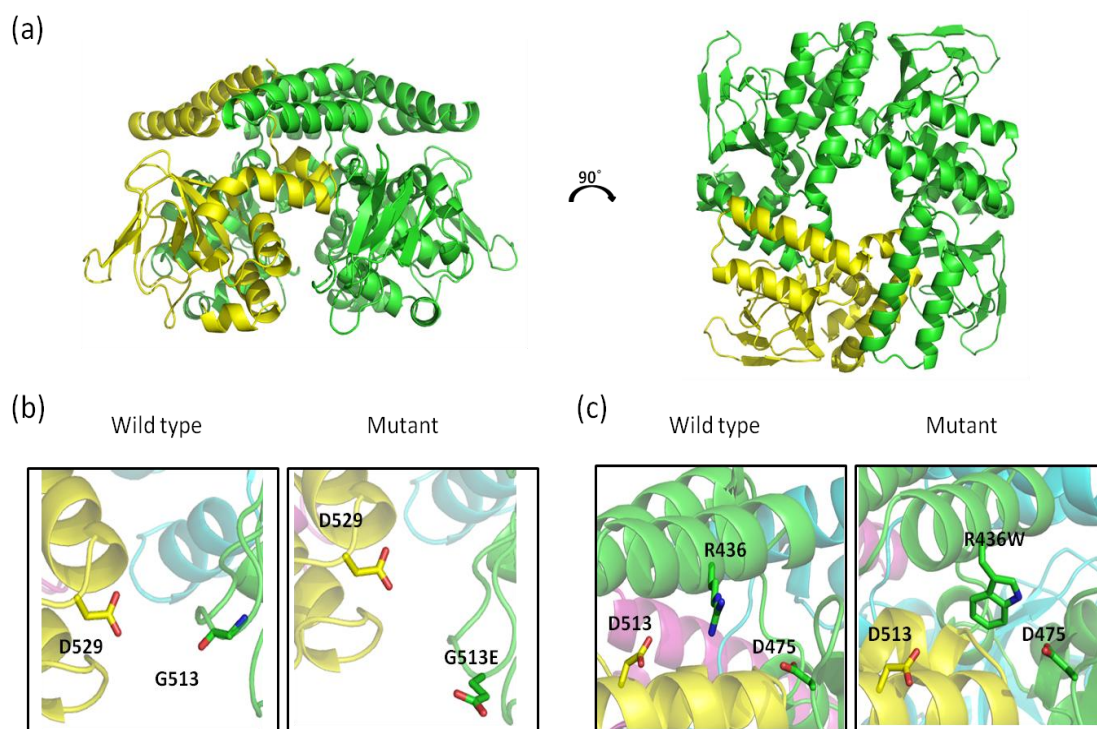
Figure 4.9: Computational structural modeling of tetramer structure of the cytoplasmic C-terminal region of human rod cell CNGC hetero-tetramer (a) Human rod cell CNGC tetramer composed of three CNGA3 (green) and one CNGB3 subunits (yellow) viewed perpendicular (left) and parallel (right).(b) CNGA3-CNGB3 interaction of CNGA3:G513 and CNGB3:D529 (Wild type) and CNGA3:G513E and CNGB3:D529 (Mutant). (c) CNGA3-CNGB3 interaction of CNGA3: R436 and CNGB3:D475 (Wild type) and CNGA3:R436W and CNGB3: D475 (Mutant).

4.3.4. FPLC analysis indicates alterations of multimerization of S100 and S137 mutants

Electrophysiological studies and biochemical analyses of animal CNGCs have indicated that several distinct subunits form functional channels *in vivo* (Kaupp and Seifert 2002). In contrast, the native composition of CNGCs *in planta* remains to be elucidated, and there is currently no information available about the inter-subunit interactions in plant CNGCs (Moeder *et al.*, 2011). Thus, to explore the above hypothesis that the two mutations, AtCNGC11/12:G459R and AtCNGC11/12:R381H, affect channel function by altering the tetramerization of the channels, recombinant proteins of the cytosolic C-terminal region of both mutants as well as AtCNGC11/12 were expressed in *E.coli* and multimerization was analyzed by fast protein liquid chromatography (FPLC).

Previously, the recombinant cytosolic C-terminal region of AtCNGC11/12 was expressed in *E.coli* (Baxter *et al.*, 2008). Although it was successful, the expression level was relatively low (Baxter and Yoshioka unpublished data). To improve the expression efficiency, a new construct was made in accordance to published data on the crystal structures of the C-terminal regions of HCN2 and SPIH (Zagotta *et al.,* 2003; Flynn *et al.,* 2007). Structural modeling of the C-terminal domain of AtCNGC11/12 (same as AtCNGC12) was performed using the structure prediction tool, Swiss-Model© (http://swissmodel.expasy.org//SWISS-MODEL.html) with both SpIH1 and HCN2 as templates to detect the C-terminal region of the AtCNGC11/12 that structurally aligned with the crystallized C-terminal region of these channels. Based on this model, a fragment beginning at S350, just after the end of the 6th trans-membrane domain (6S),

113

extending through the C-linker and CNBD, and ending at R569 was obtained using RT-PCR from cDNA of *AtCNGC11/12* as a template and the resulting construct was cloned into the *E. coli* expression vector pET28a+ (Novagen, http:// www.emdbiosciences.com/html/NVG/home.html) under the control of the T7 promoter. The expressed protein showed the expected size of 26kD including the polyhistidine tag (HIS tag) and the yield of the expressed protein was significantly higher compared to that of Baxter *et al.* (2008) (data not shown).

Expressed proteins were then subjected to FPLC analysis using a size exclusion column (Superdex-200, GE Health Care). As shown in Figure 4.10a, the elution of the AtCNGC11/12 C-terminal recombinant protein resulted in two peaks. The second peak is about ~26kDa, which is the size of the predicted monomer peptide. The first peak was eluted much earlier (suggesting a mass of > 150 kDa), indicating the multimerization or aggregation of monomer peptides (Figure 4.10a). These peaks were collected separately and subjected to SDS-polyacrylamide gel electrophoresis (PAGE). Under denaturing conditions, both peaks showed the monomeric peptide of ~26kDa, supporting the idea that the first peak is a multimer of the AtCNGC11/12 C-terminal recombinant protein (Figure 4.10b, upper panel). The ratio of the protein amounts of the first and second peaks was 0.35 : 1 (Figure 4.10a). To investigate if the two mutations, G459R and R381H, affect this multimerization/aggregation pattern, both recombinant proteins, the C-termini of AtCNGC11/12:G459R and AtCNGC11/12:R381H, were also subjected to FPLC analysis. As shown in Figure 4.10c, the same two peaks were observed, but the elution pattern of the AtCNGC11/12:G459R protein was shifted towards the first peak resulting in a ratio of the first and the second peak of 0.6 : 1. On

the other hand, although the same two peaks were observed again, the elution pattern of AtCNGC11/12:R381H was shifted towards the second peak resulting in a ratio of the first and the second peak of 0.15 : 1. The two peaks of C-AtCNGC11/12: R381H and AtCNGC11/12:G459R were also collected and subjected to SDS-PAGE as well as Western blotting using an α-His antibody to detect the His-tagged proteins. It was confirmed that the first peak is a multimer of the second peaks similar to AtCNGC11/12 (data not shown and Figure 4.10b, lower panel). This analysis was repeated at least three times using independently extracted recombinant proteins for all three constructs with almost identical results.

The FPLC analysis supports the hypothesis generated by the computational prediction. As shown in Figure 4.8b (upper right panel) G459R seems to create a new salt bridge with D433 in the neighboring subunit. This interaction may cause tighter subunit interactions resulting in the shift towards multimerized peptides shown by the FPLC analysis. Similarly, as explained earlier, R381H seems to disrupt the interaction between R381 and E412 (Figure 4.8c upper right panel). This may be the reason for the shift towards the monomer peak seen in the FPLC analysis, however, the possibility of non-specific aggregation of the peptides cannot be excluded.

Thus, we created mutant peptides by site-directed mutagenesis to address the specificity of the effect of the mutations. The expressed peptides were subjected to the same FPLC analysis. For AtCNGC11/12:G459R, the AtCNGC11/12:D433S construct was generated. D433 is the predicted partner of the salt bridge with G459 (Figure 4.8b). In D433S the charge of the position D433 changes from negative to neutral (Aspartic acid to Serine, Figure 4.11 upper panels). Since G459 is also neutral, this mutation

should not create a salt bridge with G459 (Figure 4.11 upper right panel). When we analyzed the AtCNGC11/12:D433S peptide by FPLC, as shown in Figure 4.10e, the ratio of the first peak and second peak was 0.35 : 1, which is identical to the ratio seen with AtCNGC11/12 in Figure 4.10a. Thus, these data strongly indicate that the salt bridge created by G459R is the cause of the increased multimerization.

For AtCNGC11/12:R381H, the AtCNGC11/12:E412L construct was created by site-directed mutagenesis. As shown in Figure 4.8c (upper panels), R381 forms a salt bridge with E412 in AtCNGC11/12. This bridge was disrupted in AtCNGC11/12:R381H, since the charge has been changed from positive (R) to neutral (H) (Figure 4.8c upper panels and Figure 4.11 lower panels). In AtCNGC11/12:E412L, the partner of the salt bridge of R381 (E412) was mutated to change the charge of this position from negative (E) to neutral (L). By this mutation, the same disruption of the salt bridge should be recreated from the salt bridge partner side. As shown in Figure 4.10f, the FPLC elution pattern of AtCNGC11/12:E412L shifted towards to the second peak as seen with AtCNGC11/12:R381H in Figure 4.10d. The ratio between the first and the second peaks was 0.15 : 1, which is similar to that observed for AtCNGC11/12:R381H. The experiment was repeated twice with independently extracted proteins with the same results.

Taken together, the FPLC analysis indicates that both AtCNGC11/12:G459R and AtCNGC11/12:R381H influence the multimerization of CNGC subunits through the creation/disruption of salt bridges between neighbouring subunits, which support the predictions from our computational modeling.

Figure 4.10

(a) AtCNGC11/12 (12)

(b)

(c) AtCNGC11/12:G459R

(d) AtCNGC11/12:R381H

(e) AtCNGC11/12:D433S
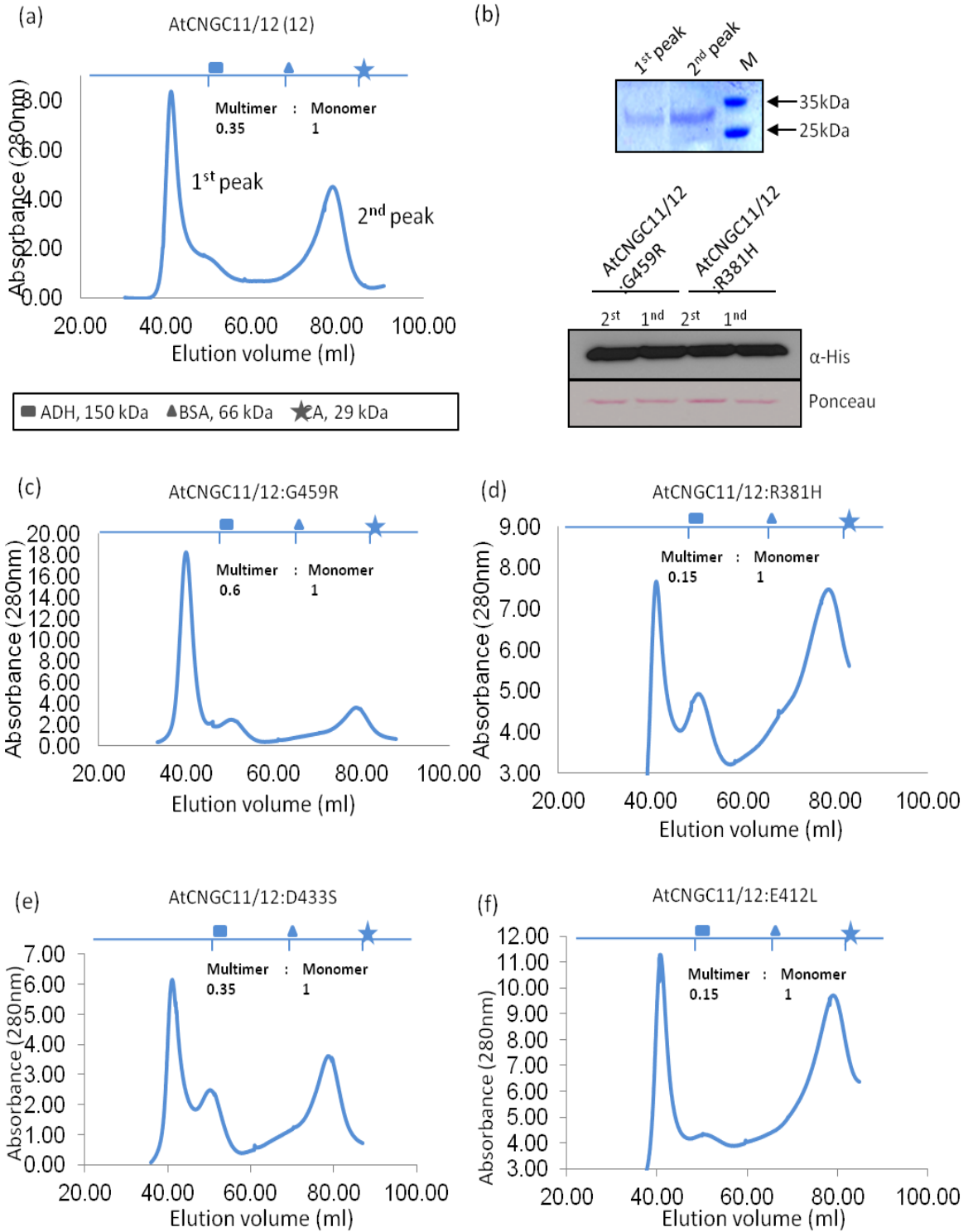
(f) AtCNGC11/12:E412L

Figure 4.10: Analysis of recombinant cytosolic C-terminal peptides (a) Size exclusion chromatography (Superdex-200 16/60 FPLC column) of AtCNGC11/12 C-terminal revealed two peaks. The ratio of 1st (multimer) to 2nd (monomer) peak was 0.35 : 1. Molecular size markers are indicated by square (ADH, 150kDa), triangle (BSA, 66kDa) and star (CA, 29kDa) (b) Upper panel: SDS-PAGE of 1st and 2nd peaks of AtCNGC11/12. Both peaks migrated as monomers under denaturing conditions. Lower panel: Western Blot of 1st and 2nd peak of AtCNGC11/12:G459R AtCNGC11/12:R381H using an α-His antibody. (c) FPLC analysis of AtCNGC11/12:G459R C-terminal peptides showed two peaks. The ratio of 1st to 2nd peak was 0.6 : 1. (d) FPLC analysis of AtCNGC11/12:R381H C-terminal detected two peaks. The ratio of 1st to 2nd peak was 0.15 : 1. (e) FPLC analysis of AtCNGC11/12:D433S C-terminal detected two peaks. The ratio of 1st to 2nd peak was 0.35 : 1. (f) FPLC analysis of AtCNGC11/12:G459R C-terminal detected two peaks. The ratio of 1st to 2nd peak was 0.15 : 1. All experiments were repeated at least two times using independently extracted peptides with almost identical results.

Figure 4.11
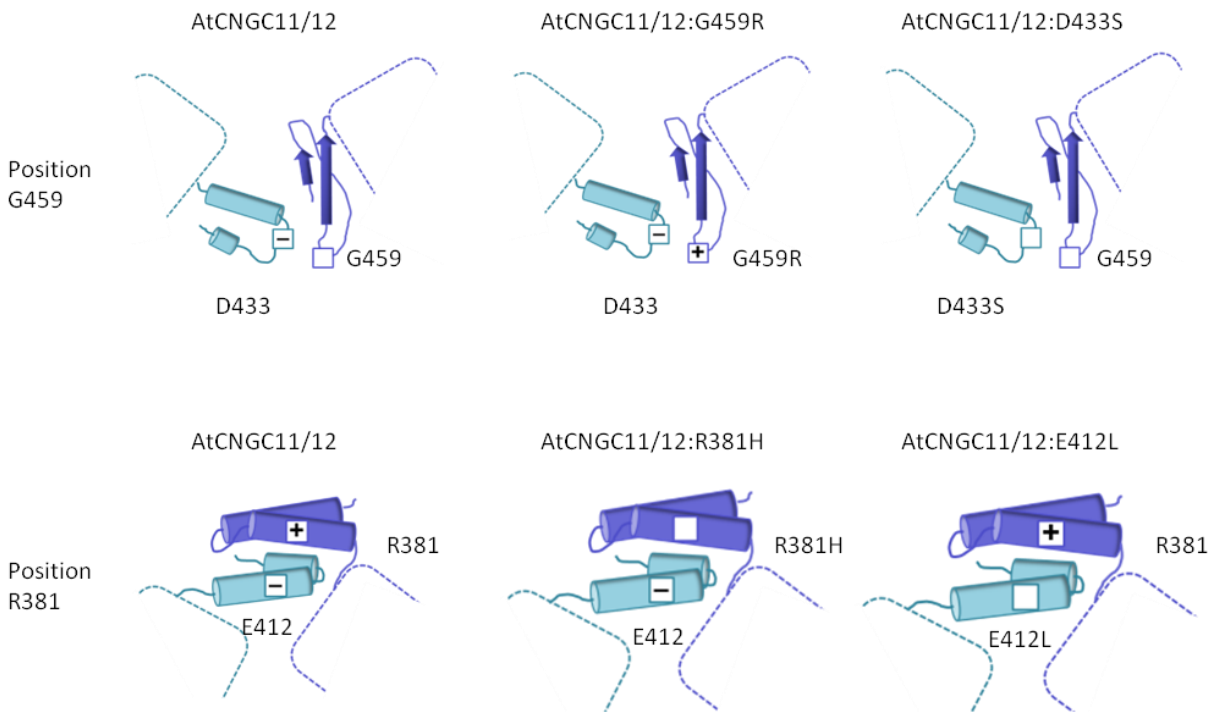
Figure 4.11: Diagram of predicted interactions of G459 and R381 in AtCNGC11/12 tetramer. Squares indicate specific residues with their electric charge. Blank square: neutral residue, square with plus: positively charged residue, square with minus: negatively charged residue. The upper panel shows the interaction of G459 in AtCNGC11/12, AtCNGC11/12:G459R and AtCNGC11/12:D433S, respectively. The lower panel shows the interaction of R381 in AtCNGC11/12, AtCNGC11/12:R381H and AtCNGC11/12:E412L. Only two subunits are shown by two different colors to depict the interactions.

4.4. Discussion

The oligomerization (tetramerization) of plant channels has been well studied for plant shaker-type potassium channels such as AKT1, SKOR, GORK, KDC1, KAT1 and KAT2, which have a similar structure to plant CNGCs (Daram *et al.*, 1997; Dreyer *et al.*, 1997; Zimmermann *et al.*, 2001; Urbach *et al.*, 2000; Dreyer *et al.*, 2004; Naso *et al.*, 2009). For example, Daram *et al.* (1997) demonstrated the tetramerization of *A. thaliana* AKT1 biochemically. They successfully expressed full length of AKT1 in *Sf9* insect cells. Size-exclusion chromatography using recombinant AKT1 revealed monomers, dimers and tetramers of AKT1. Here, although we have not observed peaks that show the exact size of dimers or tetramers, we have detected monomers and multimers by size-exclusion chromatography. The reason for not seeing peaks that show the exact size of the tetramers is currently unknown, but it could be related to the difference in biochemical characteristics between AKT1 and *A. thaliana* CNGCs.

Using a yeast two hybrid system Daram *et al.* (1997) also identified two important domains in AKT1 that are involved in subunit interactions. Both domains are located in the cytosolic C-terminal region: one at the beginning of this region including the CNBD and the other at the C-terminal end of this region. The former one, which was revealed to be the essential domain for subunit interactions, is equivalent to the C-linker domain of plant CNGCs, which contains mutation S137 characterized in this study. This indicates the importance of the C-linker domain for subunit interaction of plant shaker-type channels in general.

S137 (R381H) is one of the most interesting positions among the 29 mutations discovered in this study. Not only is this mutation equivalent to a human CNGA3

mutation that causes achromatopsia (Wissinger *et al.*, 2001), but this position was previously reported to be important for subunit interaction, affecting channel gating in hyperpolarization-activated cyclic nucleotide-modulated channel 2 (HCN2) and CNGA1 (Craven and Zagotta, 2004). The C-linker domain comprises of six α-helices (A'-F') and the CNBD comprises of three α-helices (A-C) and eight anti-parallel β-strands (β 1 - β 8) that form a β-barrel structure between the A and B helices. Through the crystal structure of the tetramer of the cytosolic C-terminal region of HCN2, Zagotta *et al.* (2003) discovered that all of the inter-subunit interactions in the cytosolic C-terminal region occur between the C-linker domains of each subunit. The interacting region was described as "elbow on the shoulder" where the A' and B' helices of one subunit (elbow) rest on the C' and D' helices (shoulder) of its neighboring subunit and their interaction involves many hydrogen bonds, hydrophobic interactions, and salt bridges (Zagotta *et al.*, 2003). Craven and Zagotta (2004) further conducted a precise analysis of one of these C-linker interactions and identified two salt bridges: an important inter-subunit interaction between the C-linkers of neighboring subunits, and a less important intra-subunit interaction between the C-linker and its CNBD. These two salt bridges are created by three residues, one positively charged residue in the B' helix of the C-linker (R/K), and two negatively charged residues: one on D' helix at the C-linker domain (E) and another in the loop between β1 and β2 of the CNBD domain (D) (Figure 4.12a). Based on our model, the positions of these three residues are equivalent to R436 (positively charged), E467 and D507 (negatively charged) in CNGA3 (Figure 4.8c, lower left panel). Craven and Zagotta (2004) created point mutations to disrupt these salt bridges in HCN2 and CNGA1 and discovered that the disruption of these salt bridges

favored channel opening. In other words, these interactions are involved in stabilizing the resting configuration (closed form) of the channels. These three residues are very well conserved among HCN and CNG channels (Craven and Zagotta, 2004 and Figure 4.12a), further indicating their importance. As explained in the result section, R436 in CNGA3 is the equivalent position to R381 in S137 in AtCNGC11/12 (12). Furthermore, our computational modeling revealed a salt bridge between R381 and E412 in the neighboring subunit (Figure 4.8c upper left panel) which is almost identical to the interaction between R436 and E467 in CNGA3 (Figure 4.8c lower left panel), as well as the interaction in HCN2 and CNGA1 described by Craven and Zagotta (2004). R381 and E412 are conserved in 19 out of 20 *A. thaliana* CNGCs, further indicating the importance of this salt bridge (data not shown). The less important second salt bridge between R436 and D507 in CNGA3 (Figure4.8c lower left panel), which is involved in intra-subunit interaction, does not exist in 18 out of 20 *A. thaliana* CNGCs including AtCNGC12 (11/12). This salt bridge was predicted when we modeled homo-tetramers of AtCNGC2 and AtCNGC4 (Figure 4.12b). Both AtCNGC2 and 4 have a negatively charged E450 instead of S450 at this position and this residue creates a salt bridge with R381 similar to that formed between D507 and R436 in CNGA3 or the equivalent positions in HCN2 and CNGA1 (Figure 4.12a and Craven and Zagotta, 2004). Based on sequence similarity, the 20 members of the *A. thaliana* CNGC family are classified into four groups, I, II, III and IV, while group IV was further divided into IVA and IVB. *AtCNGC2* and *4* are the sole members of the group IVB and share high sequence similarity as well as physiological function (Mäser *et al.*, 2001; Moeder *et al.*, 2011).

Figure 4.12

(a)

C-linker   CNBD

B'   C'   D'   E'   F'   A   β1

```
HCN2         FRQKIHDYYEHRYQG-KMFDEDSILGELNGPLREEIVNFNCRKLVASMPLFANADPN-FVTAMLTKLKFEVFQPGDYIIREG
CNGA1        MEKRVIKWFDYLWTNKKTVDEKEVLKYLPDKLRAEIAINVHLDTLKKVRIFADCEAG-LLVELVLKLQPQVYSPGDYICKKG
CNGA3        LETRVIRWFDYLWANKKTVDEKEVLKSLPDKLKAEIAINVHLDTLKKVRIFQDCEAG-LLVELVLKLRPTVFSPGDYICKKG
AtCNGC11/12  LKERIRRFEDYKWRETKGTEEEALLRSLPKDLRLETKRYLYLDMLKRVPWLNIMDDGWLLEAVCDRVKSVFYSANSFIVREG
AtCNGC4      FRQRVRNYERQRWAAMRGVDECEMVQNLPEGLRRDIKYHLCLDLVRQVPLFQHMDDL-VLENICDRVKSLIFTKGETIQKEG
AtCNGC2      LRQRVRRFERQRWNALGGEDELELIHDLPPGLRRDIKRYLCFDLINKVPLFRGMDDL-ILDNICDRAKPRVFSKDEKIIREG
```

(b)

AtCNGC2   AtCNGC4   R381

D'   R381   B'   D412   E450

+   −   −

D412   E450

Figure 4.12: An equivalent salt bridge to the one between R381 and E412 in AtCNGC11/12 in HCN2 and CNGA1 influences channel gating by affecting subunit interaction. (a) Sequence alignment of cytosolic C-terminal regions from the B' helix in the C-linker domain till the loop between β1 and β2 in the CNBD from HCN2 (NP_032252), CNGA1(NP_000078) , CNGA3 (NP_001289), AtCNGC11/12 (12) (EU541497), AtCNGC2 (NP_197045) and AtCNGC4 (NP_200236). (b) Computational structural modeling of tetramer structure of the cytoplasmic C-terminal region of AtCNGNC 2 and 4. Left panel: Perpendicular view of AtCNGC4 tetramer model. Two center panels: close-up of the black box in the left panel in AtCNGC2 and AtCNGC4. R381 forms two salt bridges with D412 in the neighboring subunit and with E450 in its own CNBD. Right panel: diagram of the electric charges of the three residues and possible salt bridges.

It will be of interest to explore whether this difference can discriminate these two members from the others in terms of their channel gating machinery.

There are four known subunits of HCN channels, HCN1-4 (Robinson and Siegelbaum, 2003). The subunit composition of native HCN channels is not known. But since HCN2 can form functional homomeric channels in heterologous systems, Zagotta *et al.* (2003) solved the crystal structure of HCN2 as a homo-tetramer and their work has become an important base for subsequent findings on the gating machinery of HCN as well as CNG channels. Similarly, there are 20 members of *A. thaliana* CNGCs and to date no information about the subunit composition of native channels is available. Since the expression of AtCNGC1, 2, 3, 11, 12 or AtCNGC11/12 can functionally complement various yeast ion channel mutants by themselves (Köhler *et al.*, 1999; Leng *et al.*, 1999; Chin *et al.*, 2009; Yoshioka *et al.*, 2006; Baxter *et al.*, 2008; Chin *et al.*, 2010), these subunits are believed to form functional homomeric channels in this heterologous system. In addition, electrophysiological studies using AtCNGC1, AtCNGC2 and AtCNGC4 have shown that these subunits also can function as homo-oligomers (Leng *et al.*, 1999; Balagué *et al.*, 2003). Therefore, in this study we generated a model of a homo-tetramer and identified two mutations that likely affect subunit interactions.

For future work, elucidating the subunit composition of native channels will be essential. To date, we have tested potential interactions between several selected *A. thaliana* CNGC subunits using similar yeast two-hybrid analysis like Daram *et al.* (1997) reported for AKT1 but so far, we have not seen any conclusive interactions (Urquhart and Yoshioka unpublished data). 20 members in *A. thaliana* can potentially create

countless combinations of heterotetramers. Thus, this aspect of plant CNGCs will remain to be a challenging, but unavoidable topic in the future.

Chapter 5

Characterisation of CaM-binding domain(s) of

AtCNGCs

Thomas A. DeFalco provided the data for Figures 5.10 and 5.16

5.1. Summary of research

The calmodulin binding domains (CaMBDs) of AtCNGCs were characterized. The structure based CaMBD prediction tool and *in silico* three dimensional (3D) homology modeling predicted two CaMBDs, one in the N-terminal and another one in the C-terminal cytosolic part in AtCNGC12. On the other hand, only one CaMBD was predicted in the N-terminal cytosolic region in AtCNGC11. These predictions were experimentally confirmed by tryptophan fluorescence spectroscopy and NMR.

5.2. Introduction

5.2.1. CaM and CaMBD

CaM is a highly conserved small acidic Ca^{2+} sensor protein present in all eukaryotic cells (Chin and Means, 2000; Yang and Poovaiah, 2003; Bouché *et al*., 2005). It has two approximately symmetrical globular domains (lobes) connected by a long α-helix. Each lobe consists of two helices (E and F helices) separated by a flexible linker region (Figure 5.1A). This structure is referred to as EF hand motifs. This EF hand "helix-loop-helix" structure is the most common Ca^{2+}-binding motif. Each EF hand in CaM (it has a total of four EF hands) enables to bind one Ca^{2+} ion (Yap *et al.,* 1999). CaM itself has no enzymatic activity, but in general the conformational changes induced by Ca^{2+} binding enables CaM to bind to its diverse target proteins, which in turn regulates their activity (Chin and Means, 2000; Vetter and Leclerc, 2003) (Figure 5.1A).

In the *A. thaliana* genome, there are seven CaM genes that encode CaM proteins with almost 100% identity to each other. They share greater than 95% identity to vertebrate CaMs (McCormack and Braam, 2003). In particular the EF hands and the

Ca^{2+} binding loops, which connect the E-helix with the F-helix, are highly conserved in plant (*A. thaliana*) and animal CaMs, suggesting the importance of these regions for CaM function. Massively parallel signature sequencing (MPSS) data and the data compiled from ~900 *A. thaliana* Affymetrix microarray chip experiments of *A. thaliana* CaMs indicated that all seven CaMs are expressed throughout the plant during all developmental stages (McCormack *et al.*, 2005). In addition to CaMs, *A. thaliana* also possesses a fifty-member CaM-like (CML) family that encodes more diverse proteins containing EF-hands that share at least 16% identity with CaM (McCormack and Braam, 2003; McCormack *et al.*, 2005; DeFalco *et al.,* 2009).

The molecular bases of CaM binding to target proteins have been extensively studied in animal systems. It has been reported that CaM can bind to target domains in both Ca^{2+}-dependent and independent manners. For Ca^{2+}-dependent targets, the relative positions of two hydrophobic residues in the CaM-binding motifs that anchor the two lobes of CaM, can be used to classify the CaM binding motifs (Rhoads and Friedberg, 1997). Early work has suggested that CaMBDs have a common characteristic, which is a positively charged (basic) amphiphilic α-helix consisting of approximately 20 residues (O'Neil and DeGrado, 1990). Later, the precise binding mode of CaM was investigated by multi-dimensional NMR solution structure of the complex of CaM and synthetic peptides corresponding to the CaMBD from skeletal smooth muscle myosin light chain kinase (skMLCK, Ikura *et al.*, 1992). This work revealed a helical structure with two hydrophobic side chains separated by a stretch of 12 residues bound by the N- and C-terminal lobes of CaM, which is later called "1-14" motif (Figure 5.1B and Table 5.1, Rhoads and Friedberg, 1997). The 1-14 motif may also include

additional hydrophobic residues in position 5 or 8 (1-5-14 or 1-8-14, respectively, Table 5.1, Rhoads and Friedberg, 1997). Since then, many CaMBD motifs have been reported (Alexander *et al.*, 1988; Vetter and Leclerc, 2003; Terrak *et al.*, 2005; Spratt *et al.,* 2007). Some of the well characterized motifs related to the current work were summarized in Table 5.1.

The motif called "1-10" was first found in a complex of CaM and with peptides corresponding to CaMBD of a CaM-dependent kinase II (CaMKII). In this case, the two lobes of CaM are bound to hydrophobic residues flanking a shorter segment of 10 amino acids. This 1-10 class may have an additional hydrophobic residue in position 5 (1-5-10), (Table 5.1, Vetter and Leclerc, 2003). The structural flexibility of CaM is manifested in the 1-16 motif which was found in a complex with a CaM kinase kinase (CaMKK) CaMBD peptide (Vetter and Leclerc, 2003, Figure 5.1B, Table 5.1). This binding motif was not entirely helical, and has hydrophobic anchors flanking a longer segment.

A large number of proteins such as myosin, nitric oxide synthase and cyclic nucleotide phosphodiesterase (PDE), can interact with Ca^{2+}-free (apo) CaM in Ca^{2+}-independent manner (Liu and Storm, 1990; Urbauer *et al.,* 1995, Spratt *et al.,* 2007, Yuan *et al.,* 1999). Many of these proteins contain what is known as IQ motif. The IQ motif was first described in neuromodulin (Alexander *et al.*, 1988). The motif comprises of the sequence IQXXXRGXXXR (Figure 5.1B, Table 5.1). Some proteins with IQ motifs including neuromodulin, can bind with apo-CaM only in the absence of Ca^{2+}, whereas others remain associated with CaM in the presence and absence of Ca^{2+}

Figure 5.1

A
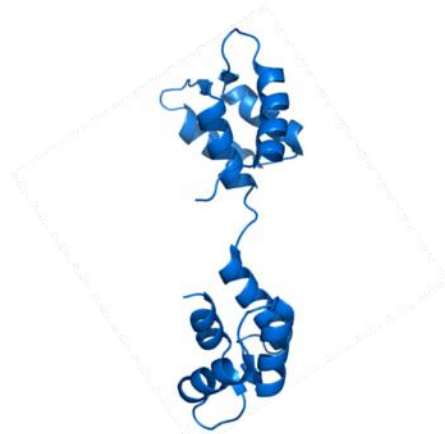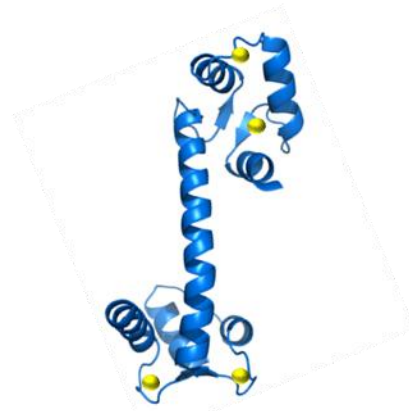
Apo-CaM   Ca²⁺-CaM

B
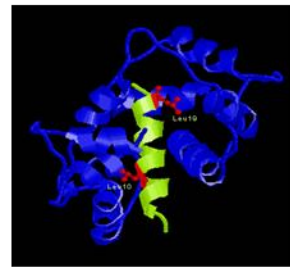
"1-14" motifs   "1-10" motifs
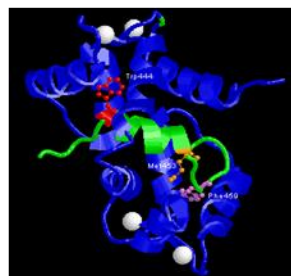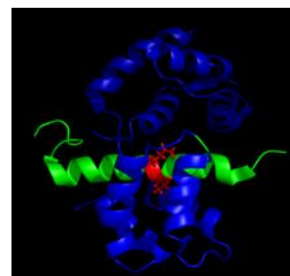
"1-16" motifs   IQ motifs

Figure 5.1: Ribbon presentations of CaM and CaM in complex with target peptides. CaM is colored blue, the CaM targets are green, Ca^{2+} ions are yellow. Structural data were taken from the Protein Data Bank (PDB), accession codes: (A) apo-CaM (1LKJ) and Ca^{2+}/CaM (3CLN). (B) 1-14 motif; skMLCK with Ca^{2+}-CaM created with RasMac v2.6 (2BBN), 1-10 motif; CaMKII and Ca^{2+}-CaM created with RasMac v2.6 (not available from PDB), 1-16 motif; CaMKK with Ca^{2+}-CaM created with RasMac v2.6 (not available from PDB) and IQ motif; $Na_V1.5$ with apo-CaM created with the protein fold recognition server (Phyre) (2L53).

Table 5.1: Various CaMBD motifs

Motif name	Sub class	Consensus sequence[1]
1-14	1-14	(FILVW)xxxxxxxxxxxx(FILVW)
	1-8-14	(FILVW)xxxxxx(FAILVW)xxxxx(FILVW)
	Basic 1-8-14	(RK)(RK)(RK)(FILVW)xxxxxx(FAILVW)xxxxx(FILVW)
	1-5-8-14	(FILVW)xxx(FAILVW)xx(FAILVW)xxxxx(FILVW)
1-10	1-10	(FILVW)xxxxxxxx(FILVW)
	1-5-10	xxx(FILVW)xxxx(FAILVW)xxxx(FILVW)
	Basic 1-5-10	(RK)(RK)(RK)(FAILVW)xxxx(FILV)xxxx(FILVW)
1-16	1-16	(FILVW)xxxxxxxxxxxxxx(FILVW)
IQ	IQ	(FILV)Qxxx(RK)Gxxx(RK)xx(FILVWY)
	IQ like	(FILV)Qxxx(RK)xxxxxxxx

[1] Residues within parentheses may substitute for each other.

(Zhang *et al.,* 1995). IQ motifs have been reported to frequently occur in tandem. For example Myosin V, which is a double-headed molecular motor involved in organelle transport, has six IQ motifs in tandem, suggesting the possibility to interact with multiple CaMs (Terrak *et al.*, 2005).

5.2.2. Calmodulin binding domains in CNGCs

Animal CNGCs have been reported to be regulated by CaM (Kaupp and Seifert, 2002). They have at least one CaMBD either in their N-termini (CNGA2 and 3) or C-termini (CNGA1 and 4), or in both N- and C-termini (CNGB1a, 1b and CNGB3) (Ungerer *et al.,* 2011).

In plants, it was suggested that CNGCs possess a CaMBD in the cytosolic C-terminus (Shuurink *et al.,* 1998; Köhler and Neuhaus, 2000; Arazi *et al.,* 2000). Shuurink *et al.* (1998) have cloned the first plant CNGC, *HvCBT1* (*Hordeumvulgare* CaM-binding transporter), as a CaM-binding protein in barley. They have identified the CaMBD to the region encoding amino acids 482-702, which is adjacent to its putative cyclic nucleotide binding domain (CNBD). Following this report, Arazi *et al.* (2000) and Köhler and Neuhaus (2000) reported CaMBDs located at the predicted αC-helix within the putative CNBD in *Nicotiana tabacum* CNGC, NtCBP4 and *A. thaliana* AtCNGC1 and 2, respectively. In addition, Chin *et al.* (2010) reported that the mutation in S58, which is a conditional suppressor of *A. thaliana cpr22* (AtCNGNC11/12), was found to be in the putative CaMBD of this channel, thereby indicating the importance of CaM in the regulation of plant CNGCs (Chin *et al.*, 2010; Abdel-Hamid *et al.,* 2010). Yet, very little is still known about the regulation of plant CNGCs by CaM (Hua *et al.,* 2003b; Kaplan *et*

al., 2007; Chin *et al.,* 2010). Furthermore, it is still not clear if there are additional CaMBDs beside the one in the αC-helix within the putative CNBD.

5.3. Results

5.3.1. Computational analysis of CaMBDs of AtCNGCs

The CaMBDs of AtCNGC1, AtCNGC2 and NtCBP4 have been reported to be located in the predicted αC-helix of the CNBD. Common CaMBDs are reported to contain specific features such as hydrophobic or aromatic residues, and the ability to form an amphiphilic α-helix, where one side of the wheel contains predominantly hydrophobic residues while the other side contained mostly basic residues (Köhler and Neuhaus, 2000). To determine the location of the CaMBD in the rest of the eighteen AtCNGCs, multiple sequence alignment (MSA) of all AtCNGCs was performed along with NtCBP4 based on their amino acid sequence. This analysis detected equivalent sequences to the previously reported CaMBDs of AtCNGC1, AtCNGC2 and NtCBP4 in the rest of the eighteen AtCNGCs (Figure 5.2A). These regions locate in the CNBDs of their C-terminal regions, agreeing well with the notion that the CaMBDs of plant CNGCs overlap with their CNBDs. Overall the corresponding sites of the AtCNGC family share very high homology, especially within their groups, with only the exception of AtCNGC12. AtCNGC12 belongs to group 1. The outstanding difference of the CaMBD sequence of AtCNGC12 is clearer when the residues of these sequences are shown with color coding specifying hydrophobicity and electric charge (Figure 5.2B). The characteristics of CaMBDs have been well documented and the hydrophobicity and electric charges are two key factors. Figure 5.2B depicts the differences in such

properties of the predicted CaMBDs of AtCNGC12 in group1 as well as the difference between groups. Especially group IVA and IVB are quite different from the other groups as well as between them. To investigate this difference further, helical wheel predications of AtCNGC12 along with AtCNGC11 (group1) and AtCNGC2 (group IVB) are shown in Figure 5.3. The predicted helical wheels of the CaMBDs of AtCNGC11 and 2 showed characteristic CaMBDs with a hydrophobic region on one side and a positively charge region on the other side (Köhler and Neuhaus, 2000). In contrast, the predicted CaMBD sequence of AtCNGC12 did not possess such characteristic. This raises two intriguing possibilities: 1. AtCNGC12 may not bind to CaM or 2. AtCNGC12 may have a CaMBD in a different region with a significantly different sequence.

To investigate the second possibility, another *in silico* CaMBD prediction was conducted using the Calmodulin Target Database, (http://calcium.uhnres.utoronto.ca/ctdb/ctdb/home.html) (Yap *et al.,* 2000). This tool, unlike MSA, is based on predicted structures. Using this tool, different areas for five out of eighteen members of the AtCNGC family were predicted. For example, a CaMBD for AtCNGC11 was predicted to be located in the N-terminus, not the C-terminal cytosolic region, whereas AtCNGC12 was predicted to have two CaMBDs; one each in the C-terminal and N-terminal cytosolic regions (Figure 5.4). The predicted location of the CaMBD in the AtCNGC12 C-terminus, however, was different from the region predicted by MSA (Figure 5.4). It shifted 16-17 aa toward to the C-terminal end.

Figure 5.2

A

	AtCNGC3	LSADDLKFVATQYR-RLHSKQLRHMFRFYSVQWQTWAACFIQAAW
	AtCNGC11	ISADDLKFVATQYR-RLHSKQLQHMFRFYSLQWQTWAACFIQAAW
	AtCNGC10	LTAEDLKSVASQFR-RLHSKQLQHTFRFYSVQWRTWSVSFIQAAW
Group I	AtCNGC13	LAADDLKLVASQFR-RLHSKQLQHTFRFYSVQWRTWGASFIQAAW
	AtCNGC1	LKADDLKFVASQFR-RLHSKQLRHTFRYYSQQWKTWAACFIQAAW
	AtCNGC12	LLPDDIKFIASHLN-VFQRQKLQRTFRLYSQQWRSWAAFFIQAAW
	AtCNGC12(Ws)	LLPDDIKFIASHLN-VFQRQKLQRTVRLYSQQWRSWAAFFIQAAW
	AtCNGC6	LIADELKFVASQFR-RLHSRQVQHTFRFYSQQWRTWAACFMQAAW
	AtCNGC9	LIADELKFVASQFR-RLHSRQVQHTFRFYSQQWRTWAAIFIQAAW
Group II	AtCNGC5	LTSEELKFVASQFR-RLHSRQVQHTFRFYSHQWRTWAACFIQAAW
	AtCNGC7	LEAEELKFVASQFR-RLHSRQVQQTFRFYSQQWRTWASCFIQAAW
	AtCNGC8	LEAEELKFVASQFR-RLHSRQVQQTFRFYSQQWRTWAACFIQAAW
	AtCNGC15	LKAEDLQFVASQFR-RLHTKQLRHKFRFYSHQWRTWAACFIQAAW
	AtCNGC14	LQAGDLKFVANQFR-RLHSKKLQHTFRYYSHQWRTWAACFVQVAW
Group III	AtCNGC17	LRAEDLKFVANQFR-RLHSKKLQHTFRFYSHHWRTWAACFIQAAW
	AtCNGC16	LRAEDLKFVANQFR-RLHSKKLQHAFRYYSHQWRAWGTCFIQAAW
	AtCNGC18	LSAEDLKFVAHQFK-RLQSKKLQHAFRYYSHQWRAWGACFVQSAW
Group VIA	AtCNGC19	LSVADLEDVTSLFSRFLRSHRVQGAIRYESPYWRLRAAMQIQVAW
	AtCNGC20	LSVADLEDVTSLFSRFLRSHRVQGAIRYDSPYWRLRAARQIQVAW
Group VIB	AtCNGC2	LGSEDLRYITDHFRYKFANERLKRTARYYSSNWRTWAAVNIQMAW
	AtCNGC4	LDAEDVKYVTQHFRYTFVNEKVKRSARYYSPGWRTWAAVAVQLAW
	NtCBP4	LVADDLKLVASQFR-RLHSKQLRHTFRFYSGQWRTWAACFIQAAW

B

AtCNGC1	FR-RLHSKQLRHTFRYY
AtCNGC3	YR-RLHSKQLRHMFRFY
AtCNGC10	FR-RLHSKQLQHTFRFY
AtCNGC13	FR-RLHSKQLQHTFRFY
AtCNGC11	YR-RLHSKQLQHMFRFY
AtCNGC12	LN-VFQRQKLQRTFRLY
AtCNGC5	FR-RLHSRQVQHTFRFY
AtCNGC6	FR-RLHSRQVQHTFRFY
AtCNGC7	FR-RLHSRQVQQTFRFY
AtCNGC8	FR-RLHSRQVQQTFRFY
AtCNGC9	FR-RLHSRQVQHTFRFY
AtCNGC14	FR-RLHSKKLQHTFRYY
AtCNGC15	FR-RLHTKQLRHKFRFY
AtCNGC16	FR-RLHSKKLQHAFRYY
AtCNGC17	FR-RLHSKKLQHTFRFY
AtCNGC18	FK-RLQSKKLQHAFRYY
AtCNGC19	FSRFLRSHRVQGAIRYE
AtCNGC20	FSRFLRSHRVQGAIRYD
AtCNGC2	FRYKFANERLKRTARYY
AtCNGC4	FRYTFVNEKVKRSARYY

Figure5.2: (A) Alignment of the area of the αB-helix and αC-helix of the CNBD in the 20 *A. thaliana* CNGCs, NCBI accession # of AtCNGCs are listed in the Appendix Table 2, and tobacco NtCBP4:AAF33670. The red box indicates the CaMBD and the black box indicates the critical four amino acids for the CaM binding suggested by Arazi *et al*. (2000). (B) Alignment of the conserved putative CaM binding regions. The conserved amino acids are highlighted with either light blue (hydrophobic residues) or gray (positively charged residues).

Figure 5.3

AtCNGC2
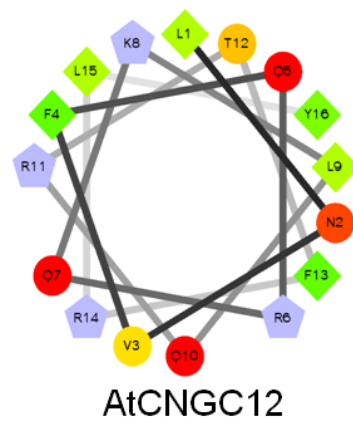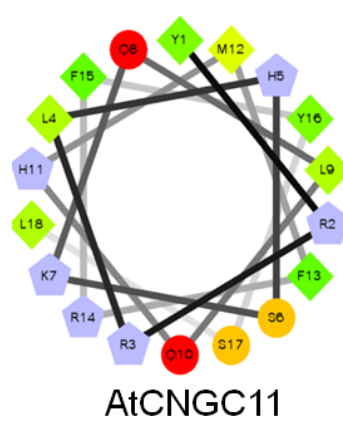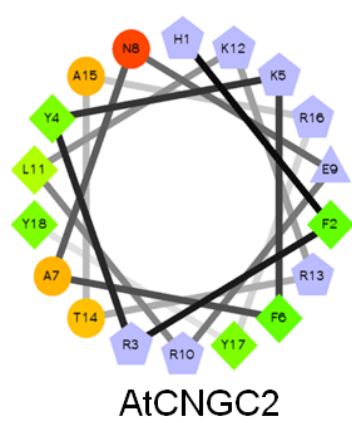
AtCNGC11

AtCNGC12

Figure 5.3: Helical wheel projection of CaM binding motifs of the C-termini of AtCNGC2, AtCNGC11 and AtCNGC12, displaying their hydrophobic and positive faces in green and blue, respectively. Hydrophilic residues are in red with pure red being the most hydrophilic (uncharged) residue, and the amount of red decreasing proportionally to the hydrophilicity.

Figure 5.4
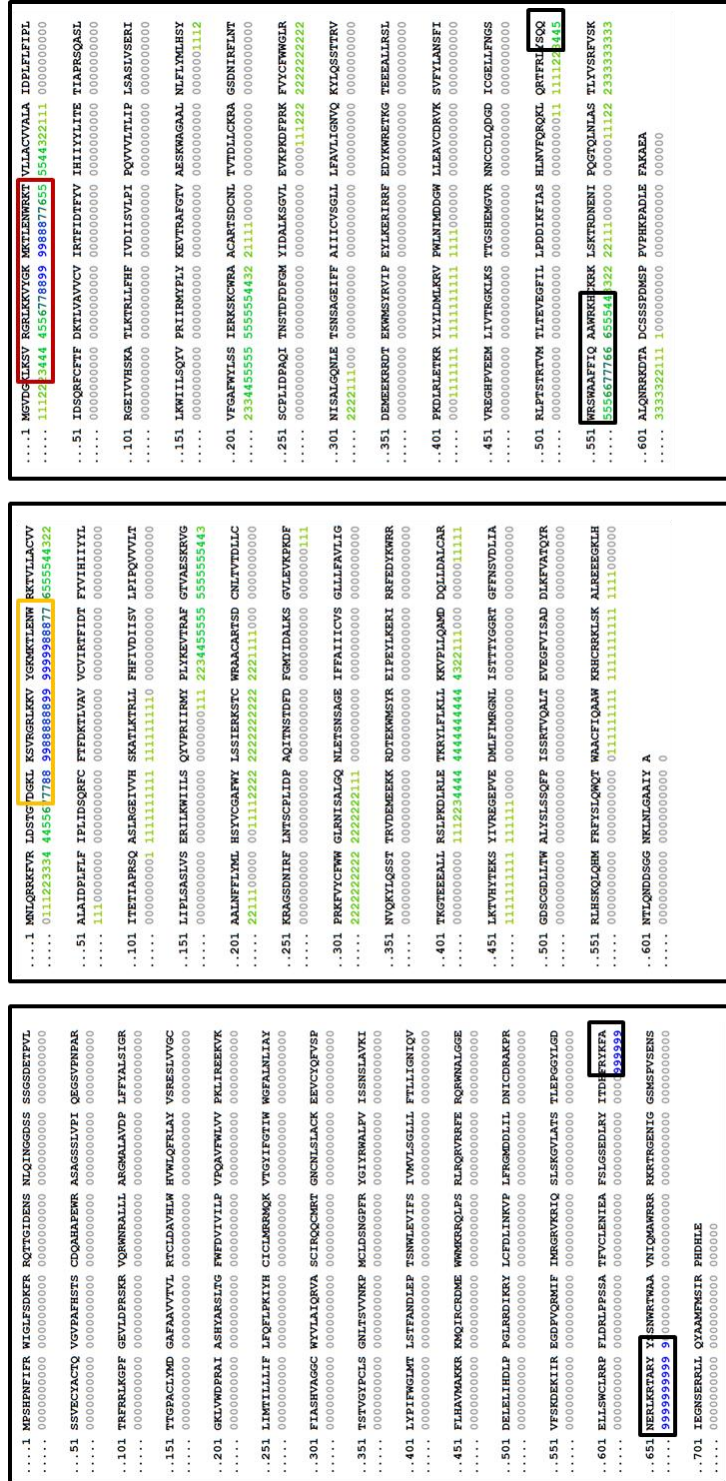
AtCNGC2

AtCNGC11

AtCNGC12

Figure 5.4: Prediction of CaMBDs of AtCNGC11 and 12 using the three dimensional structure-based CaMBD prediction tool, Calmodulin Target Database, (http://calcium.uhnres.utoronto.ca/ctdb/ctdb/home.html). The black, red and orange boxes indicate the position of the CaMBD(s) in each subunit.

Based on this analysis, AtCNGCs can be divided into three groups in terms of their CaMBDs: group I where the CaMBD is present only in the C-terminus. This group includes AtCNGC 1, 2, 3, 4, 5, 6, 8, 9, 10, 13, 14, 16, 17, 18 and 20. Group II, where the CaMBD is present only in the N-terminus. This group includes AtCNGC11 only. And group III, where the CaMBD is present in both the C- and N-termini, including AtCNGC 7, 12, 15 and 19 (Figure 5.5).

The structural model of the C-terminal region without the C-linker domain of AtCNGC2 has been reported using the crystal structure of cAMP-dependent protein kinase A (RIa) as a template (Hua *et al*., 2003). The reported CaMBD of AtCNGC2 has been shown to be at the end of the predicted αC-helix of its CNBD (Köhler and Neuhaus 2000, Hua *et al*., 2003). To identify the location of the predicted CaMBDs in their protein structure, the C-terminal regions of AtCNGC11 and AtCNGC12 were modeled using the structure prediction tool Swiss-Model© (http://swissmodel.expasy.org//SWISS-MODEL.html) along with AtCNGC2. For the current work, the crystal structure of SpIH1 was used as a temperate instead of RIa, since the structure of SpIH1 has the highest structural similarity to the C-terminal region of AtCNGCs among the crystal structures currently available (Flynn *et al.,* 2007, data not shown). As shown in Figure 5.6A, the reported CaMBD of AtCNGC2 locates to the αC-helix within the CNBD in the model, supporting the previously published predictions using RIa (Köhler and Neuhaus 2000, Hua *et al*., 2003). Similarly, the CaMBD of AtCNGC12 predicted by the Calmodulin Target Database also locates to the αC-helix of the CNBD in the 3D model (Figure 5.6B). Assuming that CaMBDs of AtCNGCs locate in the αC-helix in general, this model supports the prediction by the Calmodulin Target Database, not that by MSA.

Figure 5.5
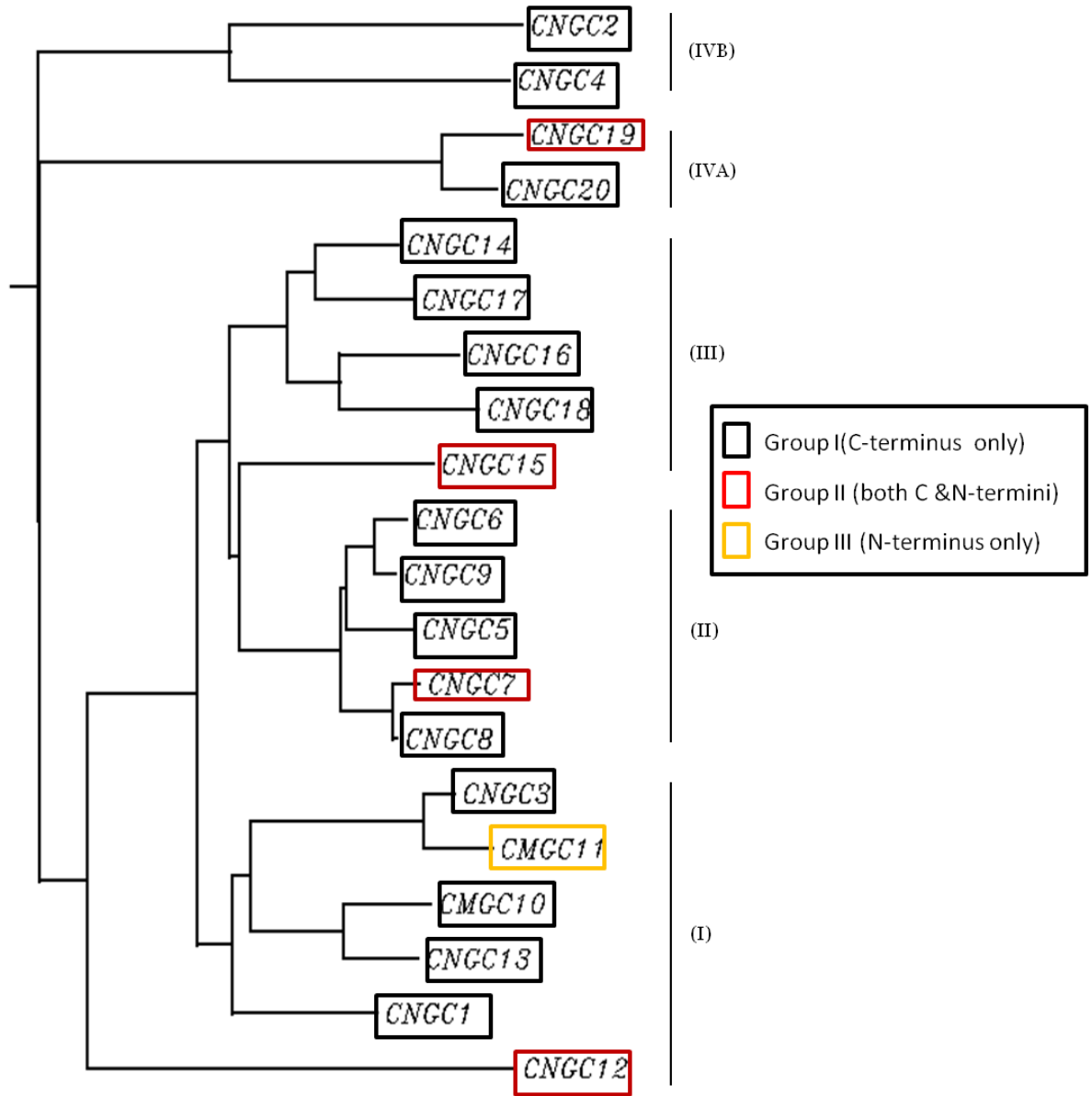
Figure 5.5: Phylogenetic tree of AtCNGCs and predicted CaMBDs. AtCNGCs cluster within 4 groups (I-IV) with the fourth group further broken into two sub-groups (IV A and IV B). The phylogenetic tree was created using ClustalW (www.ebi.ac.uk/Tools/msa/clustalw2/). The black, red and orange boxes indicate the types of group of the CaMBDs in each subunit.

Figure 5.6

AtCNGC2 (1-5-10)

AtCNGC11

AtCNGC12 (IQ-like motif)
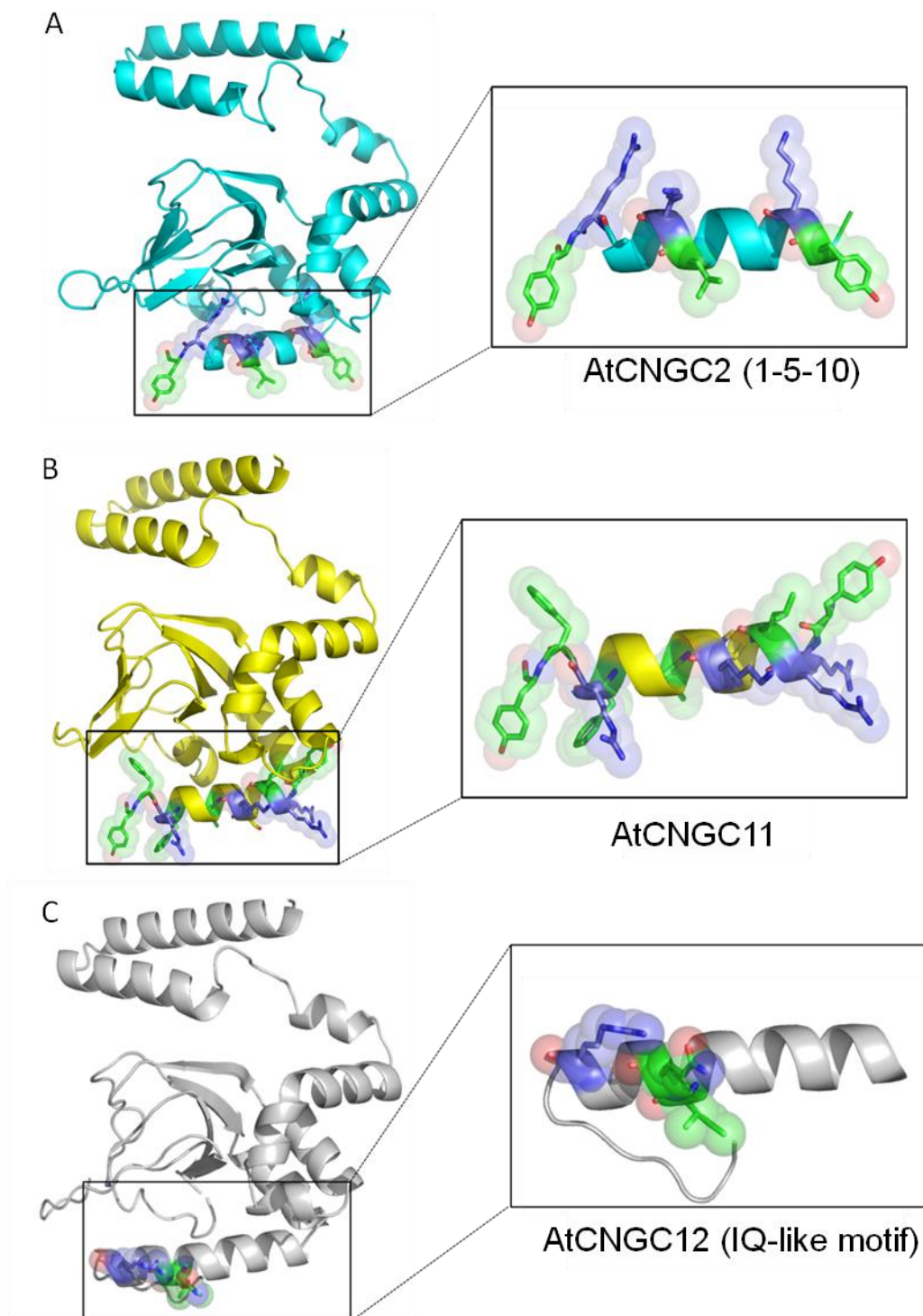
Figure 5.6: Features of CaM binding motifs of the C-termini of (A) AtCNGC2, (B) AtCNGC11 and (C) AtCNGC12. Left panel: Computational structural modeling of the cytoplasmic C-terminal region of AtCNGNC2 (cyan) in (A) AtCNGC11 (yellow) in (B) and AtCNGC12 (silver) in (C), using the crystallized structures of the cytoplasmic C-terminus of the invertebrate CNGC, SpIH (Flynn *et al.*, 2007, pdb no 2PTM). Right panel: the C-helix of each channel in the same colors. The hydrophobic and positive faces are shown in green and blue, respectively. Predicted CaM binding motifs are in the parentheses.

In this model a 1-5-10 motif was predicted in the αC-helix of the CNBD in AtCNGC2, whereas an IQ-like motif was predicted in the αC-helix of AtCNGC12 (Figure 5.6A and C, Ikura *et al.*, 1992; Cheney and Mooseker, 1992). For AtCNGC11, no CaMBD motif was predicted (Figure 5.6B).

5.3.2. The cytosolic C-terminus of AtCNGC12 binds CaM

To assess whether the C-terminal region of AtCNGC12 actually binds to CaM, the cytosolic C-terminal region of AtCNGC12, residue S357 to K578, which contains the predicted CaMBD sequences by both MSA and Calmodulin Target Database, was expressed in *E.coli* and CaM binding was tested by Nuclear magnetic resonance spectroscopy (NMR). NMR spectroscopy is a well-established method not only for the analysis of protein 3D structure, but also for protein-protein and protein-ligand interactions (Takeuchi and Wagner, 2006). One of the powerful aspects of NMR spectroscopy is its ability to characterize protein complexes under physiological conditions at atomic detail, even if the interactions are weak. Furthermore, NMR is the only method that is performed in solutions, mimicking the natural environment of proteins (Takeuchi and Wagner, 2006). The NMR spectra of CaM have been remarkably well resolved since the 1980's (Mal and Ikura, 2006).

The *A. thaliana* genome harbours seven CaM genes encoding three isoforms with almost 100% identity to each other and greater than 95% identity to vertebrate CaMs (McCormack and Braam, 2003) (Appendix, Table 4) (Figure 5.7). Therefore, the black rat CaM (pdb no 3CLN), that is uniformly ^{15}N-labelled (Mal and Ikura, 2006) was used in this NMR analysis. The analyses were conducted using the Bruker 600 MHz

system (Ikura laboratory, Department of Medical Physics at the University of Toronto). The NMR spectrum of the black rat CaM was obtained, with most of the amino acids assigned according to Mal and Ikura (2006) (Figure 5.8). As shown in Figure 5.9, chemical shifts for many residues of CaM were observed when the expressed AtCNGC12 C-terminus was added, indicating that this portion of AtCNGC12 likely contains a CaMBD. The data was not conclusive since the chemical shift was not as drastic as we expected. This could be due to the size of the expressed protein. The expressed protein is about 26kDa which is slightly larger than the limitation of protein size for NMR (≈20 kDa, Dr. Marshall, personal communication). Generally speaking, larger proteins cause slower tumbling rates and shorter NMR signal relaxation times or introduce more complexity because of more NMR-active nuclei which leads to more interactions among them. Thus, the large protein might have caused a weak (partial) shift or artificial shift of CaM. Alternatively, the binding was partial due to lack of key residues for CaM binding in the expressed protein. For example, although the expressed protein contains the CaMBD predicted by the Calmodulin Target Database, which has similarity to an IQ motif, it did not contain the second arginine residue, which is highly conserved among studied IQ motifs (IQXXXRGXXX<u>R</u>). To address these points, a peptide, which contains only the IQ like motif including this second arginine of AtCNGC12, was subsequently synthesized and analyzed.

Figure 5.7

```
CaM2/3/5  MADQLTDDQISEFKEAFSLFDKDGDGCITTKELGTVMRSLGQNPTEAELQDMINEVDADG  60
CaM6      MADQLTDDQISEFKEAFSLFDKDGDGCITTKELGTVMRSLGQNPTEAELQDMINEVDADG  60
CaM7      MADQLTDDQISEFKEAFSLFDKDGDGCITTKELGTVMRSLGQNPTEAELQDMINEVDADG  60
CaM1/4    MADQLTDEQISEFKEAFSLFDKDGDGCITTKELGTVMRSLGQNPTEAELQDMINEVDADG  60
3CLN      MADQLTEEQIAEFKEAFSLFDKDGDGTITTKELGTVMRSLGQNPTEAELQDMINEVDADG  59
          ******::**: ***********  **********  ****************
              E Helix         Loop          F Helix           E Helix

CaM2/3/5  NGTIDFPEFLNLMARKMKDTDSEEELKEAFRVFDKDQNGFISAAELRHVMTNLGEKLTDE 120
CaM6      NGTIDFPEFLNLMARKMKDTDSEEELKEAFRVFDKDQNGFISAAELRHVMTNLGEKLSDE 120
CaM7      NGTIDFPEFLNLMARKMKDTDSEEELKEAFRVFDKDQNGFISAAELRHVMTNLGEKLTDE 120
CaM1/4    NGTIDFPEFLNLMAKKMKDTDSEEELKEAFRVFDKDQNGFISAAELRHVMTNLGEKLTDE 120
3CLN      NGTIDFPEFLTMMARKMKDTDSEEEIREAFRVFDKDGNGYISAAELRHVMTNLGEKLTDE 119
          **********  :**: *************::**:*** *:**************:**
              F Helix            Loop             F Helix

CaM2/3/5  EVDEMIKEADVDGDGQINYEEFVKVMMAK 149
CaM6      EVDEMIREADVDGDGQINYEEFVKVMMAK 149
CaM7      EVDEMIREADVDGDGQINYEEFVKVMMAK 149
CaM1/4    EVEEMIREADVDGDGQINYEEFVKIMMAK 149
3CLN      EVDEMIREANIDGDGQVNYEEFVQMMTAK 148
          **:**:**:  :.*******::* **
              E Helix      Loop       F Helix
```

151

Figure 5.7: The four CaM isoforms encoded by the seven *A. thaliana* CaM genes are aligned with the black rat CaM (PDB no 3CLN), NCBI accession # of AtCaMs are listed in the Appendix, Table 4. Amino acid numbering is indicated on the left. The regions corresponding to the E helices, Ca^{2+}-binding loops and F helices are indicated by the yellow and blue boxes, respectively.

Figure 5.8

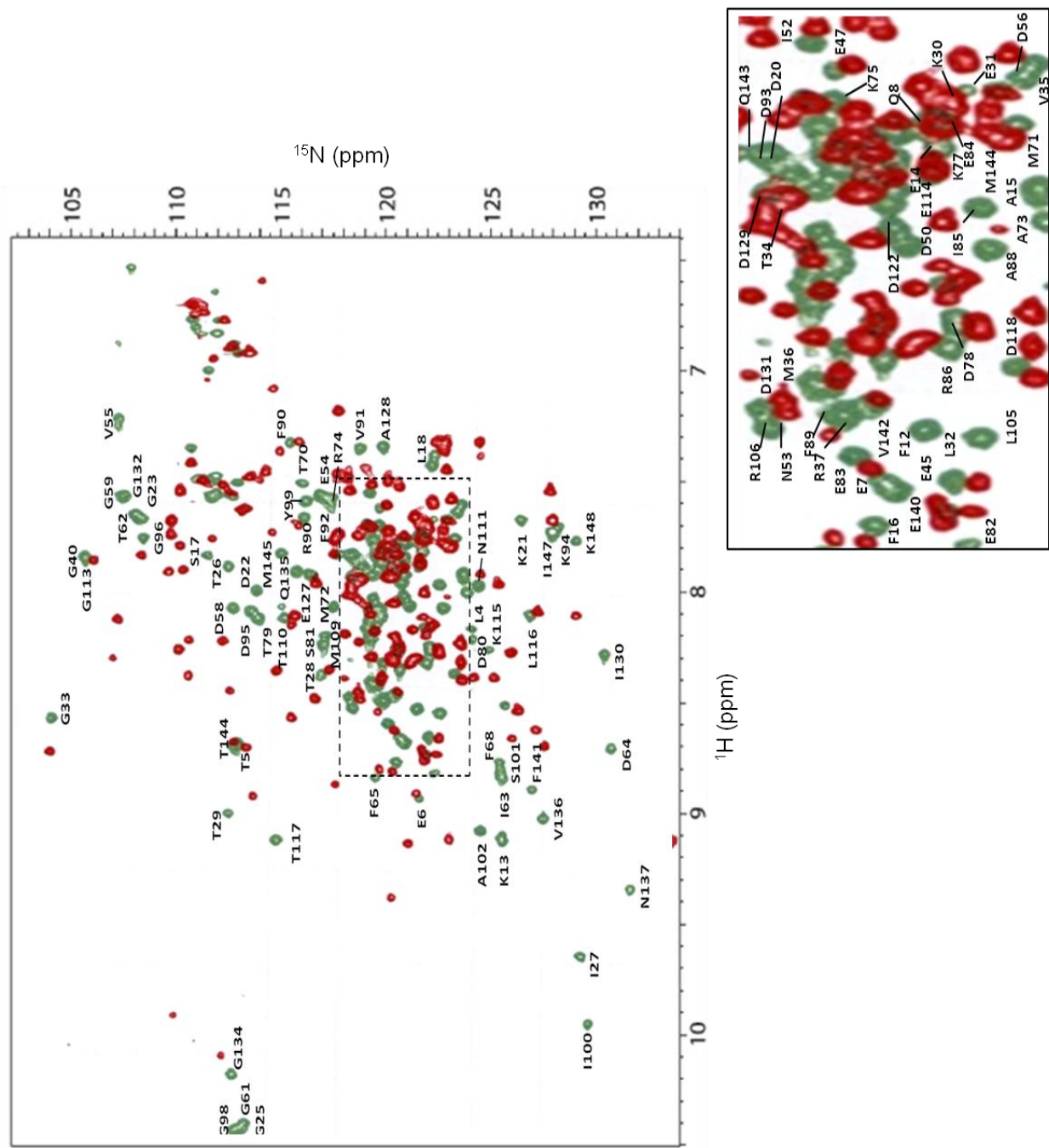**Figure 5.8:** ^{1}H-^{15}N-HSQC spectra of uniformly ^{15}N-labelled Ca^{2+}/CaM (black rat CaM, PDB ID 3CLN), without (green) and with (red) EDTA. Resonances are labelled using one letter amino acid codes.

Figure 5.9
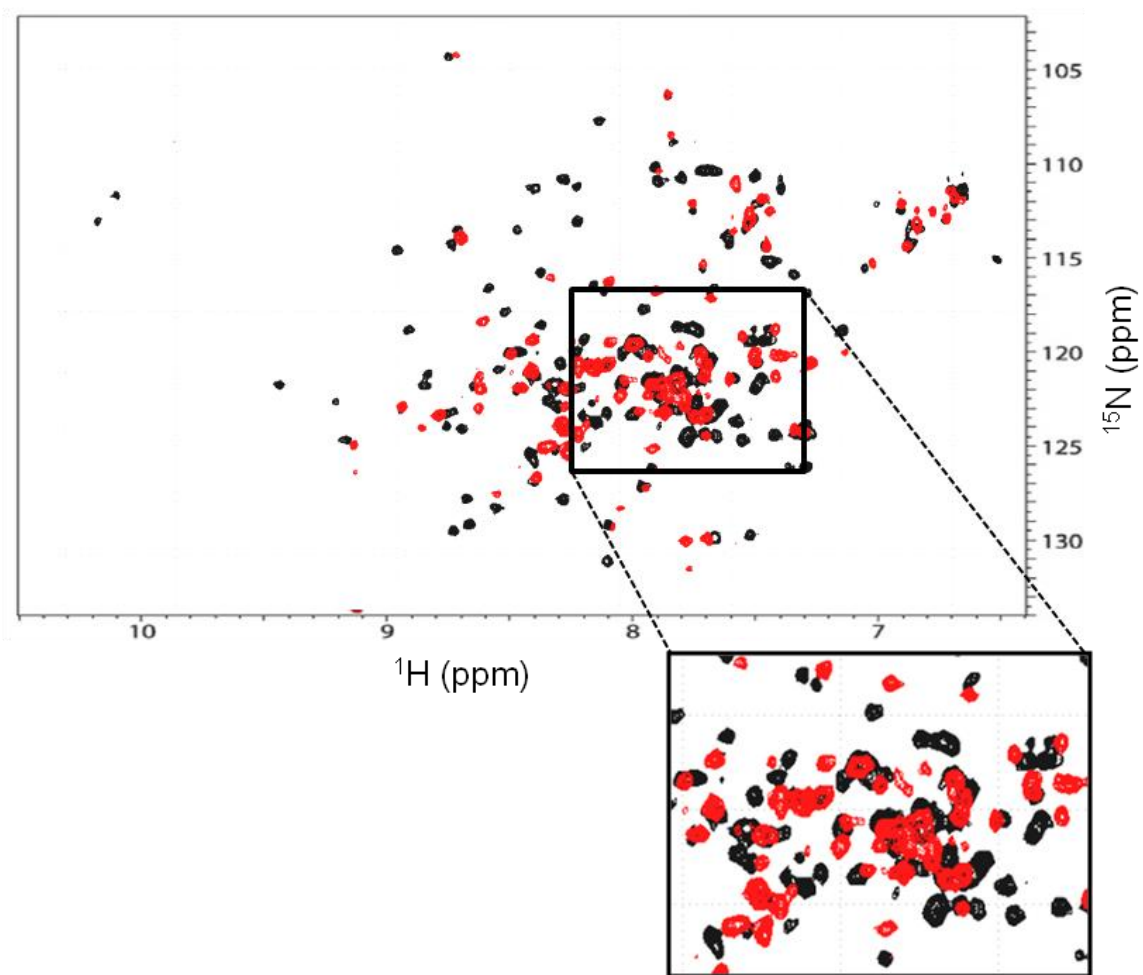
Figure 5.9: ^{1}H-^{15}N-HSQC spectra of uniformly ^{15}N-labelled Ca^{2+}/CaM (black rat CaM, PDB ID 3CLN) alone (black) and in complex with unlabeled C-terminus of AtCNGC12 (red).

5.3.3. A synthetic peptide with an IQ-like motif in AtCNGC12 binds CaM

As explained above, a peptide corresponding to the CaMBD of AtCNGC12, predicted by the Calmodulin Target Database, including the conserved second arginine (RLYSQQWRSWAAFFIQAAWRKHCK<u>R</u>) was synthesized and its binding ability to bind CaM was analyzed along with the peptide of the reported CaMBD of AtCNGC2 (Köhler and Neuhaus 2000, Appendix, Table 3).

First, the binding was evaluated by tryptophan fluorescence spectroscopy using AtCaM2 (DeFalco *et al.,* 2010). Since CaM lacks tryptophan residues and the predicted N-terminal CaMBD of AtCNGC11 and 12 contains only one tryptophan located within the predicted CaMBD (W40 and W27, respectively), it makes this method ideal for CaM binding analysis.

As shown in Figure 5.10A, addition of AtCaM2 to the AtCNGC2 peptide resulted in a shifted tryptophan emission peak with λ max from ∼353 nm to ∼347 nm, indicating that this peptide binds to AtCaM2. This result supports the published data showing the binding by yeast two hybrid analyses (Köhler and Neuhaus, 2000). Similarly, the addition of AtCaM2 to the AtCNGC12 peptide resulted in a shift in the tryptophan emission peak with λ max from ∼350 nm to ∼340 nm (Figure 5.10B), indicating that this peptide also binds to CaM.

Next for further analysis, CaM binding was tested by NMR as described above. As shown in Figure 5.11A, when the synthesized AtCNGC2 peptide was added, significant chemical shifts for almost all the residues of CaM were detected, supporting the reported analysis by Köhler and Neuhaus (2000) and the tryptophan fluorescence analysis described above. This shift was abolished by EDTA treatment, further

indicating that the CaM binding with the AtCNGC2 peptide is Ca^{2+}-dependent (Figure 5.11B). Similarly, in the case of the AtCNGC12 peptide, a chemical shift for almost all the residues of CaM was detected (Figure 5.12A). This shift was more drastic than that with the expressed larger protein mentioned above (Figure 5.9), suggesting the two concerns raised in the previous section were overcome by this synthetic peptide. This chemical shift was not completely abolished by EDTA (Figure 5.12B). This indicates that the CaM binding to this AtCNGC12 peptide is, unlike AtCNGC2, Ca^{2+}-independent. Since many IQ motif binds to CaM in a Ca^{2+}-independent manner, this data fits well to the expectation. Tryptophan fluorescence spectroscopy also supported this result. AtCNGC2 bound to CaM in Ca^{2+}-dependent manner, while AtCNGC12 bound in a Ca^{2+}-independent manner (Figure 5.10).

In the case of AtCNGC11, although the Calmodulin Target Database did not predict any CaMBD in its C-terminal region, MSA identified an equivalent sequence to the reported CaMBD of AtCNGC2 (Figure 5.2, Köhler and Neuhaus 2000). Thus, a peptide with this sequence was synthesized and analyzed by NMR, but no chemical shift of CaM was detected (Figure 5.13). This supports the prediction by the Calmodulin Target Database, but not the prediction by MSA.

Taken together, the CaMBD of the AtCNGC12 C-terminus predicted by the Calmodulin Target Database was experimentally confirmed by fluorescence analysis as well as NMR. This binding was unlike that of AtCNGC2, Ca^{2+}-independent. On the other hand, AtCNGC11 does not seem to have a CaMBD in the C-terminus as the Calmodulin Target Database predicted.

Figure 5.10
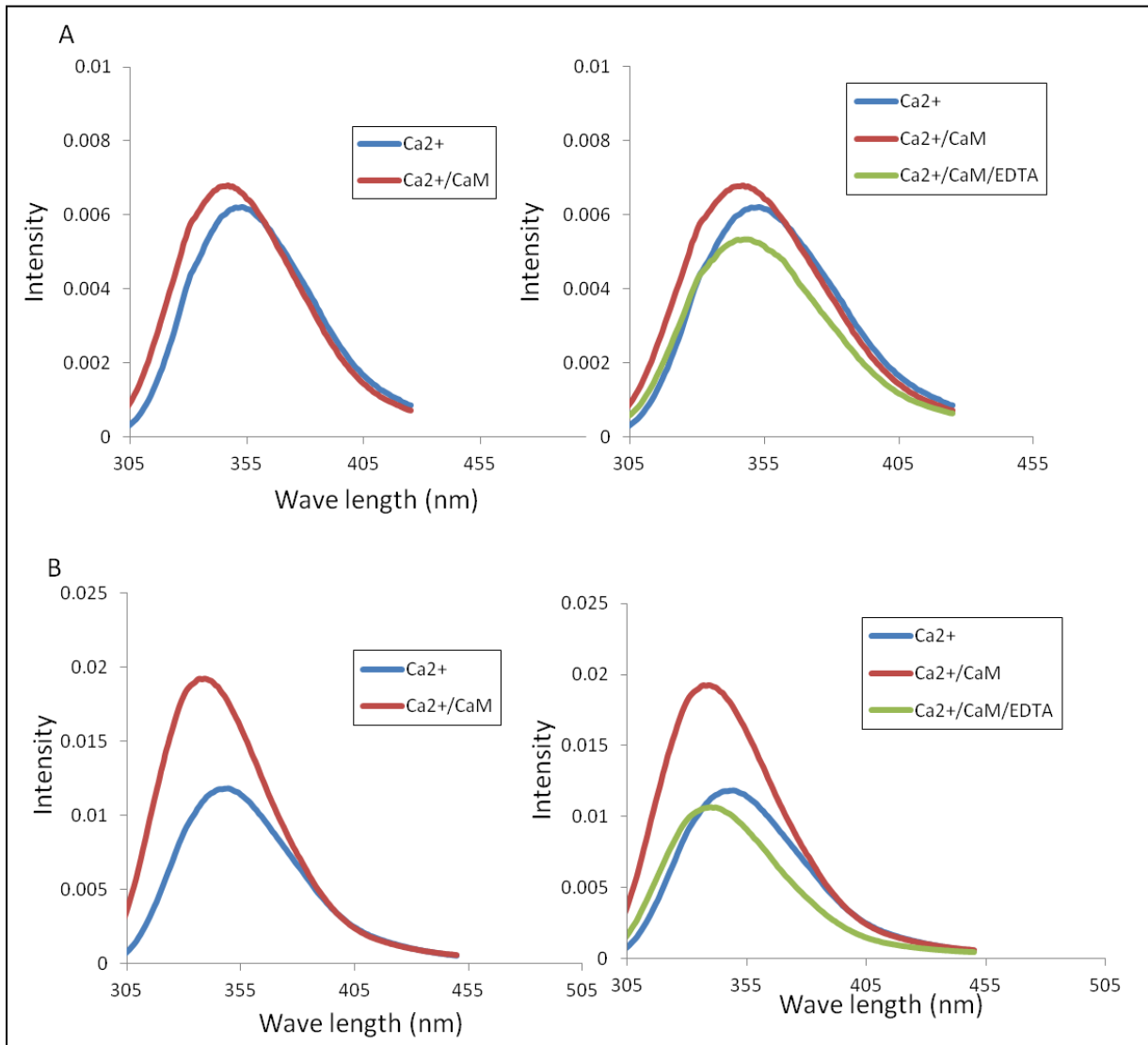
Figure 5.10: Fluorescence spectra of (A) AtCNGC2 C-terminus peptide in the absence (blue) and presence (red) of CaM, both in the presence of Ca^{2+}, and in the presence of Ca^{2+}/EDTA (green). (B) AtCNGC12 C-terminus peptide in the absence (blue) and presence (red) of CaM, both in the presence of Ca^{2+}, and in the presence of Ca^{2+}/EDTA (green).

Figure 5.11
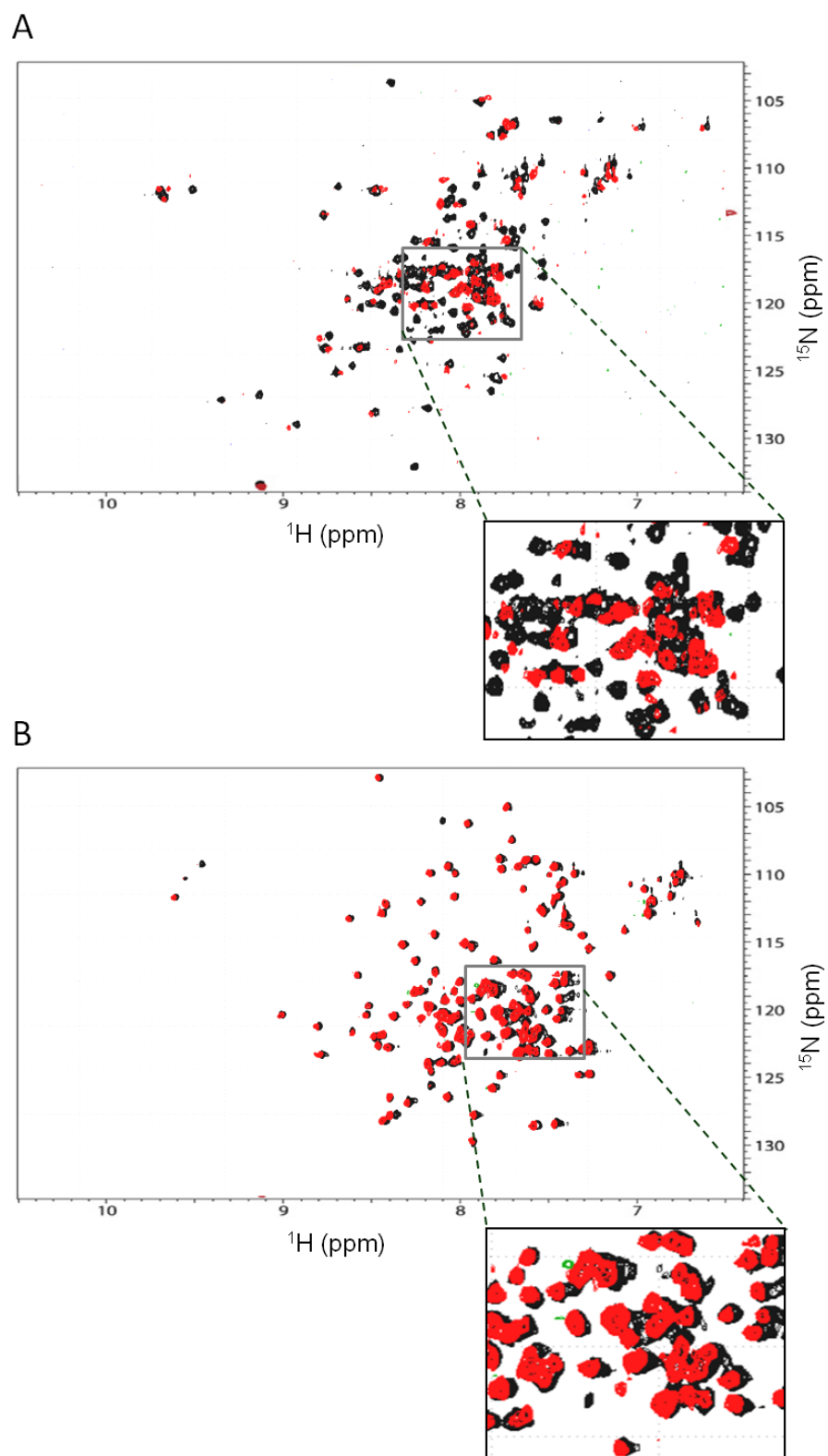
Figure 5.11: ^{1}H-^{15}N-HSQC spectra of uniformly ^{15}N-labelled Ca^{2+}/CaM (black rat CaM, PDB ID 3CLN) alone (black) and in complex with unlabeled peptide of AtCNGC2 C-terminus CaMBD (red), (A) without and (B) with EDTA.

Figure 5.12
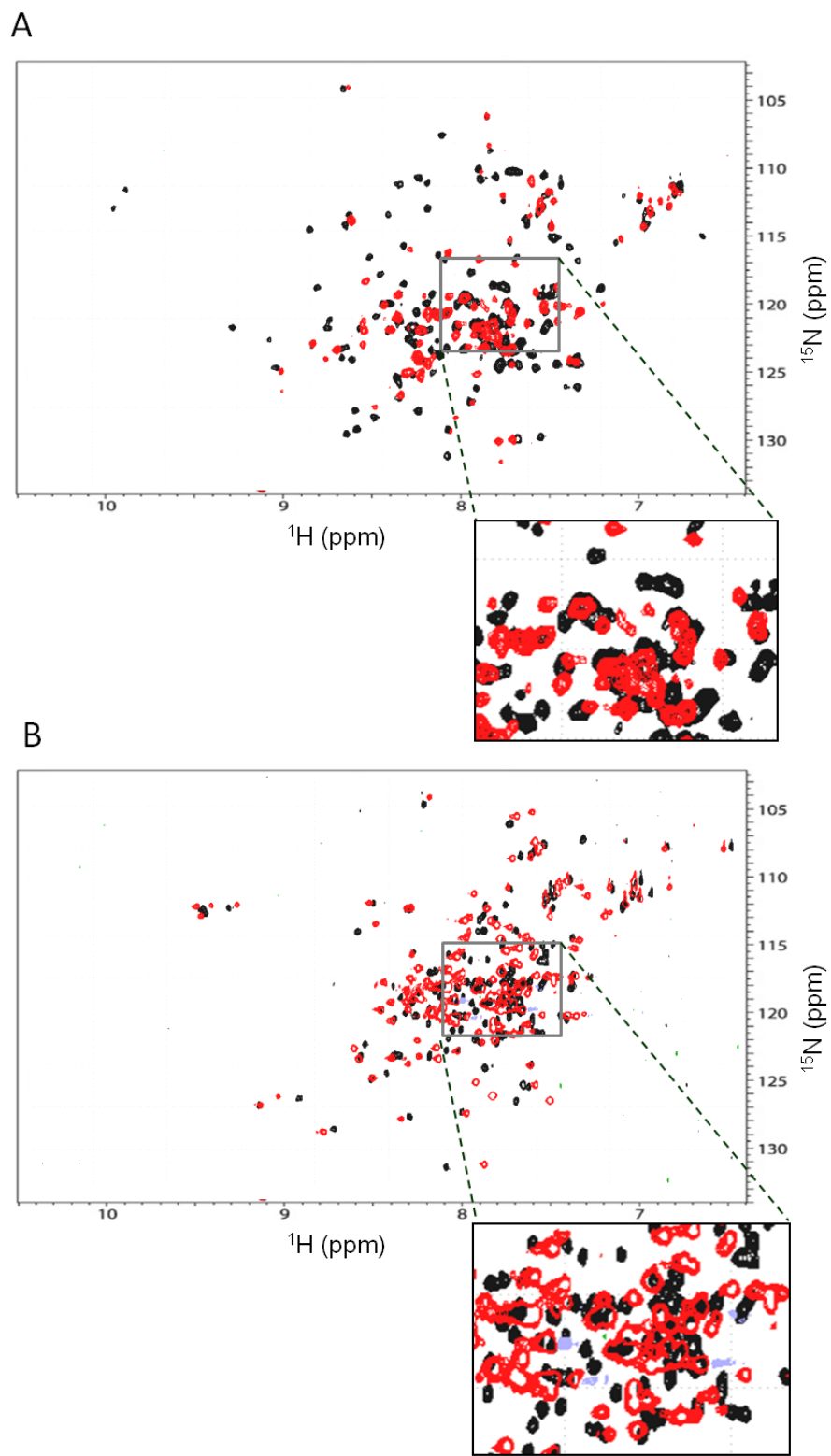
Figure 5.12: ^{1}H-^{15}N-HSQC spectra of uniformly ^{15}N-labelled Ca^{2+}/CaM (black rat CaM, PDB ID 3CLN) alone (black) and in complex with unlabeled peptide of AtCNGC12 C-terminus CaMBD (red), (A) without and (B) with EDTA.

Figure 5.13
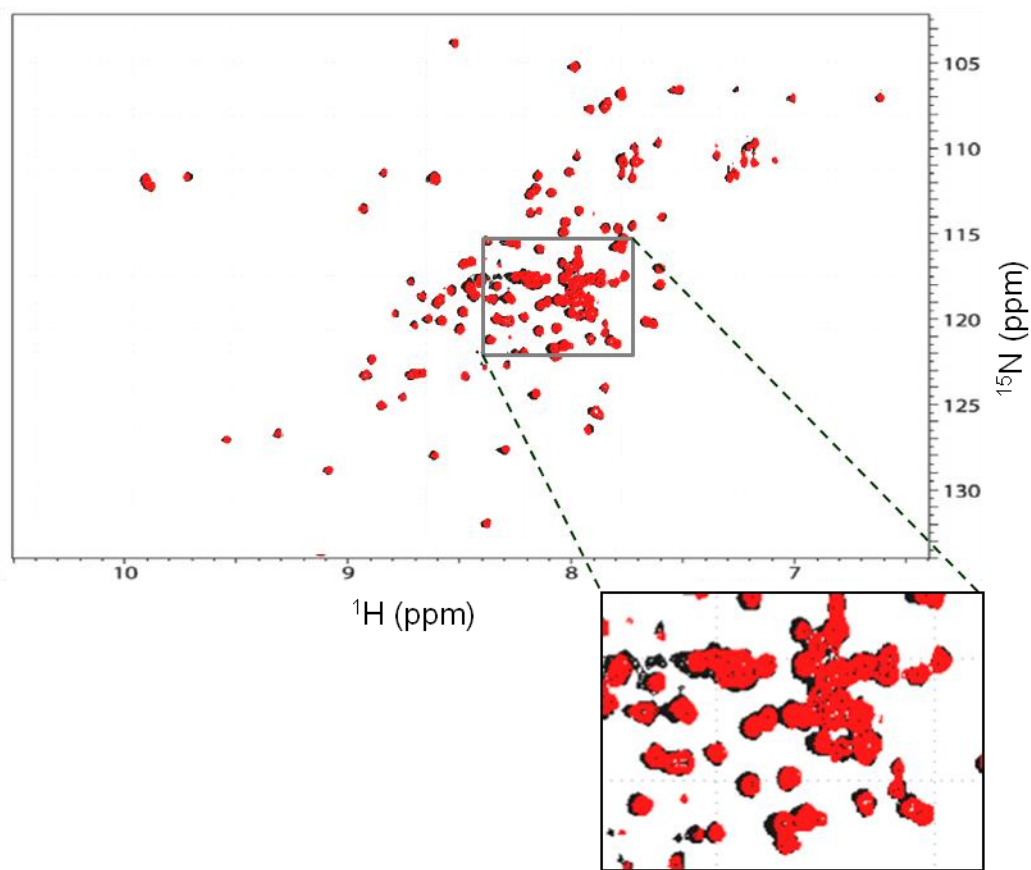
Figure 5.13: ^{1}H-^{15}N-HSQC spectra of uniformly ^{15}N-labelled Ca^{2+}/CaM (black rat CaM, PDB ID 3CLN) alone (black) and in complex with unlabeled peptide of AtCNGC11 C-terminus CaMBD (red).

5.3.4. *In silico* modeling of CaM-CaMBD interactions in AtCNGC2 and AtCNGC12 C-termini

The interactions between CaM and CaMBDs of both AtCNGC2 and 12 C-termini were modeled using PatchDock (http://bioinfo3d.cs.tau.ac.il/PatchDock/), and compared to other reported CaM-CaMBD interactions (Ikura *et al.*, 1992; Cheney and Mooseker, 1992; Bouché *et al.,* 2005; Ye *et al.,* 2008; Ishida *et al.,* 2009; Majava and Kursula, 2009; Feldkamp *et al.,* 2011). Structural modeling of the CaM-CaMBD interaction in AtCNGC2 shows a typical 1-10 motif-CaM interaction (Ikura *et al.*, 1992), where two bulky residues (F645 and L654) are separated by eight other residues and serve to anchor the CaMBD to the CaM binding pocket (Figure 5.14A). In this model, the two key hydrophobic residues, F645 and L654, fit nicely into the hydrophobic binding pocket of CaM. This hydrophobic pocket includes L18, L32, M36, M51, I52, F68, M71 and M72 (Figure 5.14A). On the other hand, the model of the CaM-CaMBD interaction in AtCNGC12 shows similarities with IQ-CaM interactions where, the IQ sequence interact with resides in one of the CaM termini (either N- or C-terminus) (Cheney and Mooseker 1992; Feldkamp *et. al.,* 2011,Figure 5.14B).

5.3.5. A possible novel CaMBD in the N-terminus of AtCNGC11 and AtCNGC12

In animal CNGCs, two different CaM binding motifs were identified: a Ca^{2+}-dependent basic amphipathic alpha helix-type and a Ca^{2+}-independent IQ-type. All animal CNGCs have at least one of those two binding sites either in their N-terminus (CNGA2 and 3) or their C-terminus (CNGA1 and 4), or in both N- and C-termini (CNGB1a, 1b and CNGB3) (Ungerer *et al.*, 2011).

Figure 5.14
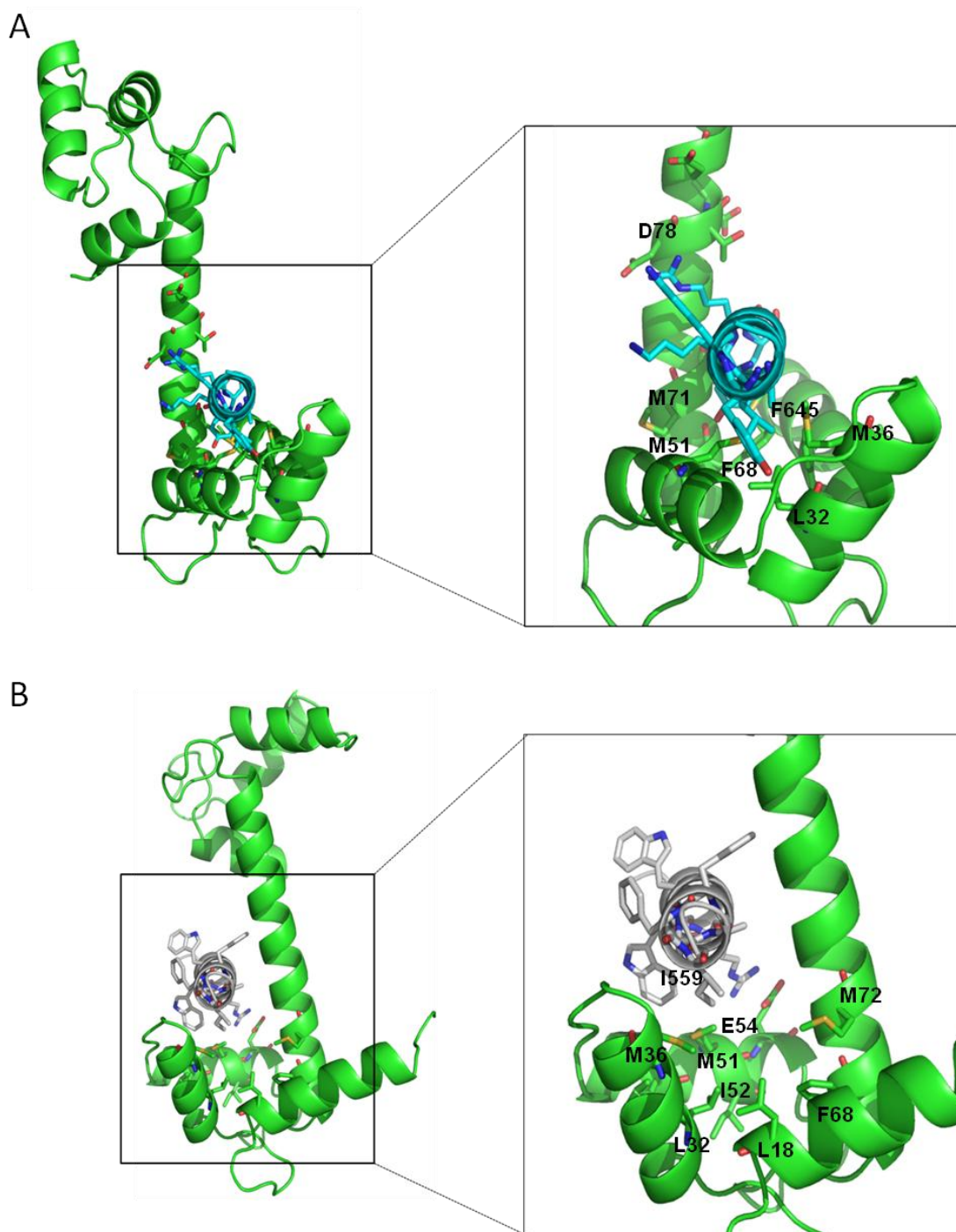
Figure 5.14: Computational structural modeling of CaM binding with AtCNGC2 and AtCNGC12. Modeling of the tertiary structure of vertebrate CaM, and the αC-helix of AtCNGC2 and AtCNGC12 was conducted using the crystallized structures of the *Rattus rattus* (black rat) CaM (PDB ID 3CLN) and the cytoplasmic C-terminus of the invertebrate CNGC, SpIH (Flynn *et al.*, 2007, PDB no 2PTM), respectively, as templates. The protein fold recognition server (Phyre) was used to model these proteins. The binding modeling was performed using an algorithm for molecular docking (PatchDock). All the images were generated using PyMOL. CaM is colored in green and (A) the αC-helix of AtCNGC2 is shown in cyan, left panel: overall binding model between rat CaM and AtCNGC2, right panel: close up of the boxed area of the left part in AtCNGC2. (B) the αC-helix of AtCNGC12 is shown in silver, left panel: overall binding model between rat CaM and AtCNGC12, right panel: close up of the boxed area of the left part in AtCNGC12.

As mentioned above, using the Calmodulin Target Database (Yap *et al.,* 2000), a CaMBD was predicted in the N-terminus of AtCNGC7, 11, 12, 15 and 19. In this region, both AtCNGC11 and 12 have an identical amino acid sequence. The tertiary structural model of the predicted site revealed an α-helix that is typical for a CaMBD (Figure 5.15, left panel). In addition, when this predicted CaMBD was inserted into a helical wheel, it formed an amphipathic helix that fits the general features of a CaMBD site, where one side of the wheel contains predominantly hydrophobic residues and the other side contained mostly basic residues (Mitsutake and Igarashi, 2005) (Figure 5.15, right panel).

5.3.6. The predicted CaMBD of AtCNGC11 and AtCNGC12 N-termini binds CaM in a Ca^{2+}-dependent manner

To provide experimental evidence for the predicted N-terminal CaMBD of AtCNGC12 (same as AtCNGC11), a synthesized peptide, corresponding to this predicted CaMBD (Appendix 1, Table 3), was examined for its ability to bind CaM.

First, tryptophan fluorescence spectroscopy was conducted. Addition of AtCaM2 to the AtCNGC12 N-terminal peptide resulted in a shift in the tryptophan emission peak with λ max from ~356 nm to ~352 nm, indicating significant binding of CaM (Figure 5.16A). This change in the tryptophan emission peak was reversed upon chelation of Ca^{2+} by EDTA treatment (Figure 5.16B), indicating that this interaction is Ca^{2+}-dependent.

Figure 5.15
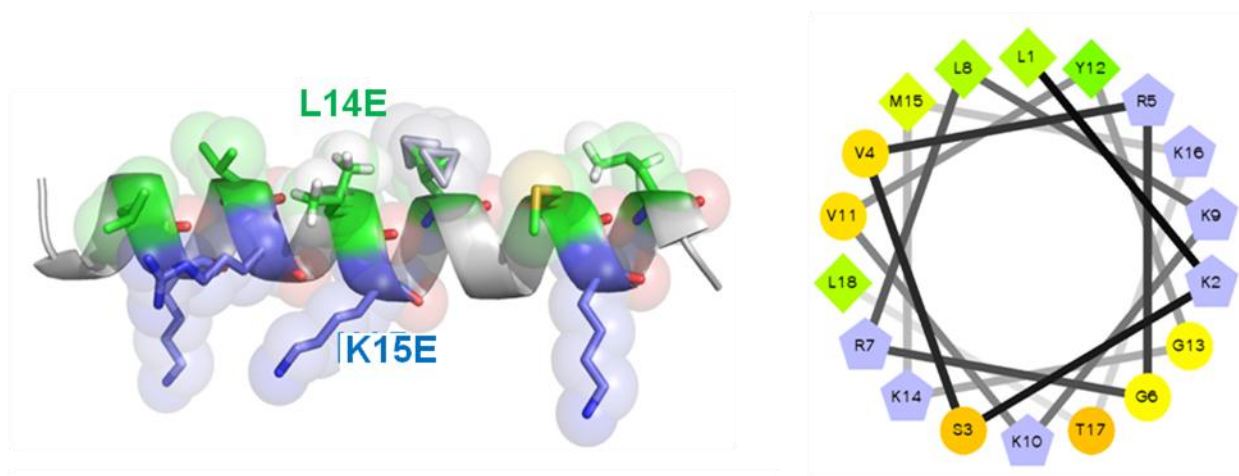
Figure 5.15: Features of CaM binding motif of the N-terminus of AtCNGC12 (same as 11) and L14E-K15E N-terminus peptides (the N-terminus mutant of AtCNGC12). Left panel: N-terminus of AtCNGC12 sequence modeled as an ideal α-helix. Right panel: Helical wheel projection of CaM binding motif of AtCNGC12 N-terminus displaying its hydrophobic and polar faces in green and blue, respectively.

Figure 5.16
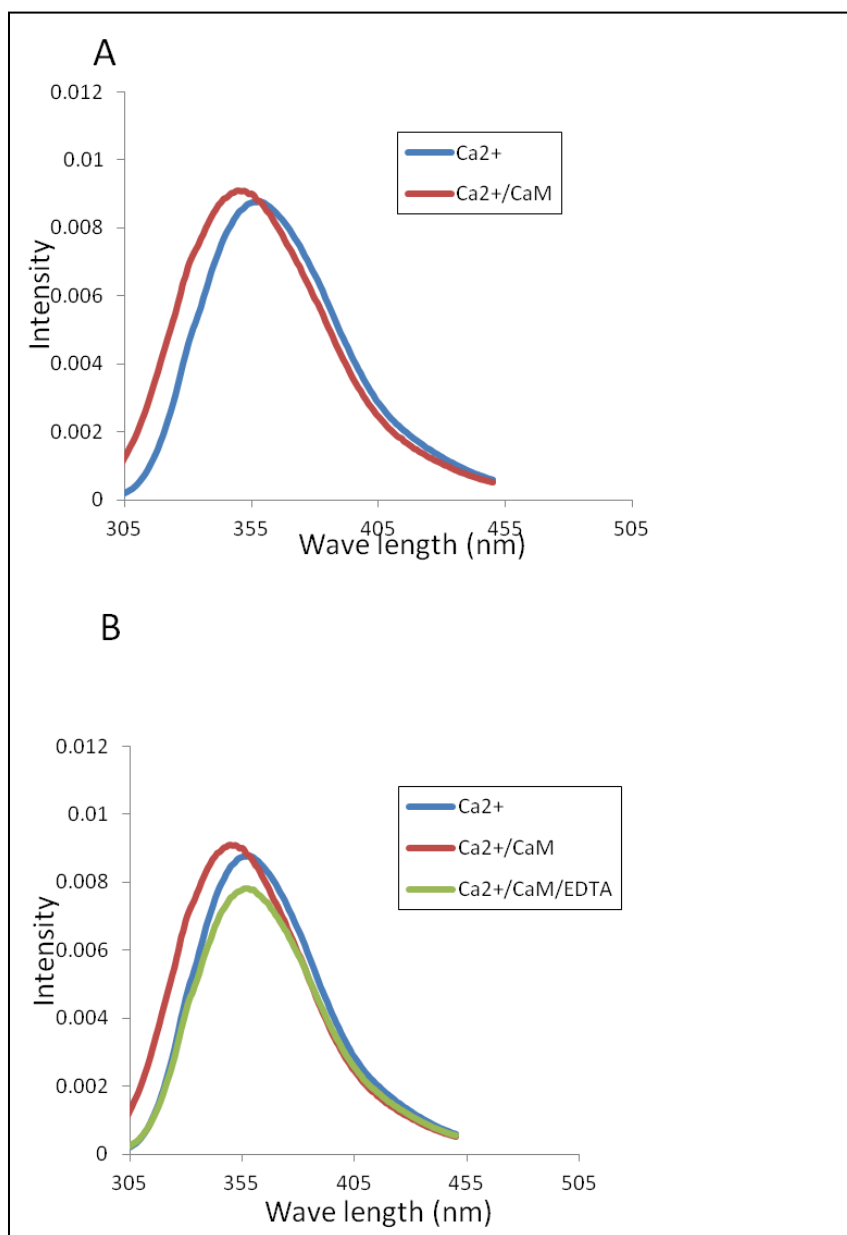
Figure 5.16: Fluorescence spectra of (A) AtCNGC12 N-terminal peptide in the absence (blue) and presence (red) of CaM, both in the presence of Ca^{2+} and (B) AtCNGC11 and 12 N-terminus peptide in the absence (blue) and presence (red) of CaM, both in the presence of Ca^{2+}, and also in the presence of Ca^{2+}/EDTA (green).

To further characterize this binding, NMR analysis was conducted as described above. When the peptide was added, a significant chemical shift for almost all the CaM residues was detected compared to CaM alone, indicating strong binding of CaM to the predicted N-terminal CaMBD (Figure 5.17A). As already observed by tryptophan fluorescence spectroscopy, this shift was Ca^{2+}-dependent, since EDTA treatment abolished this shift (Figure 5.17B).

5.3.7. Titration of CaM with AtCNGC11/AtCNGC12 wild type and L14E-K15E mutant N-terminus peptides using NMR

To further characterize the physical binding of CaM to the N-terminal putative CaMBD, a mutated version of this N-terminal peptide was synthesized. In this peptide, nonpolar L14 and positively charged K15 were changed to the negatively charged residue E (Figure 5.15, left panel). These mutations should disrupt both hydrophobic and basic sites of the amphipathic α-helix of the predicted N-terminal CaMBD, which should lead to a disruption of the CaM binding (Figure 5.15, left panel).

To observe the precise alteration of CaM binding, a titration analysis was conducted using NMR. In the titration of wild type N-terminal peptide, the signals shifted in a typical slow exchange manner, which represents strong binding of this peptide to CaM (Figure 5.18A). The chemical shift change reached saturation when one mol of peptide per one mol of CaM was added, indicating that they bind in a 1:1 ratio. On the other hand, for the mutated peptide (L14E-K15E), the signals shifted in a typical fast exchange manner where the spectrum did not reach saturation even in a 1:5 (CaM: L14E-K15E peptide) ratio (Figure 5.18B and data not shown). This indicates that the

L14E-K15E mutation disrupted CaM binding as expected. These results suggest that the predicted N-terminal CaMBD binds CaM as the helical model predicted and it is specific binding with the predicted helical structure. Furthermore the titration analysis using the wild type peptide indicates that this binding is very strong.

5.4. Discussion

In plant CNGCs, it has been reported that the CaMBD is located in the C-terminus overlapping with the CNBD. Schuurink *et al.* (1998) first reported that the cytosolic C-terminus of HvCBT1 binds AtCaM2 and a bovine CaM. Subsequently, yeast two hybrid analysis suggested that a 19–20 amino acid sequence in this region, which can form a basic amphiphilic α-helix and locates at the putative αC-helix, functions as a CaMBD in AtCNGC1 and AtCNGC2 (Köhler and Neuhaus, 2000). Supporting this report, Arazi *et al* (2000) biochemically demonstrated that a 23 amino acid sequence overlapping with this 19–20 amino acids sequence is the CaMBD in the tobacco CNGC, NtCBP4. All these data suggest that plant CNGCs have a putative CaMBD at the αC-helix in the CNBD in cytosolic C-terminal region. Recently, AtCaM2 was shown to interact with the C- but not the N-terminus of AtCNGC10 (Li *et al.,* 2005). It is worth mentioning that AtCNGC10 was predicted, in the current study, to have only one CaMBD located in the C-terminus of the channel, which agrees with this previous study (Li *et al.,* 2005).

Figure 5.17

A
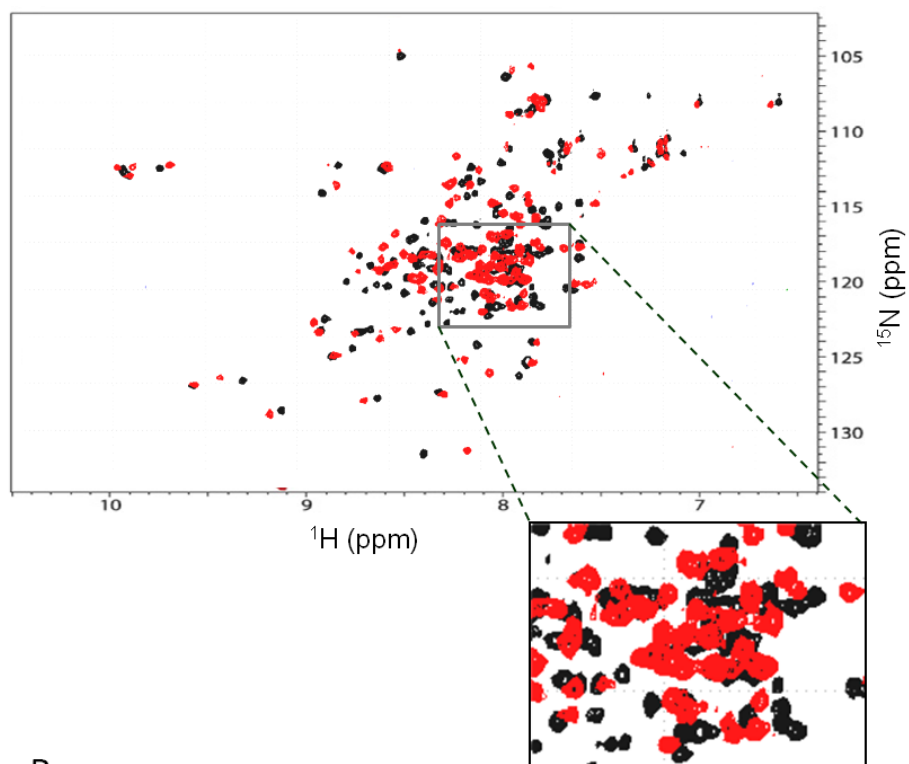
B
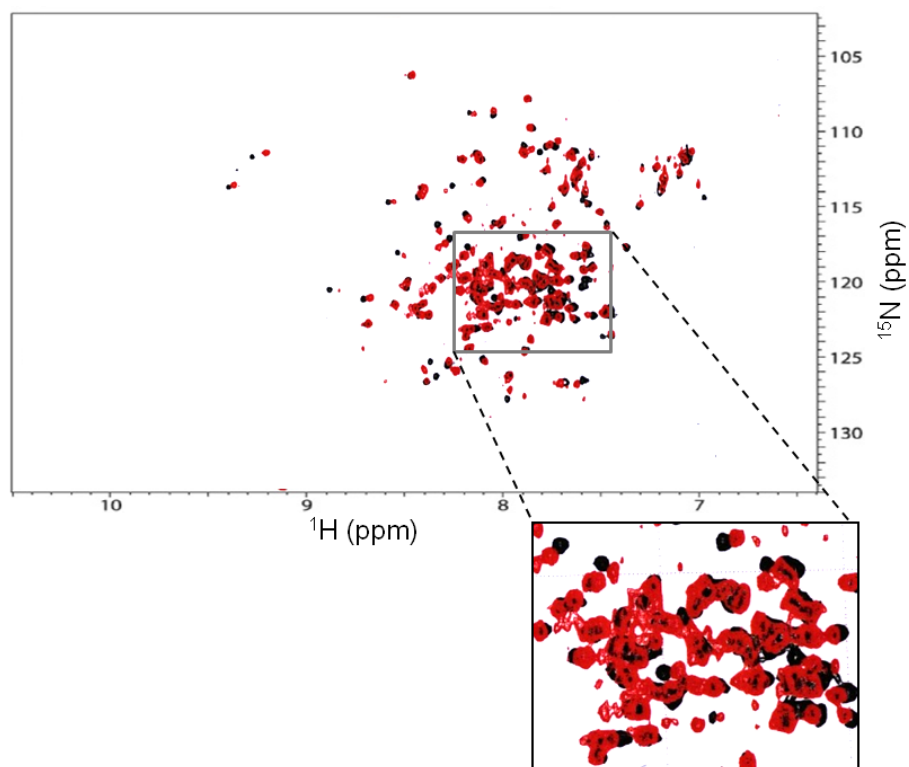
Figure 5.17: ^{1}H-^{15}N-HSQC spectra of uniformly ^{15}N-labelled Ca^{2+}/CaM (black rat CaM, PDB ID 3CLN) alone (black) and in complex with unlabeled peptide of AtCNGC12 N-terminal CaMBD (red), (A) without and (B) with EDTA.

Figure 5.18
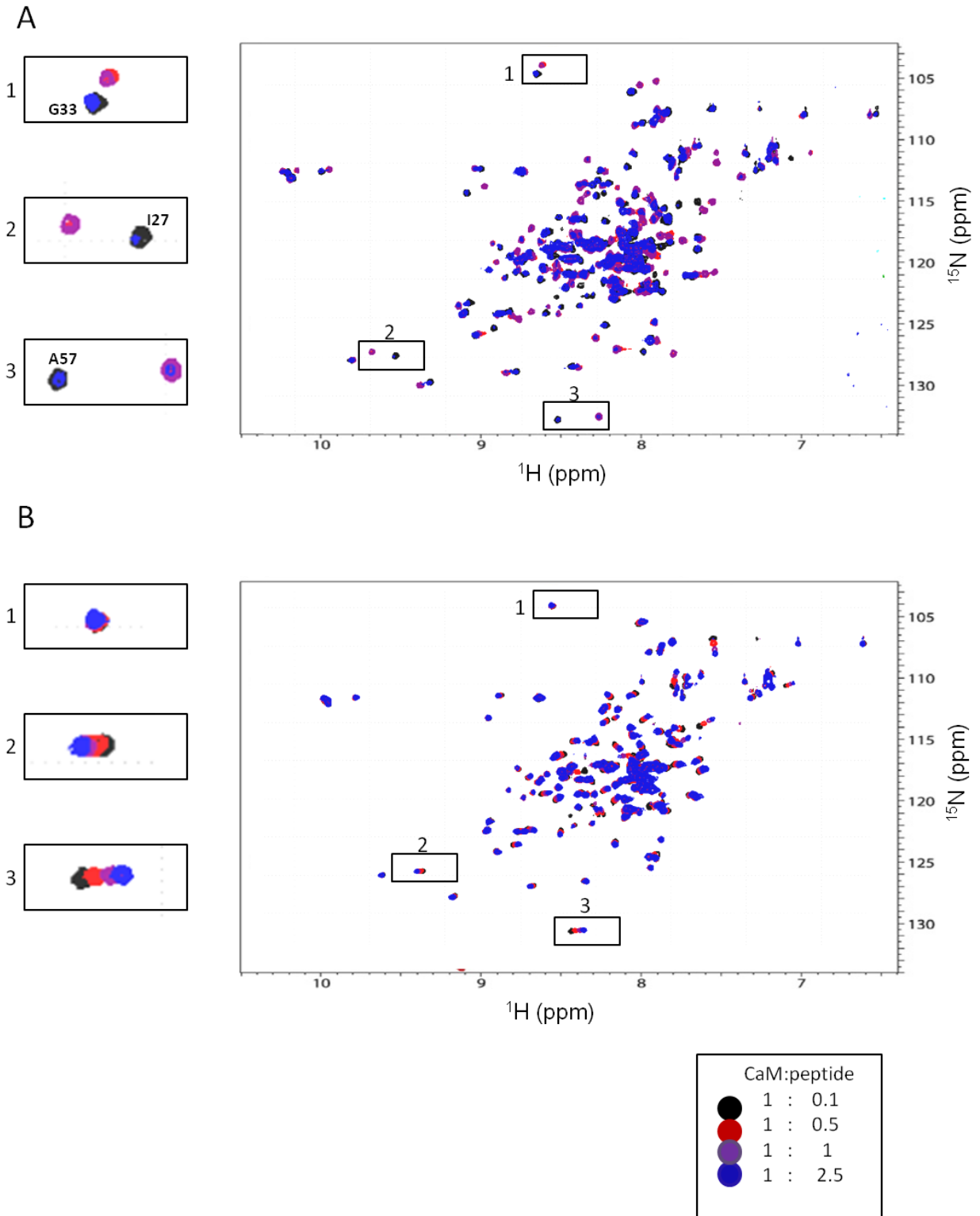
Figure 5.18: Overlay of ^{1}H-^{15}N-HSQC spectra of uniformly ^{15}N-labelled Ca^{2+}/CaM (black rat CaM, PDB ID 3CLN) titrated with (A) AtCNGC12 N-terminal peptide and (B) L14E-K15E N-terminal peptides, CaM:peptide = 1:0.1 (black), 1:0.5 (red), 1:1 (magenta) and 1:2.5 (blue).

In this study, the locations of the CaMBDs in the rest of the AtCNGC family members were investigated by MSA and the structure based Calmodulin Target Database. Some new predictions of CaMBD location were made. AtCNGC12 was predicted to have CaMBDs not only in its C-terminal, but also in the N-terminal cytosolic region. CaM binding was validated experimentally. Furthermore the predicted CaMBD in the AtCNGC12 C-terminus was not the same area as the one reported for AtCNGC1 and 2. It shifted about 10 aa toward the C-terminal end (Figure 5.4). This sequence has significant similarity to an IQ motif, which often binds to CaM in a Ca^{2+}-independent manner (Alexander *et al.*, 1988; Zhang *et al.,* 1995; Terrak *et al.*, 2005). Considering that the CaM binding of the AtCNGC12 C-terminal CaMBD is Ca^{2+}-independent, as shown in this study, it can be concluded that it is an IQ motif CaMBD. This IQ-like motif sequence of AtCNGC12 is well conserved among all AtCNGC family members, although the Calmodulin Target Database did not predict them as CaMBD (data not shown). This raises the question whether this area in other AtCNGCs also binds to CaM. If so, do some other AtCNGCs have two CaMBDs in their C-terminal region about 10 aa residues apart? Interestingly, the animal CNGC, ether á go-go (EAG) potassium channel has been reported to have three CaMBDs, one in its N-terminal cytosolic region and two in its C-terminal region just after the αC-helix of the CNBD (Ziechner *et al.*, 2006). EAG channels are regulated by intercellular Ca^{2+}: increased concentrations of Ca^{2+} inhibit channel function, presumably through CaM (Ziechner *et al.*, 2006). Thus the finding of multiple CaMBD suggests that EAG channels are regulated in a complex manner by multiple CaM molecules. Considering the remarkable similarity, AtCNGCs may be regulated in a similar manner as EAG channels. In addition, in this study it is

suggested that the location and number of CaMBD varies among AtCNGC subunits similar to animal CNGCs. It suggests diversity in the regulation by CaM among subunits. Currently there is no report about the channel subunit composition in AtCNGCs. The classification of AtCNGC members by the number and location of CaMBDs may provide a clue of the subunit composition.

In terms of N-terminal CaMBD, the animal CNGCs, CNGB1 and CNGB3 were also reported to have CaMBDs in both C- and N-termini similar to AtCNGC12 (Bradley *et al.* 2004 and Ungerer *et al.*, 2011). Bradley *et al.* (2004) and Ungerer *et al.* (2011) showed that a single lobe of CaM is permanently associated (Ca^{2+}-independent) with the N-terminus of the CNGB1b subunit and the second lobe of CaM becomes competent to bind the CaMBD of another subunit after elevation of cytosolic Ca^{2+} concentrations (Ca^{2+}-dependent). In the current study, it was shown that AtCNGC12, and possibly other AtCNGCs, have two CaMBDs in both C- and N-termini. This suggests a similar mechanism of binding, where apo-CaM is permanently associated (Ca^{2+}-independent) to the IQ-like binding site in the C-terminus with one lobe. It is possible that this apo-CaM could function as a Ca^{2+} sensor where elevations in Ca^{2+} concentrations cause a conformational change and allow binding to other binding sites located within the same or neighbouring subunits. This idea was summarized in Figure 5.19.

Figure 5.19

183
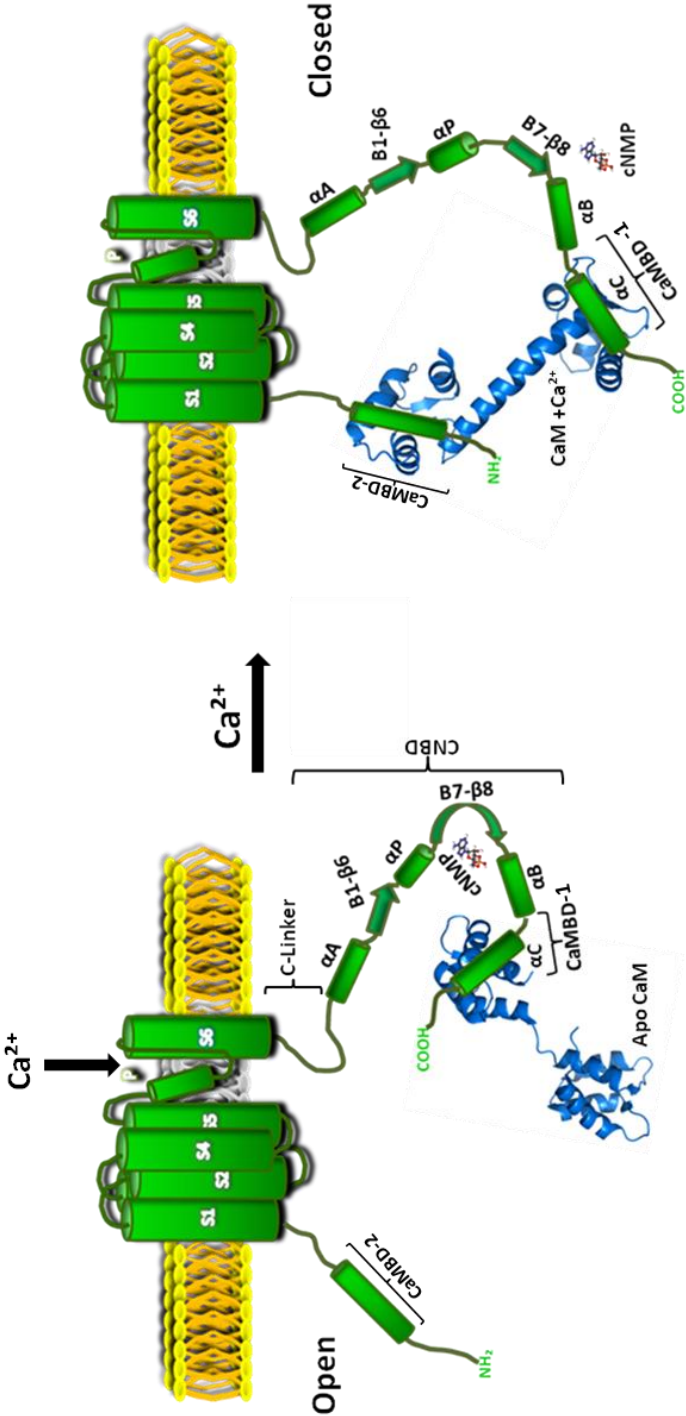
Figure 5.19: Working model for the regulation of AtCNGC12 by CaM. Apo-CaM is permanently associated to the IQ-motif in the αC-helix of the CNBD. When cNMP is bound to the CNBD of CNGC12, it causes opening of the channel, and cations can pass through the pore (between transmembrane helices 5 and 6). Upon elevation of Ca^{2+} levels in the cytosol, Ca^{2+} binds to CaM, it changes configuration and binds to the CaMBD in the cytosolic N-terminus of AtCNGC12, thus probably preventing binding of cNMPs to the channel and forcing it to close.

Chapter 6

Characterisation of the cyclic nucleotide binding domain(s) of AtCNGCs

6.1. Summary of research

The cyclic nucleotide binding domain (CNBD) of AtCNGCs was characterized, and the binding affinity of both cAMP and cGMP to the CNBD was investigated. Through computational modeling and biophysical analysis, the C-terminus of AtCNGC12 was shown to have a higher affinity to bind cAMP over cGMP. Moreover, the current work demonstrates the validity of using the thermal shift assay to determine the binding affinity of cNMP to cyclic nucleotide activated channels in general.

6.2. Introduction

6.2.1. Identification and biosynthesis of cyclic nucleotide monophosphate

cNMPs are intracellular secondary messengers that were first identified in the animal system by Rall *et al.* (1957). Through that study, cNMPs were identified as heat-stable active factors, but the actual chemical structure was determined by Lipkin and colleagues (1959). The biosynthesis of two main cNMPs, namely cyclic adenosine-3', 5' monophosphate (cAMP) and cyclic guanosine-3', 5' monophosphate (cGMP), has been well characterized in the animal system. Large numbers of adenylyl cyclases (ACs) (Hanoune and Defer, 2001), and guanylyl cyclases (GCs) (Garbers, 1999; Lucas *et al*., 2000), were identified and proved to be involved in the synthesis of both cAMP and cGMP, respectively.

cNMPs are known to regulate a wide array of physiological processes. This regulation by cNMPs is carried out by direct binding to a variety of proteins including protein kinases, ion channels, transcription factors, and guanine nucleotide exchange proteins (Baruscotti and Difrancesco, 2004; Biel *et al*., 2002; Pape, 1996; Robinson and Siegelbaum, 2003; Flynn *et al.,* 2007).

In contrast to the animal system, little is known about cNMPs in the plant system where the existence of plant cNMPs remained debatable until the end of the twentieth century (Newton *et al.,* 1999). The controversy about the existance of cNMPs is due to the small numder of ACs and GCs identified in the plant system. There are two identified GCs and both are in *A. thaliana.* One is *AtGC1,* which was identified through a search for a GC catalytic domain motif in the *A. thaliana* genomic sequence (Ludidi and Gehring, 2003). The other GC was also discovered from the *A. thaliana* sequence database and was annotated as a hormon receptor (Kwezi *at al.,*2007). Few plant proteins have been also identified to have AC activities. For example, a soluable AC was identified in alfalfa roots and tobacco (Carricarte *et al.,* 1988; Ichikawa *et al.,* 1997).

Simillar to the animal system, cNMPs are known to regulate some physiological processes in plants by direct binding to variety of proteins including cyclic nucleotide responsive protein kinasas, cyclic nucleotide binding proteins, and cyclic nucleotide gated ion channels (Newton and Smith, 2004).

In general, the study of cNMPs synthesis and their targets in the plant system still in its infancy compared to the well characterized ones in the animal system, which indicates the lack of knowledge of cNMP signalling in plants.

6.2.2. Activation of CNGCs by cyclic nuceotide mono phosphates

The CNBD of both plant and animal CNGCs share many similarities to other cNMP-binding proteins such as cAMP and cGMP-dependent protein kinases, the bacterial catabolite activator protein (CAP) and other voltage and ligand-gated ion

channels such as HCN and EAG channels (Arazi *et al.*, 2000; Hua *et al.*, 2003b; Anderson *et al.*, 1992; Sentenca *et al.*, 1992; Robinson and Siegelbaum, 2003).

The architecture of the CNBD and C-linker regions was revealed by the X-ray crystallographic structures of the C-terminal regions of the HCN2 channel (Zagotta *et al.,* 2003) and of another channel in the HCN family, the SpIH channel (Flynn *et al.,* 2007). In general, the CNBD is composed of two sub-domains: a roll sub-domain and a C-helix sub-domain. The roll sub-domain consists of two α-helices "A and B-helix", and β1-8-strands that are located between the helices. In addition, between the sixth and the seventh β-strands there is P-loop (Zagotta *et al.,* 2003; Flynn *et al.,* 2007). The C-helix sub-domain is a single α-helix that is believed to contain the CaMBD in plant CNGCs.

Based on the crystal structure and electrophysiological analyses for HCN2 and SpIH1, it was suggested that cNMPs (cAMP and cGMP) first bind to the β-roll then interact with the C-helix. It has also been shown that cGMP binds in the β-roll in the syn-configuration in contrast to the anti-configuration seen for cAMP (Zagotta *et al.*, 2003; Craven and Zagotta, 2006; Flynn *et al.,* 2007; Zhou and Siegelbaum*,* 2007) (Figure 6.1). The mechanism of cGMP binding specificity was proposed as follows: cGMP first docks in the syn-configuration in the CNBD through interactions with a threonine in the β-roll. This docking causes configuration change that induces binding of the C-helix to cGMP through an aspartate in the C-helix which subsequently promotes channel opening (Shapiro and Zagotta, 2000; Flynn *et al.,* 2007). In contrast, isoleucine as well as other residues in the C-helix, were proposed to contribute to cAMP selectivity over cGMP (Zagotta *et al.*, 2003; Flynn *et al.,* 2007; Zhou and Siegelbaum*,* 2007).

Figure 6.1

cAMP
anti configuration

purine ring

phosphoribose

cGMP
syn configuration

purine ring

phosphoribose
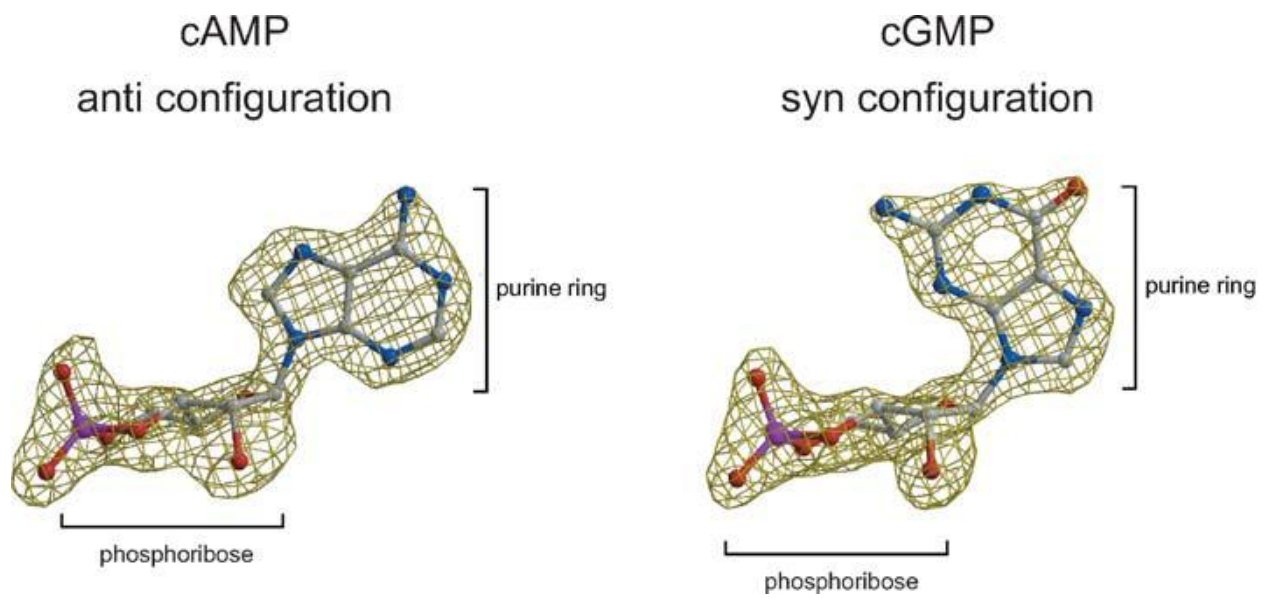
Figure 6.1: Cyclic nucleotide crystal structures. Density from X-ray crystallography showed for cAMP (left) and cGMP (right), with the chemical structure of the molecules shown in ball-and-stick format. Elements are coded with color: carbon (gray), nitrogen (blue), phosphorous (purple), hydrogen (red) (adapted from Craven and Zagotta, 2006).

It has been previously suggested that cAMP, but not cGMP, enhanced the activation of AtCNGC11/12, a chimeric channel protein that was identified in the *A. thaliana* mutant *cpr22*, as well as wild type AtCNGC12 by a yeast complementation assay (Yoshioka *et al.*, 2006). Baxter *et al.* (2008) later reported that the CNBD of AtCNGC11/12, which is identical to that of AtCNGC12, binds cAMP *in vitro.* Furthermore, it was shown that AtCNGC11/12 (AtCNGC12) selectively binds cAMP over cGMP in a competition assay (Baxter and Yoshioka unpublished data). In this analysis, the CNBD of AtCNGC11/12 (AtCNGC12) was pre-incubated with either cAMP or cGMP. Upon addition of cAMP-agarose, pre-incubation with cAMP reduced binding to the resin, whereas cGMP did not affect binding to cAMP agarose (Baxter and Yoshioka unpublished data). These results were not conclusive, due to the lack of *in vivo* data and structural data. Therefore, further analyses were required.

In this chapter, to further investigate cNMP binding occurs in plant CNGCs, structural modeling and cNMP binding analyses were performed.

6.3. Results

6.3.1. Computational modeling suggests that a specific positively charged residue in the C-helix of the CNBD is important for cAMP selectivity in AtCNGCs

A three-dimensional model for the predicted CNBD of AtCNGC12 was obtained based on the crystal structures of the C-terminal regions of HCN2 and SpIH1 channels (Zagotta *et al.,* 2003; Flynn *et al.,* 2007), where all the residues predicted to interact with either cAMP or cGMP were mapped (Figure 6.2A and B).The theoretical model revealed many similarities between the CNBDs of AtCNGC12 and both HCN2 and

SpIH1. Both HCN2 and SpIH1 were proven to have higher affinity to bind cAMP over cGMP (Flynn *et al.,* 2007; Zhou and Siegelbaum*,* 2007).

In the generated model, residues that form the cNMP binding pocket of HCN2, namely E582, R591 and T592 in the β-roll, and R632, R635 and I636 in the αC-helix, aligned well with E494, R507 and T508 in the β-roll, and A561, R564 and K565 in the αC-helix of AtCNGC12 in the presence of either cAMP or cGMP (Figure 6.2A).

The selectivity of cGMP occurs in the presence of a threonine in the β-roll (in this case T592 in HCN2). This threonine residue forms two hydrogen bonds with cAMP and three with cGMP (Figure 6.2B). Additionally, the presence of a negatively charged residue (either aspartate or glutamate) in the αC-helix further drives the channel to the open state. This negatively charged residue selectively forms two hydrogen bonds with the guanine ring of cGMP, as was shown in animal CNGCs that were reported to have higher sensitivity to cGMP (Varnum *et al.*, 1995; Zagotta *et al.*, 2003; Flynn *et al.,* 2007; Zhou and Siegelbaum*,* 2007). According to my 3D models, the threonine (T592) in the β-roll of HCN2 (homologues to V621 in SpIH1) superimposed with T508 in AtCNGC12 (Figure 6.2B). This threonine is also conserved in seventeen out of twenty AtCNGCs, as shown in the multiple sequence alignment (MSA) of the twenty members of the AtCNGC family (Figure 6.3), indicating the importance of this threonine. Also my 3D analysis showed that the negatively charged residue (either aspartate or glutamate) in the αC-helix of animal CNGCs superimposed with a positively charged residue K565, in AtCNGC12, and I636 in HCN2 (Figure 6.2C). I636 was reported to form a hydrophobic interaction with the purine ring of cAMP (Zagotta *et al.*, 2003). Replacement of I636 with the aspartate present in CNGA1 converts HCN2 into a cGMP selective channel.

Molecular dynamics MD simulations indicate that the aspartate forms a favorable electrostatic interaction with the partial positive charge on the guanine ring and a repulsive electrostatic interaction with the partial negative charge on the N7 atom of adenine ring (Zhou and Siegelbaum, 2007). This suggests that K565 in AtCNGC12, create a repulsive interaction with the guanine ring of cGMP (Figure 6.2C right panel), but a stabilizing electrostatic interaction with the partial negative charge on the adenine N7 atom of cAMP. Therefore, the model generated indicates a higher affinity of AtCNGC12 to cAMP (Figure 6.2C left panel).

The MSA of the twenty members of AtCNGCs also revealed that K656 is unique to AtCNGC12, where the other nineteen members have arginine (R) instead of lysine (K) (Figure 6.3). Although lysine and arginine share similar biochemical properties, change from lysine to arginine might have an impact on the structure of the CNBD in the rest of the AtCNGCs. To test if this difference has an impact on the structure of the cNMP binding pocket, computational model of AtCNGC12:K565R was created. As shown in Figure 6.4, overall structure of cNMP binding pocket in AtCNGC12:K565R is similar to the original AtCNGC12 (Figure 6.2A lower panel and Figure 6.4A). Also, Figure 6.4B showed that K565R created a repulsive interaction with the guanine ring of cGMP and a stabilizing electrostatic interaction with the partial negative charge on the adenine N7 atom of cAMP. The created model suggests a similar mode of interaction as predicted in AtCNGC12. (Figure 6.2C lower panel and Figure 6.4B).

6.3.2. AtCNGC12 has higher affinity to bind cAMP over cGMP

The fluorescence-based thermal shift assay is a well established method for determining protein-ligand binding affinities (Vedadi *et al.*, 2006). This assay was recently used in a screen for inhibitors of protein kinases, and in determining the stabilizing effect of salicylate on a multiple antibiotic-resistance repressor (MarR) family protein (Vedadi *et al.*, 2006; Niesen *et al.*, 2007; Saridakis *et al.*, 2008). Figure 6.5A illustrates this method. In this assay, the environmentally-sensitive fluorescent dye, Sypro Orange, is masked in an aqueous environment. Upon denaturation by heat, the protein of interest undergoes thermal unfolding, thereby exposing its hydrophobic core. This hydrophobic environment then allows the dye to fluoresce (excitation wave length= 492). This can be monitored by a real-time PCR system (Niesen *et al.,* 2007). In the presence of the ligand, the protein of interest becomes more stable; consequently the unfolding temperature of the protein goes up compared to that of the protein without ligand. Since, this assay has not been used to detect the binding affinity of cNMPs to the CNBD of CNGCs, I first tested HCN2, which is known to have high affinity for cAMP over cGMP (Zagotta *et al.*, 2003; Flynn *et al.,* 2007; Zhou and Siegelbaum*,* 2007). cDNA of the C-terminus of HCN2 was provided by Zagotta laboratory (University of Washington) and it was expressed in *E. coli* cells. Soluble protein was extracted and purified using a Ni²⁺-affinity chromatography and size exclusion chromatography. Thermal denaturation of this protein was conducted with increasing concentrations of either cAMP or cGMP, and Sypro Orange dye was used as a fluorescent indicator to monitor the denaturation of the protein.

As shown in Figure 6.5B, the presence of cNMP (either cAMP or cGMP) was shown to stabilize the C-terminus of HCN2, which is evident by an increase in the temperature at which the protein unfolds. Consistently, the unfolding temperature of the C-terminus of HCN2 increases nonlinearly with increasing concentrations of cNMP. The titration profile obtained is saturable, thus indicating that both cAMP and cGMP are binding specifically to the CNBD of HCN2. The results show that binding with cAMP is more stable than that with cGMP upon thermal denaturation of the C-terminus protein of HCN2, where cAMP required higher temperatures for the protein to unfold compared to cGMP. This result indicates a higher binding affinity of cAMP over cGMP to the CNBD of HCN2. This agrees with previously published work that reported a higher sensitivity of HCN2 to cAMP over cGMP (Zagotta *et al.*, 2003; Flynn *et al.,* 2007; Zhou and Siegelbaum*,* 2007), indicating the suitability of this method for cNMP binding analysis.

After validating this method using HCN2, the same procedure was used to assess the binding affinity of cNMPs to the CNBD of AtCNGC12 expressed in *E. coli* cells. C-terminal soluble protein was extracted and purified using a Ni^{2+}-affinity column and FPLC. As shown in Figure 6.5C, the results indicate a higher stabilization effect of cAMP over cGMP on the thermal denaturation of the C-terminus of AtCNGC12. Higher temperatures were needed to unfold the protein in the presence of cAMP compared to cGMP, thereby reflecting a higher binding affinity to cAMP over cGMP (Figure 6.5C). These results are consistent with my computational prediction mentioned in 6.3.1 section.

Figure 6.2
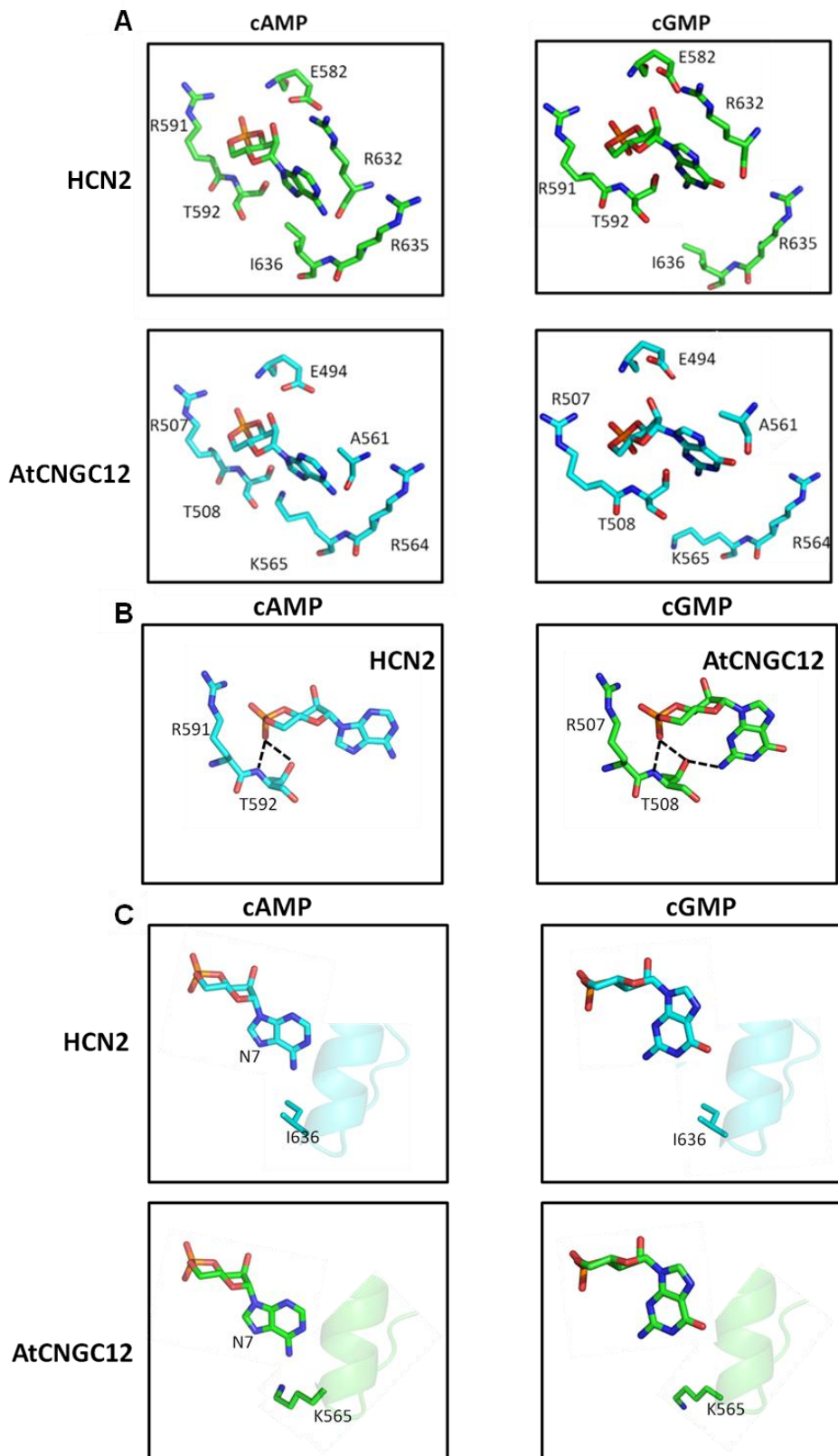
Figure 6.2: Computational modeling of the CNBD of both HCN2 and AtCNGC12 showing (A) Interactions of CNBD residues of HCN2 (upper panel) and AtCNGC12 (lower panel) with cAMP (left) and cGMP (right), (B) Interactions of T592 and T508 of HCN2 and AtCNGC12, respectively, with cAMP (left) and cGMP (right). T592 forms two hydrogen bonds (dashed lines) with cAMP and three with cGMP. (C) Interactions of I636 of HCN2 (upper panel) and K565 of AtCNGC12 (lower panel) with cAMP (left) and cGMP (right). T592 forms two hydrogen bonds (dashed lines) with cAMP and three with cGMP.

Figure 6.3

Figure 6.3: Alignment of the CNBD areas of the 20 AtCNGCs, NCBI accession # are listed in Appendix, Table 2. The red boxes indicate the position of T508 and K565 in AtCNGC12.

Figure 6.4

A   cAMP

AtCNGC12:K565R

E494
R507
A561
T508
K565R
R564

B   cAMP   cGMP

AtCNGC12:K565R
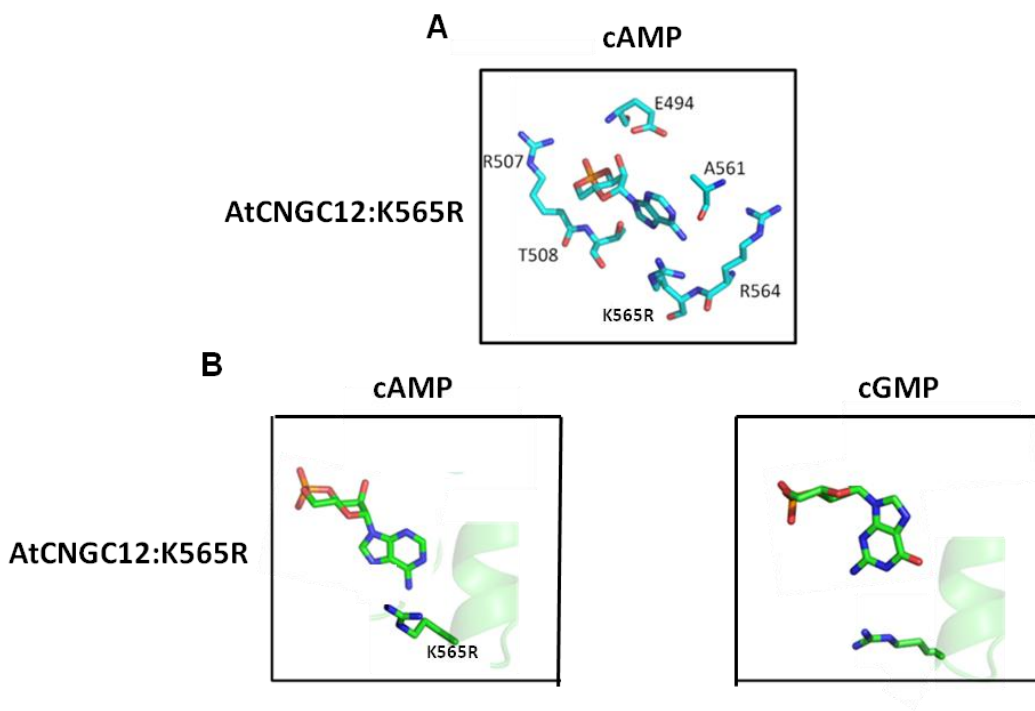
K565R

Figure 6.4: Computational modeling of the CNBD of AtCNGC12:K565R showing (A) Interactions of CNBD residues of AtCNGC12:K565R with cAMP, (B) Interactions of K565R of AtCNGC12:K565R with cAMP (left) and cGMP (right).

Figure 6.5
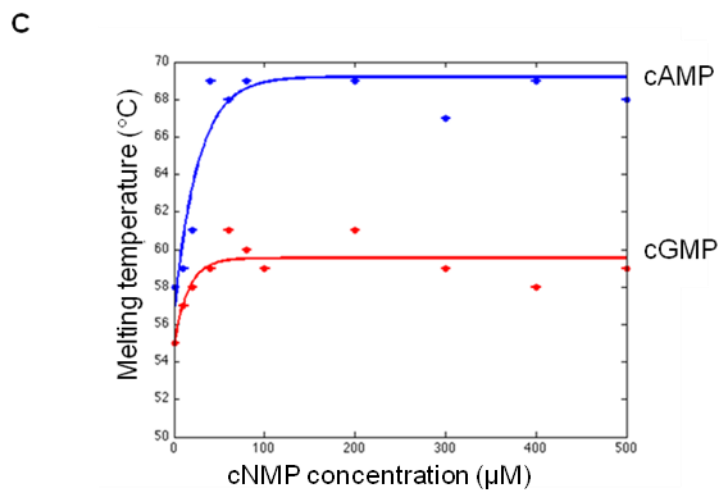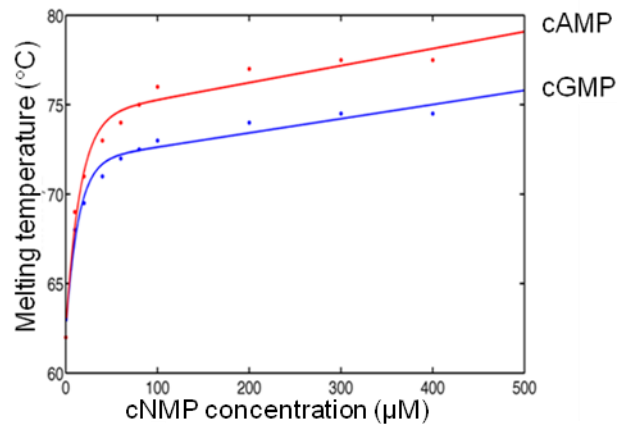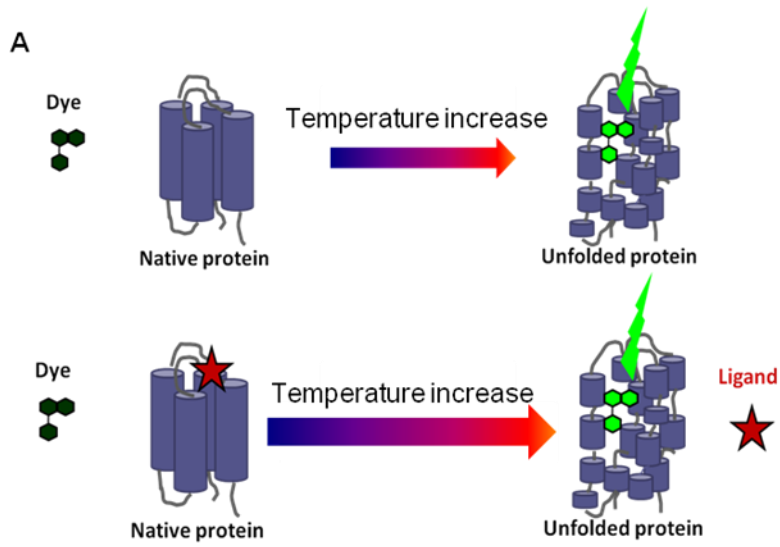
Figure 6.5: Fluorescence-based thermal shift assay of both HCN2 (positive control) and AtCNGC12. (A) Cartoon of the mechanism of the method. (B) The effect of cNMPs (µM) on the thermal denaturation of the C-termini of HCN2 and (C) AtCNGC12.

6.4. Discussion

The selectivity of cNMPs in CNGCs has been well studied in the animal system (Altenhofen *et al.*, 1991; Kumar and Weber, 1992; Scott *et al.*, 1996; Weber *et al.*, 1989; Zagotta *et al.*, 2003; Flynn *et al.,* 2007; Zhou and Siegelbaum*,* 2007). Mammalian CNGCs are activated solely by cGMP, whereas HCN channels are fully activated by cAMP and partially by cGMP. The high affinity to cGMP over cAMP arises from the presence of a threonine residue in the β-roll and an aspartate residue in the C-helix that stabilize the docking of cGMP in the syn-configuration in the CNBD (Shapiro and Zagotta, 2000; Flynn *et al.,* 2007). On the other hand, Zhou and Siegelbaum*,* 2007 reported that cAMP selectivity in HCN2 is distributed across a number of the C-helix residues, including R632, R635 and I636 (equivalent to A561, R564 and K565 in AtCNGC12). However, it is not clear how such residues generate selectivity.

It was also reported that Mesorhizobium loti K1 channel (MlotiK1), the prokaryotic homolog of cyclic nucleotide-dependent ion channels, has a higher affinity to bind cAMP over cGMP (Altieri *et al.,* 2008; Schnuke *et al.*, 2010). The specificity of binding cAMP over cGMP in this channel was revealed using both NMR and crystallography. These studies showed that two positively charged residues, R307 in the β-roll and R348 in the αC-helix of the CNBD (equivalent to R591 and R635 in HCN2, and R507 and R564 in AtCNGC12), play crucial roles in this selectivity (Schnuke *et al.*, 2010). Moreover, the crystal structure of the CNBD of MlotiK1 with cGMP showed specific hydrogen bonds occurring with the binding pocket. In particular, the N2 amine forms a hydrogen bond with the hydroxyl group of S308 (Altieri *et al.,* 2008). A similar interaction was reported in the HCN2's CNBD-cGMP crystal structure, where T592 (equivalent to S308 in

MlotiK1 and T508 in AtCNGC12) forms a hydrogen bond with the N2 of cGMP (Zagotta *et al.,* 2003). Mutations in these residues (S308A and S308V) in MlotiK1 reduced the channel sensitivity to cGMP, but not to cAMP (Altieri *et al.,* 2008).

Similar interaction between a serine residue in the β-roll of the CNBD and cGMP, was also reported in other cyclic nucleotide binding proteins such as cGMP-dependent protein kinases (PKGs) (Kim *et al.*, 2011) and Phosphodiesterase 5 (PDE5) (Heikaus *et al.,* 2008). This indicates the importance of a serine/threonine residue in the β-roll of the CNBD in the selective interaction with cGMP.

In the plant system, electrophysiological studies have shown differences in cNMP binding affinities to CNGCs. For example, AtCNGC4 is activated more strongly by cGMP than cAMP (Balagué *et al.*, 2003), while AtCNGC2 is activated similarly by both cAMP and cGMP (Leng *et al.*, 1999, Leng *et al.*, 2002). Also, the complementation of a K^+-uptake deficient yeast mutant with AtCNGC11/12, as well as AtCNGC12, was enhanced in the presence of cAMP but not cGMP (Yoshioka *et al.*, 2006).

To characterize the CNBD of AtCNGCs, computational modeling and biophysical analysis were utilized. The structure modeling of the CNBD of AtCNGCs showed similarities to other cyclic nucleotide-binding proteins such as cAMP-dependent protein kinase (Su *et al.*, 1995), a bacterial cyclic nucleotide-regulated potassium channel (Clayton *et al.*, 2004), HCN2 channel (Zagotta *et al.*, 2003) and SpIH channel (Flynn *et al.,* 2007), where the cNMP is bound to the interface between the β-roll and the C-helix.

In my model, the presence of a positively charged residue, either lysine (K565) in the CNBD of AtCNGC12 or arginine at the equivalent location in the other 19 AtCNGCs, suggests a higher affinity of AtCNGCs to bind cAMP over cGMP. To test the binding

affinity of cNMP to the CNBD of AtCNGC12, a fluoresce based thermal shift assay was conducted to measure the affinity of protein-ligand interaction (Niesen *et al.,* 2007). Here, I used this method for the first time to determine the selectivity of cAMP or cGMP binding in a plant CNGC. In this work, I showed that AtCNGC12 binds cAMP with higher affinity than cGMP, which agrees with my computational modeling and previous data using yeast complementation assay (Yoshioka *et al.*, 2006). This method could be useful to assess cNMP interactions in cyclic nucleotide-activated channels in general, and to identify important residues necessary for these interactions to occur.

This work has confirmed previous data on selectivity between cNMPs in plant CNGCs. Also, it introduced a new method that could be useful in determining the cNMP binding affinity to its target.

Chapter 7

Conclusions and Future Work

7.1. Conclusions

The *A. thaliana* CNGC family has twenty members and the biological functions of some of them have been identified. For example, some AtCNGCs are involved in plant development including senescence, gravitropism and pollen tube growth, while others have multiple functions in pathogen defense signalling (Köhler *et al.*, 2001; Sunkar *et al.,* 2000; Balagué *et al.*, 2003; Chan *et al.*, 2003; Li *et al.*, 2005; Ma *et al.*, 2006; Gobert *et al.*, 2006; Yoshioka *et al.*, 2006; Borsics *et al.*, 2007; Urquhart *et al.*, 2011). On the other hand, the structure-function relationship in this group of ion channels is still in its infancy.

Prior to this current study, two other studies, Baxter *et al.*, (2008) and Chin *et al.,* (2010), explored the relationship between the structure and the function of AtCNGCs using the *A. thaliana* mutant *cpr22*. In these studies, two amino acids, E519 and R557 in AtCNGC11/12, have been reported to have an essential role, either in basic channel function, through an interaction between the C-linker and the CNBD of the same subunit (E519), or in the regulation of channel through the alteration of CaM binding (R557). Through the same suppressor screening, twenty seven more residues, which are potentially important for *cpr22* phenotype or basic channel function, were identified and eleven were investigated for their role in channel function from a structural point of view. Two amino acids, out of eleven, R381 and G459 have been concluded to have essential roles in the function of the channel through an inter-subunit interaction with other residues on the neighbouring subunit.

Also, in this study the CNBD and CaMBD have been characterized. The binding affinity of cNMP, either cAMP or cGMP, to the CNBD has been investigated through

computational modeling and biophysical analysis. The results showed higher affinity of the CNBD in AtCNGC12 to bind cAMP over cGMP which supported the computational analysis. Furthermore, the thermal shift assay was used for cNMP affinity analysis for the first time. The result using HCN2 showed that this method can be a convenient alternative way to analyze cNMP affinity for CNGCs.

The CaMBD has also been structurally characterized for its mode of binding to CaM. In terms of CaMBD, AtCNGCs can be classified into three groups, based on the analysis by the three dimensional structure based CaMBD prediction tool. The first group has only one predicted CaMBD in the cytosolic C-terminus. An example of this group is AtCNGC2. The second group has a predicted CaMBD in the cytosolic N-terminus, like AtCNGC11. The third group contains AtCNGCs that have two CaMBDs in both C-and the N-termini. Example of this type is AtCNGC12. These predictions were experimentally validated by biophysical analyses using tryptophan fluorescence spectroscopy and NMR. Through these analyses, it has been concluded that AtCNGC2 has a CaMBD in the C-terminus, whereas AtCNGC11 has a CaMBD in the N-terminus. The CaMBD of these two AtCNGCs binds CaM in a Ca^{2+}-dependent manner. On the other hand, AtCNGC12 has been shown to harbour two CaMBDs in both C- and N-termini of the channel. The N-terminus CaMBD was shown to bind CaM in a Ca^{2+}-dependently fashion, whereas the C-terminus was shown to bind CaM in a Ca^{2+}-independent manner. These results agree well with the computational prediction, indicating the power of our computational analysis.

Collectively, these findings contribute to the better understanding of how structure translates into function in AtCNGCs in general.

7.2. Future work

Important biological roles of several AtCNGCs has been reported (Köhler *et al.*, 2001; Sunkar *et al.,* 2000; Balague *et al.*, 2003; Chan *et al.*, 2003; Li *et al.*, 2005; Ma *et al.*, 2006; Gobert *et al.*, 2006; Yoshioka *et al.*, 2006; Borsics *et al.*, 2007). On the other hand, little is known about the structure-function relationship of these channels, and the crystal structure of these AtCNGCs remains to be resolved. One profound question which remains to be answered is how these channels are regulated. Do cNMPs activate plant CNGCs in a fashion similar to the once described for animal CNGCs, or are plant CNGCs regulated negatively by cNMPs? In some cases, the CNBD and CaMBD occur as overlapping regions. In these cases, what is the role of CaM in terms of channel regulation? Does CaM compete with the cNMP as suggested? How many CaMBD exists in each subunit? All these questions have to be answered to understand the regulation of plant CNGCs. Such knowledge will thus allow us to further understand their roles in signal transduction.

The thesis presented here provides insights into the structure-function relationship of AtCNGCs, however, further studies of AtCNGC structure, including their different domains and how these domains interact with their predicted ligands, are required. In addition, investigating how these interactions affect the functionality of these channels will contribute to the plant CNGC research significantly. The outcome of these studies could further be used in the manipulation of plant CNGCs for the generation of pathogen resistant crops.

7.2.1. Determining the atomic resolution structure of the C-terminus of AtCNGC11/12(12)

In this thesis, I have modeled 3D structures of AtCNGCs using the crystal structure of SpIH since there is no similar plant channels crystalized so far and the structure of SpIH provides the highest similarity to AtCNGCs. Based on these models, I have made hypotheses of the structure-function relationship and in some cases, they were validated experimentally. This suggests that the models created by SpIH are for some extent accurate, however, considering the significant sequence difference between AtCNGCs and SpIH, especially after the β-roll in the CNBD (Dr. Zagotta, personal communication), the accuracy of the models is not so clear yet. Thus, crystallization of AtCNGCs is essential to understand the precise structure-function relationship. Indeed, I have planned to crystalize cytosolic C-terminal of AtCNGC12, however the expression in *E.coli* was not high enough. Currently, another Yoshioka lab member is attempting to increase the expression and solubility level with multiple constructs.

Crystallization and structure determination of AtCNGC12, in the presence or absence of cNMP, is the ultimate way to understand the structure of this channel and, possibly, the rest of the AtCNGCs. It will also show the mode of interaction between these channels and their predicted ligand(s).

7.2.2. Functional analysis of CaMBDs in AtCNGCs

The location and functionality of CaMBDs has been well studied in the animal system electrophysiologically (Bradley *et al.*, 2004; Craven and Zagotta, 2006; Ungerer

et al., 2011). For example, Bradley *et al.* (2004) reported that CNGB1b has two CaMBDs in both cytoslic N- and C- terminal domains. Both CaM-binding sites contribute to the negative regulation of the channel by binding CaM in a Ca^{2+}-dependent and independent manner.

In the plant system, yeast-two-hybrid analyses were used to determine CaM-binding in several CNGCs (Köhler and Neuhhaus, 2000 and Arazi *et al.,* 2000). For example, Köhler and Neuhaus (2000) showed that both AtCNGC1 and 2 bind AtCaM2/3/5 and AtCaM4. Also, fluorescence emission spectrum was used in other studies to show CaM binding (Hua *et al.*, 2003; Li *et al.,* 2005; Ali *et al.*, 2005). Li *et al.* (2005) demonstrated that AtCaM2 interacts with the C- but not the N-terminus of AtCNGC10 using this method.

In the presented work, the locations of CaMBDs of AtCNGCs were investigated and the physical binding of these domains to CaM were assessed using tryptophan fluorescence spectroscopy and NMR.

To investigate the biological significance of the CaMBDs in AtCNGCs, reliable electrophysiological studies will be required. It will be interesting to determine if AtCNGC12 has a similar mode of regulation as the animal CNGC, CNGB1b. It has been reported that CNGB1b has two CaMBDs in both cytoslic N- and C- terminal domains contribute to the negative regulation of the channel by binding CaM in a Ca^{2+}-dependent and independent manner (Bradley *et al.* 2004). We recently established collaboration with the Zagotta laboratory in the Department of Physiology and Biophysics at the University of Washington to pursue electrophysological analyses.

In addition, to study the structure-function relation of the CaMBD in AtCNGCs, and their mode of interaction with CaM, above mentioned X-ray crystallography is required.

7.2.3. Functional analysis of CNBDs in AtCNGCs

The results from this work indicated that AtCNGCs have a higher affinity to bind cAMP over cGMP, through computational modeling and thermal shift assay. So far cNMP selectivity in AtCNGC12 has been analyzed by either *in vitro* binding assay (Baxter *et al.* 2008), or yeast complementation analysis (Yoshioka *et al.*, 2006). All these analyses agreed well with the computational modeling conducted in this study. To connect this affinity (physical binding of cNMPs and AtCNGCs) to the efficacy of actual channel gating by cNMPs, electrophysiological analysis will be required. This approach can be combined with site-directed mutagenesis of the residues predicted to participate in the interaction between the CNBD and its ligand. One such residue of interest is K565 in the C-helix of AtCNGC12 CNBD. According to my computational analysis, mutation of this residue to an acidic residue should generate novel interactions with cGMP. This would convert cGMP to a full agonist of AtCNGC12. Similar work in Flynn *et al.,* (2007) showed that mutating I636 in the C-helix to aspartate converted HCN2 to a cGMP-specific binding protein. The thermal shift assay, which I used in this thesis work, can also be used to validate this hypothesis and by combining with bioassays the biological importance of cNMP specificity can be revealed.

The demonstration of AtCNGCs specificity toward either cAMP or cGMP would be of great interest and would be the first of its kind.

7.2.4. Hetero-tetramerization of AtCNGCs

In the animal system, CNGCs have been proven to form heterotetramers. The combination of subunits greatly affects the functionality of these channels. For example, it has been shown that the native olfactory CNGCs are composed of three different subunits (CNGA2, CNGA4, and CNGB1b) (Bradley *et al.*, 2004). The expression of CNGA2 subunits alone can form functional homomeric channels in heterologous system that shows slower inhibition by Ca^{2+}/CaM. This is due to the lack of sufficient CaMBDs in this subunit type. On the other hand, the sole expression of either CNGA4 or CNGB1b did not form functional homomeric channels, which indicates that those subunits are modulatory ones (Trudeau and Zagotta, 2003; Bradley *et al.*, 2004).

CNGCs in the plant system have only been speculated to form heterotetramers. There are twenty *A. thaliana* CNGC members compared to six in vertebrates which suggests large variation in channel properties and modes of regulation can be achieved through heterotetramerization.

Previous work that has been done by the Yoshioka lab indicates heterotetramerization of AtCNGCs. For example, the RNAi-induced double silenced lines of *AtCNGC11* and *12*, exhibit similar impairment in resistance against avirulent pathogens to single *AtCNGC11* and *12* knockout lines, (Moeder *et al.*, 2011). Since, the loss of both subunits does not have additive effect; it suggests that AtCNGC11 and 12 could form one channel together, where the loss of either one abolishes the function of this channel, however, further analysis, to have more definitive data, is required.

Several approaches can be taken to investigate heterotetramerization in AtCNGCs, including yeast-two-hybrid analysis. Attempts of yeast-two-hybrid analysis

were found to be experimentally challenging in the past, but might provide valuable data once the conditions have been successfully fine-tuned and adjusted.

Another possible approach to investigate heterotetramerization (*in planta*) is using bimolecular fluorescence complementation (BiFC) or Fluorescence resonance energy transfer (FRET). The advantage of using such techniques is their ability to observe protein-protein interactions in different cellular compartments including membranes. Also, using BiFC of FRET is more biologically relevant, it allows observing these interactions *in planta*. In Yoshioka laboratory, BiFC is currently being tested using *N. benthamiana* transient expression system.

Through studies such as the ones proposed in this chapter, a better understanding of how this channel family is regulated through its domains, including the CNBD and the CaMBD, will be obtained. These studies will help researchers to better understand the structure-function relationship of these channels in general.

Appendix

Appendix

Table 1: Primer sequences

Primer	Oligonucleotide sequences	Vector
Huda-cpr22-F	5'-AAGAGCTCTAGAATGAATCTTCAGAGGAGAAAA-3'	pYES2 (yeast expression) pJB (plant expression)
Huda-cpr22-R	5'-TTGCGGCCGCTGGATCCGCTTCAGCCTTTGCA-3'	pYES2 (yeast expression) pJB (plant expression)
CNGC12-pET28-F	5'-AAGCTAGCTCTACTACTAGAGTAGATGAA-3'	pET28a-modified
CNGC12-pET28-R	5'-TTGGATCCTTTCCTCCATGCCGCTTGAAT-3'	pET28a-modified
100-D433S-F	5'-CGTGTTCCATGGCTTAACATCATGGATAGTGGTTGGCTACTAG-3'	pBluescript
100-D433S-R	5'-CTAGTAGCCAACCACTATCCATGATGTTAAGCCATGGAACACG-3'	pBluescript
137-E412L-F	5'-TCTTCCTAAAGACCTGAGACTCTTAACCAAACGCTATCTTTACTTG-3'	pBluescript
137-E412L-R	5'-CAAGTAAAGATAGCGTTTGGTTAAGAGTCTGAGGTCTTTAGGAAGA-3'	pBluescript
β-tubulin-F	5'-CGTGGATCACAGCAATACAGAGCC-3'	
β-tubulin-R	5'-CCTCCTGCACTTCCACTTCGTCTTC-3'	

Table 2: NCBI accession # of AtCNGCs

AtCNGCs	NCBI accession #
AtCNGC1	AAK43954
AtCNGC2	NP_197045
AtCNGC3	CAB40128
AtCNGC4	NP_200236
AtCNGC5	T52573
AtCNGC6	AAC63666
AtCNGC7	AAG12561
AtCNGC8	NP_173408
AtCNGC9	CAB79774
AtCNGC10	AAF73128
AtCNGC11	AAD20357
AtCNGC12	AAd23055
AtCNGC12(Ws)	EU541495
AtCNGC13	AAL27505
AtCNGC14	AAD23886
AtCNGC15	AAD29827
AtCNGC16	CAB41138
AtCNGC17	CAB81029
AtCNGC18	CAC01886
AtCNGC19	BAB02061
AtCNGC20	BAB02062

Table 3: Predicted CaMBD peptide sequences

CaMBDs	peptide sequences
AtCNGC2 C-terminus	HFRYKFANERLKRTARYYSSNWRTWA
AtCNGC11 C-terminus	TQYRRLHSKQLQHMFRFYSLQWQTWA
AtCNGC12 C-terminus	RLYSQQWRSWAAFFIQAAWRKHCKR
AtCNGC12 N-terminus	VDGKLKSVRGRLKKVYGKMKTLENW
L14E-K15E N-terminus	VDGKLKSVRGREEKVYGKMKTLENW

Table 4: NCBI accession # of AtCaMs

AtCaMs	NCBI accession #
AtCaM1	NP_198594.**1**
AtCaM2	NP_001189724
AtCaM3	NP_191239.1
AtCaM4	NP_176814.1
AtCaM5	NP_180271.1
AtCaM6	NP_850860.1
AtCaM7	NP_189967.1

References

Abagyan R., Totrov M. (1994): Biased probability Monte Carlo conformational searches and electrostatic calculations for peptides and proteins. J Mol Biol **235**: 983–1002.

Abagyan R., Totrov M., Kuznetsov D. (1994): ICM - A new method for protein modeling and design: Applications to docking and structure prediction from the distorted native conformation. J Comput Chem. **15**:488–506.

Abdel-Hamid H., Chin K., Moeder W., Yoshioka K. (2011): High throughput chemical creening supports the involvement of Ca^{2+} in cyclic nucleotide-gated channel-mediated programmed cell death in Arabidopsis. *Plant Sig. Behav* **5**: 1147-1149.

Abdel-Hamid H., Chin K., Shahinas D., Moeder W., Yoshioka K. (2010): Calmodulin binding to Arabidopsis cyclic nucleotide gated ion channels. *Plant Sig. Behav.* **5**: 1-3.

Abu-Abed M., Millet O., MacLennan D.H., Ikura M. (2004): Probing nucleotide-binding effects on backbone dynamics and folding of the nucleotide-binding domain of the sarcoplasmic/endoplasmicreticulum Ca^{2+}-ATPase. Biochemistry **379**: 235–242.

Alexander K. A., Wakim B. T., Doyle G. S., Walsh K. A., Storm D. R. (1988): Identification and characterization of the calmodulin-binding domain of neuromodulin, a neurospecific calmodulin-binding protein. *J. Biol. Chem.,* **263**: 7544-9.

Ali R., Ma W., Lemtiri-Chlieh F., Tsaltas D., Leng Q., Von Bodman S., Berkowitz G.A. (2007): Death Don't Have No Mercy and Neither Does Calcium: *Arabidopsis* Cyclic Nucleotide Gated Channel 2 and Innate Immunity. Plant Cell **19**: 1081-1095.

Ali R., Zielinski R.E., Berkowitz G.A. (2005): Expression of plant cyclic nucleotide-gated cation channels in yeast. J. Exp. Bot. **57**: 125-138.

Altenhofen W., Ludwig J., Eismann E., Kraus W., Bonigk W., Kaupp U.B. (1991): Control of ligand specificity in cyclic nucleotidegated channels from rod photoreceptors and olfactory epithelium. Proc. Natl. Acad. Sci. USA **88**: 9868–9872.

Altieri S.L., Clayton G.M., Silverman W.R., Olivares A.O., De La Cruz E.M., Lise R. Thomas L.R., Morais-Cabral J.H. (2008): Structural and energetic analysis of activation by a cyclic nucleotide binding domain. J. Mol. Biol. **381**: 655–669.

Anderson J.A., Huprikar S.S., Kochian L.V., Lucas W.L., Gaber R.F. (1992): Functional expression of a probable *Arabidopsis thaliana* potassium channel in *Saccharomyces cerevisiae*. Proc. Natl. Acad. Sci. USA **89**: 3736-3740.

Arazi T., Kaplan B., Fromm H. (2000): A high-affinity calmodulin-binding site in a tobacco plasma-membrane channel protein coincides with a characteristic element of cyclic nucleotide-binding domains. Plant Mol. Biol. **42**: 591-601.

Arazi T., Sunkar R., Kaplan B., Fromm H. (1999): A tobacco plasma membrane calmodulin-binding transporter confers Ni^{2+} tolerance and Pb^{2+} hypersensitivity in transgenic plants. Plant J. **20**: 171–182.

Atkinson M., Midland L., Sims J., KeenT. (1996): Syringolide 1 triggers Ca2þ influx, Kþ efflux, and extracellular alkalization .in soybean cells carrying the disease-resistance gene Rpg4. Plant Physiol. **112**: 297–302.

Balagué C., Lin B., Alcon C., Flottes G., Malmstrom S., Köhler C., Neuhaus G., Pelletier G., Gaymard F., Roby D. (2003): HLM1, an essential signaling component in the hypersensitive response, is a member of the cyclic nucleotide-gated channel ion channel family. Plant Cell **15**: 365-379.

Baruscotti M., Difrancesco D. (2004): Pacemaker channels. Ann. N Y Acad. Sci. USA **1015**: 111–121.

Baxter J., Moeder W., Urquhart W., Shahinas D., Chin K., Christendat D., Kang H.G., Angelova M., Kato N., Yoshioka K. (2008): Identification of a functionally

essential amino acid for Arabidopsis cyclic nucleotide-gated ion channels using the chimeric AtCNGC11/12 gene. Plant J. **457**: 56-69.

Becchetti A., Gamel K., Torre V. (1999): Cyclic nucleotide-gated channels. Pore topology studied through the accessibility of reporter cysteines. J. Gen. Physiol., **114**: 377−392.

Biel M., Schneider A., Wahl C. (2002): Cardiac HCN channels: structure, function, and modulation. Trends Cardiovasc. Med. **12**: 206–212.

Biel M., Seeliger M., Pfeifer A., Kohler K., Gerstner A., Ludwig A., Jaissle G., Fauser S., Zrenner E., Hofmann F. (1999): Selective loss of cone function in mice lacking the cyclic nucleotide-gated channel CNG3. Proc. Natl. Acad. Sci. USA **96**: 7553–7557.

Bonigk W., Altenhofen W., Muller F., Dose A., Illing M., Molday R.S., Kaupp U.B. (1999): Rod and cone photoreceptor cell express distinct genes for cGMP-gated channels. Neuron **10**: 865-877.

Bonigk W., Bradley J., Muller F., Sesti F., Boekhoff I., Ronnett G. V., Kaupp U. B., Frings S. (1999): The native rat olfactory cyclic nucleotide-gated channel is composed of three distinct subunits. J. Neurosci. **19**: 5332–5347.

Borsics T., Webb D., Andeme-Ondzighi C., Staehelin L.A., Christopher D.A. (2006): The cyclic nucleotide-gated calmodulin-binding channel AtCNGC10 localizes to the plasma membrane and influences numerous growth responses and starch accumulation in *Arabidopsis thaliana*. Planta **225**: 563-573.

Bouché N., Yellin A., Snedden W.A., Fromm H. (2005): Plant-Specific Calmodulin-Binding Proteins. Annu. Rev. Plant Biol. **56**: 435–66.

Bradley J., Bonigk W., Yau K.-W., Frings S. (2004): Calmodulin permanently associates with rat olfactory CNG channels under native conditions. Nat. Neurosci. **7**: 705–710.

Bridges D., Fraser M.E., Moorhead G.B.G. (2005): Cyclic nucleotide binding proteins in the *Arabidopsis thaliana* and *Oryza sativa* genomes. BMC Bioinformatics **11**: 6.

Bruggemann A., Pardo L. A., Stuhmer W., Pongs O. (1993): Ether-a-go-go encodes a voltage-gated channel permeable to K^+ and Ca^{2+} and modulated by cAMP. Nature **365**: 445–448.

Brunet L.J., Gold G.H., Nagi J. (1996): General anosmia caused by a targeted disruption of the mouse olfactory cyclic nucleotide-gated cation channel. Neuron **17**: 681-693.

Carricarte V.C., Bianchini G.M., Muschietti J.P., Tellez-Inon M.T., Perticari A., Torres N., Flawia M.M. (1998): Adenlyate cyclase activity in a higher plant, alfalfa. Biochemical Journal 249: 807-811.

Chan C.W.M., Schorrak L.M., Smith R.K., Bent A.F., Sussman M.R. (2003): A cyclic nucleotide-gated ion channel, CNGC2, is crucial for plant development and adaptation to calcium stress. Plant Physiol. **123**: 728–731.

Chen T-Y., Illing M., Molday L.L., Hsu Y-T., Tau K-W., Molday R.S. (1994): Sub-unit 2 of retinal rod cGMP-gated cation channels is a component of the 240kDa channel-associated protein and mediates Ca^{2+}-calmodulin modulation. Proc. Natl. Acad. Sci. USA **91**: 11757-11761.

Cheney R.E., Mooseker M.S. (1992): Unconventional myosins. Curr. Opin. Cell Biol. **4**: 27-35.

Chin D., Means A.R. (2000): Calmodulin: a prototypical calcium sensor. Trends Cell Biol. **10**: 322-328.

Chin K., Moeder W., Abdel-Hamid H., Shahinas D., Gupta D., Yoshioka K. (2010): Importance of the αC-helix in the cyclic nucleotide binding domain for the stable channel regulation and function of cyclic nucleotide gated ion channels in Arabidopsis. J. Exp. Bot. **61**: 2383-2393.

Chin K., Moeder W., Yoshioka K. (2009): Biological roles of cyclic nucleotide-gated ion channels in plants - What we know and don't know about this 20 member ion channel family. Botany **87**: 668-677.

Chow J.Y., Jeffries C.M., Kwan A.H., Guss J.M., Trewhella J. (2010): Calmodulin disrupts the structure of the HIV-1 MA protein. J. Mol. Biol. **400**: 702-14.

Christopher D.A., Borsics T., Yuen C.Y., Ullmer W., Andéme-Ondzighi C., Andres M.A., Kang B.H., Staehelin L.A. (2007): The cyclic nucleotide gated cation channel AtCNGC10 traffics from the ER via Golgi vesicles to the plasma membrane of *Arabidopsis* root and leaf cells. BMC Plant Biol. **7**: 48.

Clough S.J., Fengler K.A., Yu I-C., Lippok B., Smith R.K. Jr., Bent A.F. (2000): The *Arabidopsis dnd1* "defense, no death" gene encodes a mutated cyclic nucleotide-gated ion channel. Proc. Natl. Acad. Sci. USA **97**: 9323-9328.

Craven K. B., Zagotta W. N. (2004): Salt bridges and gating in the COOH-terminal region of HCN2 and CNGA1 channels. J. Gen. Physiol. **124**: 663–677.

Craven K., Olivier N.B., Zagotta W. (2008): C-terminal Movement during Gating in Cyclic Nucleotide-modulated Channels. J. Biol. Chem. **283**(21): 14728–14738.

Craven K., Zagotta W.N. (2006): CNG and HCN Channels: Two Peas, One Pod. Annu. Rev. Physiol. **68**: 375-401.

Cukkemane A., Seifert R., Kaupp U.B. (2011): Cooperative and uncooperative cyclic-nucleotide-gated ion channels. Trends. Biochem. Sci. **36**: 55-64.

Daram P., Urbach S., Gaymard F., Sentenac H., Chérel I. (1997): Tetramerization of the AKT1 plant potassium channel involves its C-terminal cytoplasmic domain. EMBO J. **16**: 3455–3463

Davenport R. (2002): Glutamate receptors in plants. Ann. Bot. **90**: 549–57.

DeFalco T., Chiasson D., Kaiser B., Snedden W.A. (2010): Characterization of GmCaMK1, a novel calmodulin-binding receptor-like kinase from soybean (*Glycine max*). *FEBS Letters* **584**: 4717-24.

DeFalco T.A., Bender K.W., Snedden W.A. (2009): Breaking the code: Ca^{2+} sensors in plant signalling. Biochem. **425**: 27–40.

DeLano W.L. (2002): The PyMOL Molecular Graphics System, DeLano Scientific, Palo Alto, CA, USA.

Dhallan R.S., Yau K.W., Schrader K.A., Reed R.R. (1990): Primary structure and functional expression of a cyclic nucleotide activated channel from olfactory neurons. Nature **347**: 184-187.

Dietrich P., Anschütz U., Kugler A., Becker D. (2010): Physiology and biophysics of plant ligand-gated ion channels. Plant Biol. **12**: 80-93.

Dodd A.N., Kudla J., Sanders D. (2010): The Language of Calcium Signaling. Annu. Rev. Plant Biol. **61**: 593–620.

Dreyer I., Antunes S., Hoshi T., Müller-Röber B., Palme K., Pongs O., Reintanz B., Hedrich R. (1997): Plant K^+ channel alpha-subunits assemble indiscriminately. Biophys. J **72**: 2143-2150.

Dreyer I., Poree F., Schneider A., Mittelstadt J., Bertl A., Sentenac H., Thibaud J.B., Mueller-Roeber B. (2004): Assembly of plant Shaker-like Kout channels requires two distinct sites of the channel alpha-subunit. Biophys. J **87**: 858–872.

Dreyer I., Uozumi N. (2011): Potassium channels in plant cells. FEBS J. **278**: 4293–4303.

Dryja T.P., Finn J.T., Peng Y.W., McGee T.L., Berson E.L., Yau K.W. (1995): Mutations in the gene encoding the α-subunit of the rod cGMP-gated channel in autosomal recessive retinitis pigmentosa. Proc. Natl. Acad. Sci. USA **92**: 10117-10181.

Eismann E., Muller F., Heinemann S.H., Kaupp U.B. (1994): A single negative charge within the pore region of a cGMP-gated channel controls rectification, Ca^{2+} blockage, and ion selectivity. Proc. Natl. Acad. Sci. USA **91**: 1109-1113.

Fain G. L., Matthews H. R., Cornwall M. C., Koutalos Y. (2001): Adaptation in vertebrate photoreceptors. Physiol. Rev. **81**: 117–151.

Feldkamp M.D., Yu L, Shea M.A. (2011): Structural and energetic determinants of apo calmodulin binding to the IQ motif of the Na(V)1.2 voltage-dependent sodium channel. Structure **19**: 733-47.

Fesenko E.E., Kolesnikov S.S., Lyubarsky A.L. (1985): Induction by cyclic GMP of cationic conductance in plasma membrane of retinal rod outer segment. Nature **313**: 310–313.

Flynn G.E., Black K.D., Islas L.D., Sankaran B., Zagotta, W.N. (2007): Structure and rearrangements in the carboxy-terminal region of SpIH channels. Structure **15**: 671–682.

Flynn G.E., Zagotta W.N. (2011): Molecular Mechanism Underlying Phosphatidylinositol 4,5-Bisphosphate-induced Inhibition of SpIH Channels, J. Biol. Chem. **286**: 15535–15542.

Frietsch S., Wang Y.F., Sladek C., Poulsen L.R., Romanowsky S.M., Schroeder J.I., Harper J.F. (2007): A cyclic nucleotide-gated channel is essential for polarized tip growth of pollen. Proc. Natl. Acad. Sci. USA **104**: 14531-14536.

Frings S., Lynch J.W., Lindemann B. (1992): Properties of cyclic nucleotide-gated channels mediating olfactory transduction: activation, selectivity, and blockage. J. Gen. Physiol. **100**: 45-67.

Garbers D.L. (1999): The guanylyl cyclase receptors. Methods **19**:477–484.

Gavazzo P., Picco C., Eismann E., Kaupp U.B., Menini A. (2000): A point mutation in the pore region alters gating, Ca^{2+} blockage and permeation of olfactory cyclic nucleotide gated channels. J. Gen. Physiol. **116**: 311-325.

Gerstner A., Zong X., Hofmann F., Biel M. (2000): Molecular cloning and functional characterization of a new modulatory cyclic nucleotide-gated channel subunit from mouse retina. J Neurosci **20**: 1324–1332.

Giorgetti A., Nair A.V., Codega P., Torre V., Carloni P. (2005): Structural basis of gating of CNG channels. FEBS Letters **579**(9): 1968−1972.

Gobert A., Park G., Amtmann A., Sanders D., Maathuis F.J.M. (2006): *Arabidopsis thaliana* Cyclic Nucleotide Gated Channel 3 forms a non-selective ion transporter involved in germination and cation transport. J. Exp. Bot. **57**: 791-800.

Gordon S.E., Zagotta W.N. (1995): Subunit interactions in coordination of Ni^{2+} in cyclic nucleotide-gated channels. Proc. Natl. Acad. Sci. USA **92**: 10222-10226.

Goto-Omoto S., Hayashi T., Gekka T., Kubo A., Takeuchi T., Kitahara K. (2006): Compound heterozygous CNGA3 mutations (R436W, L633P) in a Japanese patient with congenital achromatopsia. Vis. Neurosci. **23**: 395–402.

Guo K. M., Babourina O., Christopher D. A., Borsic T., Rengel Z. (2010): The cyclic nucleotide-gated channel AtCNGC10 transports Ca^{2+} and Mg^{2+} in *Arabidopsis*. Physiologia Plantarum **139**: 303–312.

Halgren T. (1995): Merck molecular force field I-V. J Comp Chem. **17**:490–641.

Hanoune J., Defer N. (2001): Regulation and role of adenylyl cyclase isoforms. Annu Rev Pharmacol Toxicol. **41**: 145-74.

Heikaus C.C., Stout J.R., Sekharan M.R., Eakin C.M., Rajagopal P., Brzovic P.S., Beavo J.A., Klevit R.E. (2008): Solution Structure of the cGMP Binding GAF Domain from Phosphodiesterase 5. J. Biol. Chem. **283**(33): 22749–22759.

Hepler P. (2005): Calcium: A Central Regulator of Plant Growth and Development. Plant Cell, **17**: 2142–2155

Hoeflich K.P., Ikura M. (2002): Calmodulin in Action: Diversity in Target Recognition and Activation Mechanisms. Cell **108**: 739-742.

Holm L., Park J. (2000): DaliLite workbench for protein structure comparison. Bioinformatics **16**: 566-567.

Hoshi T. (1995): Regulation of voltage dependence of the KAT1 channel by intracellular factors. J. Gen. Physiol. **105**: 309–328.

Hua B.G., Mercier R.W., Leng Q., Berkowitz G.A. (2003a): Plants do it differently. A new basis for potassium-sodium selectivity in the pore of an ion channel. Plant Physiol. **132**: 1353-1361.

Hua B.G., Mercier R.W., Zielinski R.E., Berkowitz G.A. (2003b): Functional interaction of calmodulin with a plant cyclic nucleotide gated cation channel. Plant Physiol. Biochem. **41**: 945-954.

Huang C.W., Chen Y.H., Chen Y.H., Tsai Y.C., Lee H.J. (2009): The interaction of Glu294 at the subunit interface is important for the activity and stability of goose delta-crystallin. Mol Vis. **15**: 2358-63.

Ichikawa T., Suzuki Y., Czaja I., Schommer C., LeBnick A., Schell J., and Walden R. (1997): Identification and role of adenylyl cyclase in auxin signaling in higher plants. Nature **390**: 698-701.

Ikura M., Barbato G., Klee C.B., Bax A. (1992): Solution structure of calmodulin and its complex with a myosin light chain kinase fragment. Cell Calcium **13**(6-7): 391-400.

Ishida H., Rainaldi M., J. Vogel H.J. (2009): Structural Studies of Soybean Calmodulin Isoform 4 Bound to the Calmodulin-Binding Domain of Tobacco MAPK Phosphatase-1 Provide Insights into a Sequential Target Binding Mode. J. Biol. Chem. **41**: 28292-38305.

Jammes F., Hu H.C., Villiers F., Bouten R., Kwak J.M. (2011): Calcium-permeable channels in plant cells. FEBS Letters **278**: 4262-76

Junttila M. R., Saarinen S., Schmidt T., Kast J., Westermarck J. (2005): Singe *Strep*-tag® purification for the isolation and identification of protein complexes from mammalian cells. Proteomics **5**: 1199-1203.

Juranic N., Atanasova E., Filoteo A.G., Macura S., Prendergast F.G., Penniston J.T., Strehler E.E. (2010): Calmodulin Wraps around Its Binding Domain in the Plasma Membrane Ca²⁺ Pump Anchored by a Novel 18-1 Motif, J. Biol. Chem. **285**: 4015–4024.

Jurkowski G.I., Smith R.K. Jr., Yu I.C., Ham J.H., Sharma S.B., Klessig D.F., Bent A.F. (2004): *Arabidopsis* DND2, a second cyclic nucleotide-gated ion channel gene for which mutation causes the "defense, no death" phenotype. Molecular Plant-Microbe Interactions **17**: 511-520.

Kaplan B., Sherman T., Fromm H. (2007): Cyclic nucleotide-gated channels in plants. FEBS Letters **581**: 2237–2246.

Kaupp U.B., Niidome T., Taname T., Terada S., Bonigk W., Stuhmer W., Cook N.J., Kangawa K., Matsuo H., Hirose T., Miyata T., Numa S. (1998): Primary structure and functional expression from complementary DNA of the rod photoreceptor cyclic GMP-gated channel. Nature **342**: 762-766.

Kaupp U.B., Seifert R. (2002): Cyclic nucleotide-gated ion channels. Physiol. Rev. **82**: 769-824.

Ko C.H., Gaber R.F. (1991): *TRK1* and *TRK2* encode structurally related K⁺ transporters in *Saccharomyces cerevisiae*. Mol. Cell. Biol. **11**: 4266–4273.

Koeppen K., Reuter P., Kohl S., Baumann B., Ladewig T., Wissinger B. (2008): Functional analysis of human CNGA3 mutations associated with colour blindness suggests impaired surface expression of channel mutants A3R427C and A3R563C. Eur. J. Neurosci. **27**: 2391–2401.

Kohl S., Baumann B., Broghammer M., Jägle H., Sieving P., Kellner U., Spegal R., Anastasi M., Zrenner E., Sharpe L.T., Wissinger B. (2000): Mutations in the CNBG3 Gene encoding the β-subunit of the cone photorecepter cGMP gated channel are responsible for achromatopsia (*ACHM3*) linked to chromosome 8q21. Hum. Mol. Genet. **9**: 2107-2116.

Kohl S., Marx T., Giddings I., Jägle H., Jacobson S.G., Apfelstedt-Syllae E., Zerenner E., Sharpe L.T., Wissinger B. (1998): Total colour blindness is caused by mutations in the gene encoding the α-subunit of the cone photoreceptor cGMP-gated cation channel. Nature Genet. **19**: 257-259.

Köhler C., Merkle T., Roby D., Neuhaus G. (2001): Developmentally regulated expression of a cyclic nucleotide-gated ion channel from Arabidopsis indicates its involvement in programmed cell death. Planta **213**: 327-332.

Köhler C., Merkle T., Neuhaus G. (1999): Characterization of a novel gene family of putative cyclic nucleotide- and calmodulin-regulated ion channels in *Arabidopsis thaliana*. Plant J. **18**: 97–104.

Köhler C., Neuhaus G. (1998): Cloning and partial characterization of two putative cyclic nucleotide-regulated ion channels from Arabidopsis thaliana, designated CNGC1 (Y16327), CNGC2 (Y16328) (PGR98-062). Plant Physiol. **116**: 1604.

Köhler C., Neuhaus G. (2000): Characterization of calmodulin binding to cyclic nucleotide-gated ion channels from *Arabidopsis* thaliana. FEBS Letters **4710**: 133–136.

Korschen H.G., Illing M., Seifert R., Sesti F., Williams A., Gotzes S., Colville C., Muller F., Dose A., Godde M., Molday L., Moday R.S. (1995): A 240 kDa protein represents the complete β subunit of the cyclic nucleotide-gated channel from rod photoreceptor. Neuron **15**: 627-636.

Kramer R.H., Siegelbaum S.A. (1992): Intracellular Ca^{2+} regulates the sensitivity of cyclic nucleotide-gated channels in olfactory receptor neurons. Neuron **9**: 897-906.

Kumar V.D., Weber I.T. (1992): Molecular model of the cyclic GMP-binding domain of the cyclic GMP-gated ion channel. Biochemistry. **31**: 4643–4649.

Kwezi L., Meier S., Mungur L., Ruzvidzo O., Iving H., Gehring C. (2007): The Arabidopsis thaliana brassinosteroid receptor (AtBRI1) contains a domain that functions as a guanylyl cyclase in vitro. PLoS ONE **2**: e449.

Leng Q., Mercier R.W., Hua B.G., Fromm H., Berkowitz, G.A. (2002): Electrophysiological analysis of cloned cyclic nucleotide-gated ion channels. Plant Physiol. **128**: 400–410.

Leng Q., Mercier R.W., Yao W., Berkowitz G.A. (1999): Cloning and first functional characterization of a plant cyclic nucleotide-gated cation channel. Plant Physiol. **121**: 753–761.

Li X., Borsics T., Harrington H.M., Christopher D.A. (2005): *Arabidopsis* AtCNGC10 rescues potassium channel mutants of *E. coli*, yeast, and *Arabidopsis* and is regulated by calcium/calmodulin and cyclic GMP in *E. coli*. Funct. Plant Biol. **32**: 643–653.

Liman E. R., Buck L. B. (1994): A second subunit of the olfactory cyclic nucleotide-gated channel confers high sensitivity to cAMP. Neuron **13**: 611–621.

Lipkin D., Cook W.H., Markham R. (1959): Adenosine-3`-5`-phosphoric acid: a proof of structure. Journal of American Chemical Society **81**: 6198-6203.

Liu Y.C., Storm D.R. (1990): Regulation of free calmodulin levels by neuromodulin: neuron growth and regeneration. Trends Pharmacol. Sci. **11**: 107-111

Lucas K.A., Pitari G.M., Kazerounian S., Ruiz-Stewart I., Park J., Schulz S., Chepenik K.P., Waldman S.A., (2000): Guanylyl cyclases and signaling by cyclic GMP. Pharmacol Rev **52**: 375–413.

Ludidi N. Gehring C. (2002): Identification of novel protein with guanylyl cyclase activity in Arabidposis thaliana. The Journal of Biological Chemistry **278**: 6490-6494.

Ma W., Ali R., Berkowitz G.A. (2006): Characterization of plant phenotypes associated with loss-of-function of AtCNGC1, a plant cyclic nucleotide gated cation channel. Plant Physiol. Biochem. **44**: 494–505.

Majava V., Kursula P. (2009): Domain Swapping and Different Oligomeric States for the Complex Between Calmodulin and the Calmodulin-Binding Domain of Calcineurin A. PLoS ONE **4**(e5402): 1-8.

Mal T.K., Ikura M. (2006): NMR Investigation of Calmodulin. Graham A. Webb (ed.), Modern Magnetic Resonance, 503–516.

Marschner H. (1995): Mineral nutrition of higher plants, 2nd edn. London: Academic Press.

Mäser P., Thomine S., Schroeder J.I., Ward J.M., Hirschi K., Sze H., Talke I.N., Amtmann A., Maathuis F.J., Sanders D., Harper J.F., Tchieu J., Gribskov M., Persans M.W., Salt D.E., Kim S.A., Guerinot M.L. (2001): Phylogenetic relationships within cation transporter families of *Arabidopsis*. Plant. Physiol. **126**: 1646–1667.

Matulef K., Zagotta W.N. (2003): Cyclic nucleotide-gated ion channels. Annu. Rev. Cell Dev. Biol. 2003. **19**: 23–44.

McCormack E., Braam J. (2003): Calmodulins and related potential calcium sensors of *Arabidopsis.* New Phytol. **159**: 585-598.

McCormack E., Tsai Y.C., Braam J. (2005): Handling calcium signaling: *Arabidopsis* CaMs and CMLs. Trends Plant Sci. **10**: 383-389.

Mengel K., Kirkby E.A., Kosegarten H., Appel T. (2001): Principles of plant nutrition. Dordrecht: Kluwer Academic.

Menini A. (1999): Calcium signalling and regulation in olfactory neurons Curr. Opin. Neurobiol. **9**: 419–426.

Metropolis N., Rosenbluth AW., Rosenbluth MN., Teller AH., Teller E. (1953): Equation of state calculations by fast computing machines. J Chem Phys. **21**:1087–1092.

Michalakis S., Reisert J., Geiger H., Wetzel C., Zong X., Bradley J., Spehr M., Huttl S., Gerstner A., Pfeifer A., Hatt H., Yau K. W., Biel M. (2006): Loss of CNGB1

protein leads to olfactory dysfunction and subciliary cyclic nucleotide-gated channel trapping. J. Biol. Chem. **281**: 35156–35166.

Mitsutake S., Igarashi Y. (2005): Calmodulin Is Involved in the Ca^{2+}-dependent Activation of Ceramide Kinase as a Calcium Sensor. J. Biol. Chem. **280**(49): 40436–40441.

Moeder W., Urquhart W., Ung H., Yoshioka K. (2011): The role of cyclic nucleotide-gated ion channels in plant immunity. Mol. Plant **4**: 442-452.

Mosher S., Moeder W., Nishimura N., Jikumaru Y., Joo S-E., Urquhart W., Klessig D.F., Kim S-K., Mabara, E., Yoshioka K. (2010): The lesion-mimic mutant *cpr22* shows alterations in absisic acid signaling and absisic acid insensitivity in a salicylic acid-dependent manner. Plant Physiol. **152**: 1901-1913.

Mottig H., Kusch J., Zimmer T., Scholle A., Benndorf K. (2001): Molecular regions controlling the activity of CNG channels. J. Gen. Physiol. **118**: 183-192.

Nakaruma T., Gold G.H. (1987): A cyclic nucleotide-gated conductance in olfactory receptor cilia. Nature **325**: 442–444.

Naso A., Dreyer I., Pedemonte L., Testa I., Gomez-Porras J.L., Usai C., Mueller-Rueber B., Diaspro A., Gambale F., Picco C. (2009): The Role of the C-Terminus for Functional Heteromerization of the Plant Channel KDC1. Biophys. J. **96**: 4063–4074.

Natalie C., Strynadka J., James M.N.G. (1989): Crystal structure of the helix-loop-helix calcium-binding proteins. Annu. Rev. Biochem. **8**: 951-958.

Nemethy G., Gibson KD., Palmer KA., Yoon CN., Paterlini G., Zagari A., Rumsey S., Scheraga HA. (1992): Energy parameters in polypeptides: Ten improved geometrical parameters and nonbonded interactions for use in the ECEPP/3 algorithm, with application to proline-containing peptides. J Phys Chem **96**:6472–6484.

Newton R.P., Roef L., Witters E., van Onckelen H. (1999): Tansley Review no. 106 Cyclic nucleotides in higher plants: the enduring paradox. New phytologist **143**: 427-455.

Newton R.P., Smith C.J. (2004): Cyclic nucleotides. Phytochemistry **65**: 2423–2437

Niesen F.H., Berglund H., Vedadi M. (2007): The use of differential scanning fluorimetry to detect ligand interactions that promote protein stability. Nat. Protoc. **2**: 2212-2221.

O'Neil K.T., DeGrado W. F. (1990): A thermodynamic scale for the helix-forming tendencies of the commonly occurring amino acids. Science **250**: 646–651.

Paoletti P., Young E.C., Siegelbaum S. (1999): C-linker of cyclic nucleotide-gated channels controls coupling of ligand binding to channel gating. J. Gen. Physiol. **113**: 17-33.

Pape H.C. (1996): Queer current and pacemaker: the hyperpolarization activated cation current in neurons. Annu. Rev. Physiol. **58**: 299–327.

Park C.S., MacKinnon R. (1995): Divalent cation selectivity in a cyclic nucleotide-gated ion channel. Biochemistry. **34**: 13328-13333.

Park S.W., Kaimoyo E., Kumar D., Mosher S., Klessig D.F. (2007): Methyl Salicylate Is a Critical Mobile Signal for Plant Systemic Acquired Resistance. Science **318**: 113-116.

Peiter E., Maathuis F.J.M., Mills L.N., Knight H., Pelloux J. (2005): The vacuolar Ca^{2+}-activated channel TPC1 regulates germination and stomatal movement. Nature **434**: 404–408

Peng C., Rich E.D., Varnum M.D. (2004): Subunit configuration of heteromeric cone cyclic nucleotide-gated channels. Neuron **42**: 401–410.

Picones A., Korenbrot J.I. (1992): Permeation and interaction of monovalent cations with cGMP-gated channels of cone photoreceptors. J. Gen. Physiol. **100**: 647-673.

Pottosin I., Wherrett T., Shabala S. (2009): SV channels dominate the vacuolar Ca^{2+} release during intracellular signalling. FEBS Letters **583**: 921–926

Rall T., Sutherland E., and Berthet J. (1957): The relationship of epinephrine and glucagon to liver phosphorylase. IV. Effect of epinephrine and glucagon on the reactivation of phosphorlyase in liver homogenates. Journal of Biological Chemistry **224**: 463-475.

Rehmann H., Wittinghofer A., Boss J.L. (2007): Capturing cyclic nucleotides in action: snapshots from crystallographic studies. Natl. Rev. Mol. Cell Biol. **8**: 63-73.

Rhoads A.R., Friedberg, F. (1997): Sequence motifs for calmodulin recognition. FASEB J. **11**: 331–340.

Robinson R.B., Siegelbaum S.A. (2003): Hyperpolarization-activated cation currents: from molecules to physiological function. Annu. Rev. Physiol. **65**: 453-480.

Root M.J., MacKinnon R. (1993): Identification of an external divalent cation-binding site in the pore of a cGMP-activated channel. Neuron **11**: 459-466.

Rostoks N., Schmierer D., Mudie S., Drader T., Brueggeman R., Caldwell D.G., Waugh R., Kleinhofs A. (2006): Barley necrotic locus *nec1* encodes the cyclic nucleotide gated ion channel 4 homologous to the *Arabidopsis* HLM1. Mol. Gen. Genom. **275b**: 159-168.

Sanders D., Brownlee C., Harper J.F. (1999): Communicating with calcium. Plant Cell **11**: 691–706.

Sanders D., Pelloux J., Brownlee C., Harper. J.F. (2002): Calcium at the Crossroads of Signaling. Plant Cell, **S**401–**S**417.

Sautter A., Zong X., Hofmann F., Biel M. (1998): An isoform of the rod photoreceptor cyclic nucleotide-gated channel beta subunit expressed. Proc. Natl. Acad. Sci. USA **95**: 4696–4701.

Schneidman-Duhovny D., Inbar Y., Nussinov R., Wolfson H.J. (2005): PatchDock and SymmDock: servers for rigid and symmetric docking. Nucleic Acids Res. **33**: W363-7.

Schünke S., Lecher J., Stoldt M., Kaupp U.B., Willbold D. (2010): Resonance assignments of the nucleotide-free wildtype MloK1 cyclic nucleotide-binding domain. Biomol. NMR Assign. **4**: 147–150.

Schuurink R.C., Shartzer S.F., Fath A., Jones R.L. (1998): Characterization of a calmodulin-binding transporter from the plasma membrane of barley aleurone. Proc. Natl. Acad. Sci. USA **95**: 1944–1949.

Scott S.P., Harrison R.W., Weber I.T., Tanaka J.C. (1996): Predicted ligand interactions of 3050-cyclic nucleotide-gated channel binding sites: comparison of retina and olfactory binding site models. Protein Eng. **9**: 333–344.

Seifert R., Eismann E., Ludwig J., Baumann A., Kaupp U.B. (1999): Molecular determinants of a Ca^{2+} binding site in the pore of cyclic nucleotide-gated channels: S5/S6 segments control affinity of intrapore glutamates. EMBO Journal **18**: 119-130.

Sentenace H., Bonneaud N., Minet M., Lacroute F., Salmon J-M., Gaymard F., Grignon C. (1992): Cloning and expression in yeast of a plant potassium ion transport system. Science **256**: 663-665.

Shapiro M.S., Zagotta W.N. (2000): Structural basis for ligand selectivity of heteromeric olfactory cyclic nucleotide-gated channels. Biophys. J. **78**: 2307-2320.

Shen X., Li H., Ou Y., Tao W., Dong A., Kong J., Ji C., Yu S. (2008): The secondary structure of calcineurin regulatory region and conformational change induced by calcium/calmodulin binding. J. Biol. Chem. **283**(17): 11407-13.

Silva H., Yoshioka K., Dooner H.K., Klessig, D.F. (1999): Characterization of a new Arabidopsis mutant exhibiting enhanced disease resistance. Mol. Plant-Microbe Interact. **12**: 1053-1063.

Snedden W.A., Fromm H. (2001): Calmodulin as a versatile calcium signal transducer in plants. New Phytol. **151**: 35-66.

Song Y., Cygnar K.D., Sagdullaev B., Valley M., Hirsh S., Stephan A., Reisert J., Zhao H. (2008): Olfactory CNG channel desensitization by Ca2+/CaM via the B1b subunit affects response termination but not sensitivity to recurring stimulation. Neuron **58**: 374-386.

Spratt D.E., Taiakina V., Guillemette J.G. (2007): Calcium-deficient calmodulin binding and activation of neuronal and inducible nitric oxide synthases. Biochim. Biophys. Acta. **1774**(10): 1351-1358.

Stockwell B.R. (2004): Exploring biology with small organic molecules. Nature **432**: 846–854.

Studier F.W. (2005): Protein production by auto-induction in high density shaking cultures. Protein Expr. Purif. **41**: 207-234.

Sun Z.P., Akabas M.H., Goulding E.H., Karlin A., Siegelbaum S.A. (1996): Exposure of residues in the cyclic nucleotide-gated channel pore: P region structure and function in gating. Neuron **16**(1): 141−149.

Sundin O.H., Yang J-M., Li. Y., Zhud D., Hurd J.N., Mitchell T.N., Silva E.D., Maumenee I.H. (2000): Genetic basis of total colour blindness among the Pingelapese islanders. Nature Genet. **25**: 289-293.

Sunkar R., Kaplan B., Bouché N., Arazi T., Dolev D., Talke I.N., Maathuis F.J.M., Sanders D., Bouchez D., Fromm H. (2000): Expression of a truncated tobacco NtCBP4 channel in transgenic plants and disruption of the homologous *Arabidopsis CNGC1* gene confer Pb^{2+} tolerance. Plant J. **24**: 533–542.

Takeuchi K., Wagner G. (2006): NMR studies of protein interactions. Curr Opin Struct Biol. **16**: 109-17.

Terrak M., Rebowski G., Lu R.C., Grabarek Z., Dominguez R. (2005): Structure of the light chain-binding domain of myosin V. Proc. Natl. Acad. Sci. USA. **102**: 12718–12723*.*

Thompson J.D., Higgins D.G., Gibson T.J. (1994): CLUSTAL W: improving the sensitivity of progressive multiple sequence alignment through sequence weighting, position specific gap penalties and weight matrix choice. Nucleic Acids Res. **22**: 4673–4680*.*

Totrov M., Abagyan R. (2001): Protein-ligand docking as an energy optimization problem. In: Raffa RB, editor. Drug-receptor thermodynamics: Introduction and experimental applications. New York: John Wiley & Sons.

Totrov M., Abagyan R. (1999): Derivation of sensitive discrimination potential for virtual ligand screening. Proceedings of the Third Annual International Conference on Computational Molecular Biology. Lyon, France: ACM Press. **p** 37–38.

Trudeau M. C., Zagotta W. N. (2002a): An intersubunit interaction regulates trafficking of rod cyclic nucleotide-gated channels and is disrupted in an inherited form of blindness. Neuron **34**: 197–207.

Trudeau M. C., Zagotta W. N. (2002b): Mechanism of calcium/calmodulin inhibition of rod cyclic nucleotide-gated channels Proc. Natl. Acad. Sci. USA. **99**: 8424–8429.

Trudeau M.C., Zagotta W.N. (2003): Calcium/calmodulin modulation of olfactory and rod cyclic nucleotide-gated ion channels. J. Biol. Chem. **278**: 18705–18708.

Ungerer N., Mücke N., Broecker J., Keller S., Frings S., Möhrlen F. (2011): Distinct binding properties distinguish LQ-type calmodulin-binding domains in cyclic nucleotide-gated channels. Biochemistry. **50**: 3221-3228.

Urbach S., Chérel I., Sentenac H.,Gaymard F. (2000): Biochemical characterization of the Arabidopsis K channels KAT1 and AKT1 expressed or co-expressed in insect cells. Plant J. **4**: 527-538.

Urbauer J.L., Short J.H., Dow L.K., Wand A.J. (1995): Structural analysis of a novel interaction by calmodulin: high-affinity binding of a peptide in the absence of calcium. Biochemistry. **34**: 8099-109.

Urquhart W., Gunawardena A.H.L.A.N., Moeder W., Ali R., Berkowitz G.A., Yoshioka K. (2007): The chimeric cyclic nucleotide-gated ion channel ATCNGC11/12 constitutively induces programmed cell death in a Ca^{2+} dependent manner. Plant Mol. Biol. **65**: 747–761.

Varnum M. D., Zagotta W. N. (1997): Interdomain interactions underlying activation of cyclic nucleotide-gated channels. Science **278**: 110–113.

Varnum M.D., Black K.D., Zagotta W.N. (1995): Molecular mechanism for ligand discrimination of cyclic nucleotide-gated channels. Neuron **15**: 619–625.

Vedadi M., Niesen F.H., Allali-Hassani A., Fedorov O.Y., Finerty P.J. Jr., Wasney G.A., Yeung R., Arrowsmith C., Ball L.J., Berglund H., Hui R., Marsden B.D., Nordlund P., Sundstrom M., Weigelt J., Edwards A.M. (2006): Chemical screening methods to identify ligands that promote protein stability, protein crystallization, and structure determination, Proc. Natl. Acad. Sci. USA. **103**: 15835-15840.

Vetter S.W., Leclerc E. (2003): Novel aspects of calmodulin target recognition and activation, Eur. J. Biochem. **270**: 404–414.

Vivian S., Dea S., Xu X., Dinesh C. (2008): Structural Insight on the Mechanism of Regulation of the MarR Family of Proteins: High-Resolution Crystal Structure of a Transcriptional Repressor from *Methanobacterium thermoautotrophicum*, J. Mol. Biol. **377**: 655–667.

Wang Z., Jiang Y., Lu L., Huang R., Hou Q., Shi F. (2007): Molecular Mechanisms of Cyclic Nucleotide-Gated Ion Channel Gating. J. Gen. Genom. **34**: 477-485

Ward J.M., Maser P., Schroeder J.I. (2009): Plant ion channels: gene families, physiology, and functional genomics analyses. Annu. Rev. Physiol. **71**: 59–82.

Weber I.T., Shabb J.B., Corbin J.D. (1989): Predicted structures of the cGMP binding domains of the cGMP-dependent protein kinase: a key alanine/threonine difference in evolutionary divergence of cAMP and cGMP binding sites. Biochem. **28**: 6122–6127.

Weber I.T., Steitz T.A. (1987): Structure of a complex catabolite gene activator protein and cyclic AMP refined at 2.5 Å resolution. J. Mol. Biol. **198**: 311-326.

Weyand I., Godde M., Frings S., Weiner J., Muller F., Altenhofen W., Hatt H., Kaupp U.B. (1994): Cloning and functional expression of a cyclic-nucleotide-gated channel from mammalian sperm. Nature **368**: 859-863.

White P.J., Brown P.H. (2010): Plant nutrition for sustainable development and global health, Ann. Bot. **105**: 1073–1080.

Wissinger B., Gamer D., Jägle H., Giorda R., Marx T., Mayer S., Tippmann S., Broghammer M., Jurklies B., Rosenberg T., Jacobson S.G., Sener C., Tatlipinar S., Hoyng C.B., Castellan C., Bitoun P., Andreasson S., Rudolph G., Kellner U., Lorenz B., Wolff G., Verellen-Dumoulin C., Schwartz M., Cremers F.P.M., Apfelstedt-Sylla E., Zrenner E., Salati R., Sharpe L.T., Kohl S. (2001): *CNGA3* Mutations in Hereditary Cone Photoreceptor Disorders. Am. J. Hum. Genet. **69**: 722-733.

Yamauchi E., Nakatsu T., Matsubara M., Kato H., Taniguchi H. (2003): Crystal structure of a MARCKS peptide containing the calmodulin-binding domain in complex with Ca^{2+}-calmodulin, Nat. Struct. Biol. **10**: 226-231

Yang T., Poohvaiah B.W. (2003): Calcium/calmodulin-mediated signal network in plants. Trends Plant Sci. **8**: 505-512.

Yap K.L., Yuan T., Mal T.K., Vogel H.J., Ikura M., (2003): Structural basis for simultaneous binding of two carboxy-terminal peptides of plant glutamate decarboxylase to calmodulin, J. Mol. Biol. **328**: 193–204

Yap K.L., Ames J.B., Swindells M.B., Ikura M. (1999). Diversity of conformational states and changes within the EF-hand protein super family. Proteins, **37**: 499-507.

Ye Q., Wang H., Zheng J., Wei Q., Jia Z. (2008): The complex structure of calmodulin bound to a calcineurin peptide. Proteins **73**: 19–27.

Yoshioka K., Kachroo P., Tsui F., Sharma S.B., Shah J., Klessig D.F. (2001): Environmentally sensitive, SA-dependent defense responses in the *cpr22* mutant of *Arabidopsis*. Plant J. **26**: 447-459.

Yoshioka K., Moeder W., Kang H.G., Kachroo P., Masmoudi K., Berkowitz G., Klessig D.F. (2006): The Chimeric *Arabidopsis* Cyclic Nucleotide-Gated Ion Channel 11/12 activates multiple pathogen resistance responses. Plant Cell **18**: 747-763.

Yuan T., Walsh M.P., Sutherland C., Fabian H., Vogel H.J. (1999): Calcium-dependent and -independent interactions of the calmodulin-binding domain of cyclic nucleotide phosphodiesterase with calmodulin. Biochemistry. **38**: 1446-55.

Zagotta W. N., Siegelbaum, S. A. (1996): Structure and function of cyclic nucleotide-gated channels. Annu. Rev. Neurosci. **19**: 235–263.

Zagotta W.N., Olivier N.B., Black K.D., Young E.C., Olson R., Gouaux E. (2003): Structural basis for modulation and agonist specificity of HCN pacemaker channels. Nature **425**: 200-204.

Zagotta W.N., Siegelbaum S.A. (1996): Structure and function of cyclic nucleotide-gated channels. Ann. Rev. Neurosci. **19**: 235–263.

Zhang, M., Tanaka T., and Ikura M. (1995): Calcium-induced conformational transition revealed by the solution structure of apo calmodulin. Nat. Struct. Biol. **2**: 758–767.

Zhong H., Lai J., Yau K.W. (2003): Selective heteromeric assembly of cyclic nucleotide-gated channels. Proc. Natl. Acad. Sci. USA **100**: 5509-5513.

Zhong H., Molday L.L., Molday R.S., Yau K.W. (2002): The heteromeric cyclic nucleotide-gated channel adopts a 3A:1B stoichiometry. Nature **420**: 193–198.

Zhou L., Siegelbaum S.A. (2007): Gating of HCN channels by cyclic nucleotides: residue contacts that underlie ligand binding, selectivity, and efficacy. Structure **15**: 655–670.

Ziechner U., Schonherr R., Born A. K., Gavrilova-Ruch O., Glaser R. W. (2006): Inhibition of human ether a go-go potassium channels by Ca2+/calmodulin binding to the cytosolic N- and C-termini. FEBS J **273**: 1074–1086.

Zimmermann S., Hartje S., Ehrhardt T., Plesch G., Mueller-Roeber B. (2001): The K^+ channel SKT1 is co-expressed with KST1 in potato guard cells-both channels can co-assemble via their conserved KT domains. Plant J. **28**: 517-527.

Zong X., Zucker H., Hofmann F., Biel M. (1998): Three amino acids in the C-linker are major determinants of gating in cyclic nucleotide-gated channels. EMBO **17**: 353-362.

Zufall F., Munger S. D. (2001): From odor and pheromone transduction to the organization of the sense of smell. Trends Neurosci. **24**: 191–193.